UNIVERSITY OF OKLAHOMA

GRADUATE COLLEGE

PHYSICAL AND CHEMICAL WEATHERING IN MODERN AND PERMIAN PROXIMAL FLUVIAL SYSTEMS

A DISSERTATION

SUBMITTED TO THE GRADUATE FACULTY

in partial fulfillment of the requirements for the

Degree of

DOCTOR OF PHILOSOPHY

By

LESLIE JO KEISER
Norman, Oklahoma
2013

PHYSICAL AND CHEMICAL WEATHERING IN MODERN AND PERMIAN PROXIMAL FLUVIAL SYSTEMS

A DISSERTATION APPROVED FOR THE
CONOCOPHILLIPS SCHOOL OF GEOLOGY AND GEOPHYSICS

BY

_____
Dr. Gerilyn S. Soreghan, Chair

_____
Dr. Megan Elwood Madden

_____
Dr. Michael J. Soreghan

_____
Dr. Andrew S. Madden

_____
Dr. Susan Postawko

_____
Dr. Michal Kowalewski

For my dad who always believed in me.

ACKNOWLEDGEMENTS

I would like thank my advisor, Dr. Lynn Soreghan, for her endless patience and support even though I made it incredibly difficult at times. I had written off ever getting a PhD in Geology because I was a mother of 3 children and couldn't fathom being able to accomplish such a great feat, let alone find someone who was willing to encourage and push me through this long journey. Lynn was that person. Her lectures in Depositional Systems sparked my love for geology like never before and when I inquired about graduate school she didn't hesitate telling me she had no doubts I could do it if I wanted to. And so with Lynn's help, I tackled many obstacles just to get started and many more along the way. This degree represents not only an academic accomplishment, it represents incredible emotional, spiritual, and professional growth as an individual. Lynn helped me find strength I didn't know I had and gave me tools to cope with never-ending stress and change. I am indebted to her for life.

I thank my committee members Dr. Megan Elwood Madden, Dr. Mike Soreghan, Dr. Andy Madden, Dr. Susan Postawko, and Dr. Michal Kowalewski for their time and constructive comments throughout my years in the program. A special thanks to Dr. Megan Elwood Madden for her hours of time spent explaining seemingly simple geochemical problems to me and her encouragement to see this through to the end. I want to thank Dr. Andy Madden for the many hours spent answering my confusing questions about

clays. I also spent countless hours in Dr. Mike Soreghan's office with questions related to grain-size, climate, adobe illustrator, lab equipment, and many more topics I can't think of right now. Thank you Mike.

I would also like to thank Preston Larson for his hours of help while I learned how to use the SEM. Gary Stowe and Jeremy Jernigan in the Petroleum Engineering lab at OU provided endless support with the SEM in their lab. Without their help much of my research would not have been possible, thank you. Dr. Bill Mahaney deserves many thanks for his insight into so many things geology and for his many emails that made me laugh. His belief in me and confidence boosters via email were so important in the end when the light at the end of the tunnel seemed to be getting further away.

I also want to thank Kristen Marra, fellow PhD student, for laughing with me about things no one else would understand. Those moments, though few and far between after she moved, were great reprieves amongst the immense amount of stress that goes with getting a PhD. Her advice and help with all things lab related was essential for my success. I also want to thank Allison Stumpf, Earl Manning, and Tyler Foster for their help with fieldwork in the Wichita Mountains. Other fellow OU students who provided help along the way that I would like to thank are Alisan Sweet, Dustin Sweet, Tad Eccles, Mallory Irwinsky, Matt Miller, and Austin Shock.

I thank my mother and grandmother for their help with Aiden, Noah, and Wyatt throughout the years. I couldn't have done it without them. I thank my dad who kept pushing me even after he was gone. I want to thank Aiden,

Noah, and Wyatt for enduring the hardship of having a mother working on her PhD. They had the ability to make the stress go away in the blink of an eye. A simple hug out of nowhere or I love you for no reason gave me so much encouragement, thank you. And last but not least I have to thank my husband, Tim for his endless support through the ups and downs of our life over the past 5 years. If we can make it through this, we can make it through anything life throws at us. Thank you!

TABLE OF CONTENTS

LIST OF TABLES

LIST OF FIGURES

ABSTRACT

Chapter 1

Inferring paleoclimate from ancient fluvial strata can be challenging, and conflicting interpretations for a given system are common in the literature. This research uses a combination of physical and chemical weathering signals in an attempt to better define the paleoclimatic interpretations for the proximal Cutler Formation near Gateway, Colorado (Chapter 3) and the Post Oak Conglomerate in the Wichita Mountains, Oklahoma (Chapter 4), both Permian units. Chapter 4 includes a comparison of weathering signals from modern sediments in the Wichita Mountains. A methodology for pre-treatment techniques used for grain-size analysis was evaluated during the course of the research and is the topic of Chapter 2. This dissertation is organized as three stand-alone manuscripts and a brief summary of each is presented below.

Chapter 2

To assess the effects of drying on subsequent grain-size analyses, a variety of drying approaches, including drying in ambient air, oven drying, and freeze drying, were applied to sediment collected from modern fluvial, lacustrine, and paludal settings, and containing a wide range of clay-sized material (16-61%). Samples were subsequently rehydrated and subjected to grain-size analysis in a laser particle-size analyzer, and resultant histograms were compared with those from control samples never subjected to drying.

Results indicate that drying techniques induced no effect on grain-size distribution for samples containing <39% clay-sized material. However, for samples containing >39% clay-sized material, only freeze drying produced reproducible results statistically identical to the control samples.

Chapter 3

SEM analysis of quartz microtextures has been shown to be useful for the study of depositional environments in Quaternary strata, and more recently ancient strata. Certain microtextures such as curved grooves, straight grooves, deep troughs, and mechanically upturned plates have been found to be distinctive of glacial processes. SEM analysis of quartz microtextures from the proximal lacustrine, medial lacustrine, and fluvial facies of the Permo-Pennsylvanian Cutler Formation, along with qualitative (histograms), semi-quantitative (ternary diagram), and quantitative techniques (nMDS) were used to assess the possibility of tropical glaciation during the deposition of the this unit. The proximal lacustrine facies depositionally onlaps Unaweep Canyon, a hypothesized glacially carved paleolandform. The proximal lacustrine facies exhibits an abundance of high-stress microtextures indicative of a glacial influence. Grains from the distal fluvial facies exhibit fewer high-stress microtextures and more percussion fractures, which are expected to increase with transport distance *a priori*, owing to more prolonged entrainment in the fluvial system. Multiple approaches to data analysis, including visual inspection of raw data histograms, semi-quantitative

classification of textures using ternary diagrams, as well as quantitative statistical techniques such as the non-parametric multivariate ordination technique, nMDS, produce similar results that suggest the potential usefulness of SEM microtextural analysis for the interpretation of a possible glacial influence. These findings support the proglacial lacustrine interpretation for the proximal Cutler Formation. Despite the abundance of precipitation features inherent to sediment of this age, SEM microtextural analysis is a useful tool for the study of ancient alluvial fan systems where other climate indicators are generally lacking.

Chapter 4

The Wichita Mountains (Oklahoma) are a Permian paleolandscape presently undergoing exhumation. These granitic mountains are releasing sediment into modern streams draining the uplands. Analogously, the Lower Permian (Leonardian) Post Oak Conglomerate proximal to the mountains records drainage systems of similar size to those of the modern system (e.g. Blue Beaver Creek), and that emanated from the same granitic bedrock source. This setting thus offers a near-unique opportunity to compare and contrast weathering signals in systems of both ages, and thus refine paleoclimatic inferences for the ancient system. Significant amounts of clay, high percentages of Al_2O_3 in the mud fraction, spheroidal weathering, thick weathering rinds, and hyperconcentrated flood flow deposits are prominent in the Post Oak Conglomerate and lacking in the modern sediment of Blue

Beaver Creek, suggesting that the climate during the Early Permian was significantly different from the temperate semi-arid climate of the modern and recent systems. More specifically, more water was available for weathering in the Permian. Geochemical data from alluvial sediment in other modern climates draining generally felsic source regions support the results of this study that the Early Permian in the Wichita Mountains was much wetter than previously thought. Most importantly, the preservation of weathering signals in ancient alluvial-fluvial strata is useful for deciphering paleoclimate when other climate evidence is lacking.

1. INTRODUCTION

Inferring paleoclimatic conditions of ancient alluvial-fluvial strata in highland-proximal regions is challenging and conflicting conclusions for a single system are common in the literature. This research uses a combination of physical and chemical weathering signals in an attempt to better define the paleoclimatic interpretations for two Permian units: the Cutler Formation proximal to the Uncompahgre Uplift (Chapter 3) and the Post Oak Conglomerate proximal to the Wichita Uplift, Oklahoma (Chapter 4). Additionally, sediments from a modern fluvial system, Blue Beaver Creek of the modern Wichita Mountains were also studied as a comparison to the ancient Post Oak Conglomerate. A methodology for pre-treatment techniques used for grain-size analysis was evaluated during the course of the research (Chapter 2). These 3 chapters are organized as three stand-alone publications, briefly summarized below.

Chapter 2

Pretreatment drying of mud-sized sediment (<63 μm) resulted in clay-rich (>39%) samples exhibiting more sensitivity to drying techniques than clay-poor (<39%) samples. This demonstrates an influence of the drying technique on the granulometric results. Employing freeze drying for sample drying yielded the most consistent results. However, for samples with <39% clay-sized material, all drying techniques are equally effective, and no

apparent need exists for the extra effort (and expense) that accompanies freeze drying.

Chapter 3

Scanning Electron Microscopy is a useful tool in the study of quartz grain microtextures. Microtextures on quartz grains from the proximal Cutler Formation near Gateway, CO were documented for the presence/absence of 18 distinct microtextures. Averaging of presence/absence data for the samples provided a means to use more quantitative techniques than previously employed for SEM microtextural analysis. These continuous quantitative variables were utilized for non-metric multidimensional scaling, a purely quantitative technique that does not rely on initial assumptions of what environments produce specific microtextures.

Chapter 4

The Post Oak Conglomerate was deposited in a climate much wetter than the modern climate of the Wichita Mountains today. Significant amounts of clay, high percentages of Al_2O_3 in the mud fraction, spheroidal weathering, thick weathering rinds, and hyperconcentrated flood flow deposits are prominent in the Post Oak conglomerate and lacking in the modern Blue Beaver Creek sediment. When compared to other modern climates, the Post Oak Conglomerate fits best with a tropical climate. The climate of the region for the Early Permian is commonly interpreted to be arid. However; these

results suggest a brief time period of wet conditions in the Wichita Mountains prior to the onset of the aridity documented in younger Permian units of the area.

2. EFFECTS OF DRYING TECHNIQUES ON GRAIN-SIZE ANALYSES OF FINE-GRAINED SEDIMENT

INTRODUCTION

Grain-size analysis of mud-sized (clay and silt) sediment (<63 μm) is critical to a wide range of research questions in sedimentology, geochemistry, paleoclimatology, geomorphology, structural geology, and other areas of geoscience. Granulometry of mud-sized sediment, however, presents unique challenges owing to the potential complication of particle aggregation (Buurman et. al, 1997; Muggler et al., 1997; Konert and Vandenberghe, 1997; Vaasma 2008; Jiang and Liu, 2011). If samples require drying steps during pre-treatment, then drying-induced sample aggregation can occur, which can compromise the validity of subsequent grain-size analyses (McManus, 1988; Sperazza et al., 2005). Induced sample aggregation is of concern particularly in studies that employ chemical pretreatment of small volumes of fine-grained sediment (Lewis and McConchie, 1994). For example, studies of sediment from recent and modern lacustrine, marine, fluvial, and soil environments all involve chemical pretreatment techniques prior to grain-size analysis, and thus typically involve intermediate drying steps (Gee and Bauder, 1986; Vaasma, 2008; Marra et al., in review). Where sample sizes are limited, e.g. for core splits that must be distributed among multiple researchers, splitting the sample to avoid an intermediate drying step is precluded (Lewis and McConchie, 1994). Even if sufficient sample material is collected in the field,

chemical pretreatment can significantly decrease the amount of useable sample needed for ultimate grain-size analysis (e.g. Marra et al., in review).

Grain-size analysis of modern sediment commonly necessitates chemical pre-treatments for removal of non-silicate components (e.g., organic matter, carbonate, Fe oxides) which would otherwise invalidate grain-size analysis of the silicate fraction (Gee and Bauder, 1986; Vaasma, 2008; Marra et al., 2012). Following such pre-treatments, samples are dried to obtain the mass of the silicate fraction, prior to grain-size analysis. Unfortunately, however, surface tension can drive particle aggregation during air drying or oven drying (Brydon et al., 1963; Last, 2001), and oven drying mud also induces sample caking, and adherence to the sample container. Many researchers have thus employed freeze drying, under the assumption that freeze drying will prevent particle aggregation (e.g. Brydon et al. 1963, IAEA, 2003). However, no systematic analyses exist of the effects of drying techniques, including freeze drying, on particle-size analysis.

Given the widespread use of grain-size analysis in sedimentologic studies, it is important to establish protocols that maximize fidelity of the original particle-size distribution, especially for samples containing abundant fines and that must be pre-treated prior to analysis. This study aims to test the idea that grain-size analyses of fine-grained (clay- and silt-containing) sediment will vary as a function of pre-treatment drying techniques, and to establish protocols leading to the most accurate and reproducible results.

METHODS

Fine-grained sediment samples, representing a range of mud content, were collected from modern and recent lacustrine, paludal, and fluvial environments. Samples were collected using a scoop, and placed in sealed plastic bags to preserve the original water saturation. Average clay mineralogy was determined using XRD analysis on a split of each sample.

Each sample was wet sieved to isolate the mud (<63 μm) fraction. The mud fraction was then treated with the following processing steps: 1) 30% H_2O_2 to remove organic matter, 2) 1N HCl to remove carbonate material, and 3) the Citrate-Bicarbonate-Dithionite (CBD) method (Mehra and Jackson, 1960) to remove iron oxides. Samples were never dried during these treatments. Subsequently, four aliquots of treated mud were each dried using different drying techniques as follows: (1) freeze drying using a LABCONCO FreeZone 6 Liter Benchtop freeze-dry system (2) oven drying at 50^{o}C for 4 hours, (3) oven drying at 200^{o}C for 2 hours, and (4) drying in ambient air for 12 hours. Once dried and weighed, a portion of each sample was re-suspended in distilled water with 5 drops of 5% sodium hexametaphosphate (dispersant) solution, then sonicated for 2 minutes before being analyzed with a Beckman Coulter Laser Particle Size Analyzer (LPSA), Model LS 230, to compare granulometry results after sample drying using the four methods. A 5th aliquot of each sample was subjected to all of the chemical pretreatments, but never dried, and thus was used as the control sample. Clay mineralogy

was determined using oriented clay mounts and bulk quantitative XRD analysis.

Laser particle-size analyzers require very small sample sizes for analysis, to achieve the proper opacity (obscuration value) for laser analysis. Accordingly, the subsample must be continually agitated to ensure it is representative of the whole sample (Last, 2001). Reproducibility is compromised if techniques for sample loading are not consistent. Hence, samples are sonicated to ensure complete disaggregation and mixing prior to extraction of an aliquot for analysis by LPSA. However, for samples rich in silt and sand, rapid particle settling within the sample vial prior to extraction of the aliquot can result in biased LPSA results. For this reason, samples were analyzed multiple times on the LPSA to ensure erratic results were not being reported.

Data output included histograms (volume % by grain size), and standard statistics (e.g., mean, mode, median, skewness, kurtosis; Fig. 2.1). These statistics were calculated by the LPSA software using the Fraunhoffer model for particle-size analysis (Syvitski, 2007). Kolmogorov–Smirnov (K-S) statistics (Davis, 2002) were used to compare histograms produced from each drying technique relative to that of each control sample to determine statistical significance of any differences. The K-S test is a non-parametric test superior to the t-test in cases of irregular data distributions (i.e., data that are not normal, log-normal, etc.). Geological applications of K-S statistics include 1) comparison of detrital-zircon age-probability distributions (e.g.,

Dickinson and Gehrels, 2009; Gehrels et al., 2011), and 2) grain-size and pore-size distributions (e.g., Bouabid, et al., 1992). K-S statistics assess differences in populations of data by comparing cumulative distribution functions directly resulting in a D value. The D value represents the maximum vertical deviation in the cumulative distribution curves for the two data sets under comparison (Davis, 2002).

The LPSA measures particle size in multiple channels (n) each representing a specific particle size range. The number of particle-size channels (n) measured on the LPSA for a particular sample determines what D value is significant for that sample. This number (n) can vary based on the range of particle-sizes for a sample. For example, for samples exhibiting a two-tailed distribution with n=83 channels, and using a confidence interval of 95% (alpha = 0.05), D values >0.1324 are considered statistically significant.

RESULTS

The predominant clay minerals present in the silt-rich samples are kaolinite and chlorite, whereas smectite with subordinate chlorite and illite generally predominate in the clay-rich samples, although one clay-rich sample contains mostly kaolinite and chlorite. As determined by LPSA analysis, seven samples are relatively rich (39-61%) in clay-sized material, and seven samples are relatively poor (17-38%) in clay-sized material. Standard statistics to include mean, median, mode, standard deviation, skewness, and kurtosis are reported in Table 2.1 for all samples.

Table 2.2 lists the resultant D values for the 4 different drying techniques compared to the control samples. Results are inconsistent for samples containing >39% clay-sized material: Four of these seven samples exhibit particle-size results that differ significantly relative to their respective control samples, whereas three exhibit results that do not differ significantly relative to the controls. In contrast, all samples containing <39% clay-sized material exhibit statistically invariant granulometric results regardless of the drying techniques employed. The sample with the highest clay content (61%) exhibits significant differences in grain-size distributions between the control sample and samples treated by oven drying at 50°C, oven drying at 200°C, and drying in ambient air. Freeze drying this sample produced the only results that did not differ significantly from the control sample. The samples with 49% clay, 43% and 39% clay showed significant differences between the control and both oven-drying techniques. Drying in ambient air and freeze drying did not produce any significant differences relative to the control for these samples regardless of the drying techniques employed.

DISCUSSION AND CONCLUSIONS

Generalizing from the results above, clay-rich (>39%) samples exhibit more sensitivity to drying techniques than clay-poor (<39%) samples, demonstrating an influence of the drying technique on the granulometric results. Employing freeze drying for sample drying yielded the most consistent results. However, for samples with <39% clay-sized material, all

drying techniques are equally effective, and no apparent need exists for the extra effort (and expense) that accompanies freeze drying.

In addition to the proportion of clay-sized material, clay mineralogy likely plays a role in the results. All samples that demonstrated a significant change in particle-size distribution attributable to drying techniques were dominated by smectite, a well-known swelling clay. Smectite undergoes volume changes of up to 30% during wetting and drying events (Moore and Reynolds, 1997). Hence, the presence of swelling clays is a key factor leading to inconsistencies in grain-size results, and thus freeze-drying is the best choice for any samples containing swelling clays.

ACKNOWLEDGEMENTS

This research was conducted with the support of the National Science Foundation (EAR-0746042 and ANT-0442639), and the University of Oklahoma School of Geology and Geophysics. Any opinions, findings, and conclusions or recommendations expressed in this material are those of the author(s) and do not necessarily reflect the views of the National Science Foundation. Additional support was provided by student grants from SEPM and Sigma Xi. XRD analysis was possible with the help of A. Madden and C. Ambers.

Table 2.1: Standard statistics (mean, median, mode, skewness, and kurtosis) calculated using the Fraunhoffer model associated with the LPSA.

	Control	Freeze Dry	Air Dry	Oven Dry 50C	Oven Dry 200C	Control	Freeze Dry	Air Dry	Oven Dry 50C	Oven Dry 200C	Control	Freeze Dry	Air Dry	Oven Dry 50C	Oven Dry 200C
			51%					44%					60%		
Mean	4.557	5.617	4.113	4.35	4.242	5.42	7.63	8.78	6.41	6.81	3.487	3.275	3.738	3.274	3.747
Median	4.089	5.842	3.769	3.97	4.242	5.83	8.98	11	7.26	7.77	3.006	3.016	3.149	2.85	3.257
Mode	2.313	7.083	2.313	2.313	4.242	9.37	41.7	38	21.7	23.8	2.107	2.313	2.107	2.107	2.107
S.D.	3.722	3.305	3.42	3.634	4.242	3.55	3.88	3.98	3.82	3.67	3.334	2.803	3.48	3.164	3.362
Skew	0.139	-0.185	0.12	0.118	4.242	-0.22	-0.41	-0.5	-0.32	-0.33	0.35	0.263	0.399	0.345	0.262
Kurtos	-0.792	-0.762	-0.763	-0.812	4.242	-0.74	-0.74	-0.7	-0.76	-0.78	-0.485	-0.365	-0.447	-0.466	-0.637
			39%					61%					49%		
Mean	10.89	6.117	5.797	4.604	4.455	3.488	4.838	3.656	3.752	4.092	4.878	5.987	6.033	4.613	3.501
Median	13.78	5.506	5.333	4.178	3.813	3.017	4.454	3.196	3.252	3.505	4.395	5.919	5.617	4.127	3.042
Mode	50.22	2.539	2.313	2.313	2.313	2.313	2.787	2.313	2.107	2.313	2.787	4.877	2.313	2.313	2.107
S.D.	4.217	4.191	4.132	3.801	3.855	3.164	3.303	3.226	3.361	3.585	3.608	3.406	4.09	3.717	3.105
Skewness	-0.471	0.079	0.0402	0.0841	0.212	0.394	0.144	0.312	0.285	0.273	0.189	-0.0958	0.0121	0.11	0.339
Kurtosis	-0.709	-0.916	-0.965	-0.869	-0.798	-0.379	-0.699	-0.536	-0.604	-0.694	-0.668	-0.783	-0.941	-0.868	-0.524
			26%					22%					38%		
Mean	11.19	10.94	12.23	14.41	10.15	14.38	15.9	12.44	14.38	16.85	7.013	7.804	8.81	6.33	9.284
Median	16.01	15.77	18.44	23.28	13.07	21.44	25.31	19.53	23.62	27.04	7.862	9.111	11.1	7.15	11.64
Mode	31.5	34.58	45.75	45.75	41.68	34.58	45.75	41.68	41.68	50.22	21.69	31.5	41.7	21.7	41.68
S.D.	4.475	4.445	4.613	4.486	4.627	4.697	4.446	4.564	4.383	4.732	3.939	3.882	3.98	3.8	4.188
Skewness	-0.595	-0.617	-0.687	-0.868	-0.479	-0.643	-0.908	-0.746	-0.951	-0.871	-0.293	-0.378	-0.51	-0.32	-0.501
Kurtosis	-0.401	-0.402	-0.417	-0.139	-0.691	-0.225	0.0708	-0.339	0.0391	-0.107	-0.806	-0.77	-0.68	-0.75	-0.674
			30%					43%					28%		
Mean	9.016	10.17	11.56	11.02	12.93	6.109	6.052	6.245	5.463	5.808	10.4	7.4	9.15	9.97	10.3
Median	11.11	13.71	16.31	15.45	19.5	5.783	5.84	6.211	5.203	5.341	14.1	8.91	11.9	13.2	15
Mode	45.75	41.68	50.22	45.75	50.22	2.539	3.687	2.539	2.313	2.313	41.7	23.8	34.6	38	34.6
S.D.	4.109	4.075	4.222	4.305	4.27	4.064	3.58	4.083	3.86	3.88	4.1	3.66	3.87	3.85	3.94
Skewness	-0.447	-0.6	-0.636	-0.584	-0.673	0.00257	-0.0464	-0.082	-0.0189	0.067	-0.58	-0.45	-0.55	-0.57	-0.71
Kurtosis	-0.7	-0.577	-0.582	-0.693	-0.599	-0.918	-0.839	-0.922	-0.922	-0.883	-0.6	-0.67	-0.62	-0.65	-0.45
			17%					16%							
Mean	15.6	20.5	13.9	17.4	11.5	17.7	18.9	18.8	15	17.2					
Median	19.8	32.4	21.7	28.5	17.3	29.8	25.2	31.5	24.6	28.6					
Mode	35	45.8	41.7	50.2	38	3.87	2.71	3.85	4.06	3.82					
S.D.	2.73	3.62	3.9	3.86	3.95	-1.3	-0.82	-1.3	-0.9	-1.2					
Skewness	-0.65	-1.5	-0.91	-1.1	-0.69	0.746	-0.26	0.896	-0.19	0.671					
Kurtosis	-0.58	1.7	-0.066	0.368	-0.52	45.8	41.7	45.8	50.2	45.8					

Figure 2.1: Grain-size histograms for all analyzed samples. All plots show results for the aliquots dried using the four different methods, as well as the control for each sample. Shaded plots indicate those for which the use of different drying techniques induced statistically different grain-size distributions.

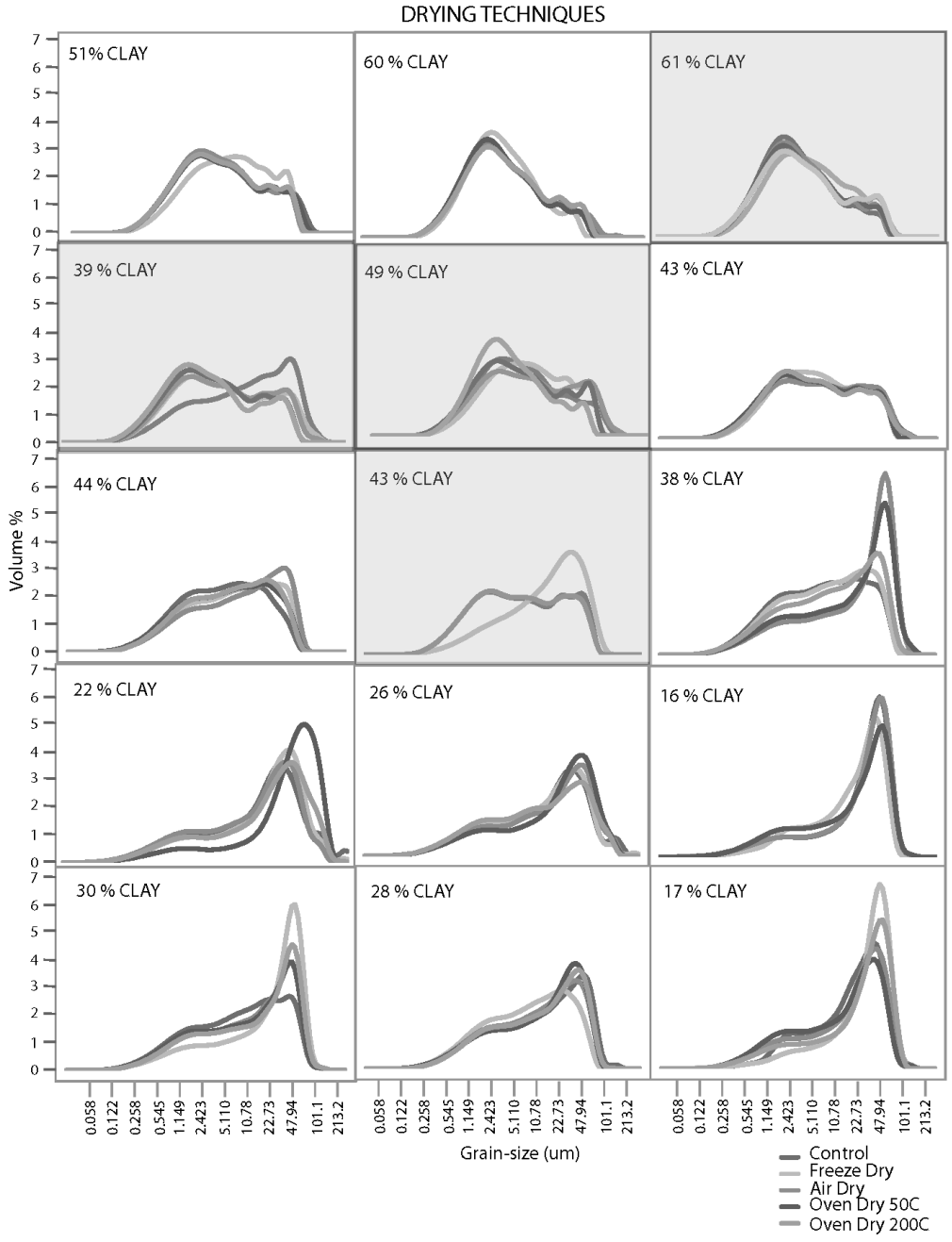
DRYING TECHNIQUES
51% CLAY
60 % CLAY
61 % CLAY
39 % CLAY
49 % CLAY
43 % CLAY
44 % CLAY
43 % CLAY
38 % CLAY
22 % CLAY
26 % CLAY
16 % CLAY
30 % CLAY
28 % CLAY
17 % CLAY
Volume %
0 1 2 3 4 5 6 7
0.058 0.122 0.258 0.545 1.149 2.423 5.110 10.78 22.73 47.94 101.1 213.2
Grain-size (um)
Control
Freeze Dry
Air Dry
Oven Dry 50C
Oven Dry 200C

Table 2.2: D-values calculated using K-S statistics are reported. The significant value is the d-value threshold that must be reached (using a 95% confidence interval) before a method can be considered significantly different from the control sample. This value is different for each sample based on the "n" listed in the far right-hand column. * = significant value

Clay %	Air Dry	Freeze Dry	Oven Dry 50	Oven Dry 200	Significant Value	n
61	0.1325 *	0.1205	0.1446*	0.1325*	0.1324	n=83
60	0.08	0.0714	0.0667	0.0706	0.1324	n=83
51	0.1067	0.1067	0.0526	0.053	0.1324	n=83
49	0.0723	0.0843	0.1446*	0.1687*	0.1324	n=83
44	0.0941	0.0706	0.0706	0.0879	0.1265	n=91
43	0.0482	0.0723	0.0723	0.1325*	0.1324	n=83
39	0.1099	0.1209	0.1429*	0.0753	0.1252	n=93
38	0.0471	0.0471	0.0471	0.0606	0.1309	n=95
30	0.0645	0.1122	0.0645	0.053	0.1324	n=83
28	0.0706	0.0824	0.0706	0.0805	0.1324	n=83
26	0.0532	0.0426	0.0532	0.044	0.1309	n=85
22	0.0909	0.0606	0.1	0.0638	0.1245	n=94
17	0.0879	0.0989	0.0769	0.0879	0.1265	n=91
16	0.044	0.0879	0.0989	0.0588	0.1309	n=85

REFERENCES

BOUABID, R, NATER, E.A., BARAK, P., 1992, Measurement of pore size distribution in a lamellar Bt horizon using epifluorescence microscopy and image analysis: Geoderma, 53, 309-328.

BRYDON, J.E., RICE, H.M., AND SCOTT, G.C., 1963, Note on the recovery of clays from suspension by freeze-drying: Canadian Journal of Soil Science, 43(2), 404-405.

BUURMAN, P., PAPE, T.H., MUGGLER, C.C., 1997, Laser grain-size determination in soil genetic studies 1. Practical problems: Soil Science, 162, 211-218.

DAVIS, JOHN C., 2002, Statistics and Data Analysis in Geology, 3rd edition: John Wiley & Sons, 638p.

DICKINSON, W.R. AND GEHRELS, G.E., 2009, U-Pb ages of detrital zircons in Jurassic eolian and associated sandstones of the Colorado Plateau: Evidence for transcontinental dispersal and intraregional recycling of sediment: Geological Society of America Bulletin, 121, 408-433.

GEE, G.W., AND J.W. BAUDER, 1986, Particle-size analysis, In A. Klute, ed., Methods of soil analysis, Part 1, 2nd ed. Agron. Monog. 9. ASA and SSSA, Madison, WI, 383–411.

GEHRELS, G.E., BLAKEY, R., KARLSTROM, K.E., TIMMONS, M.J., DICKINSON, B., and PECHA, M., 2011, Detritial zircon U-Pb geochronology of Paleozoic strata in the Grand Canyon, Arizona: Lithosphere, 3(3),183-200.

JIANG, Z. AND LIU, L., 2011, A pretreatment method for grain size analysis of red mudstones: Sedimentary Geology, 241,13-21

INTERNATIONAL ATOMIC ENERGY AGENCY, 2003, Collection and preparation of bottom sediment samples for analysis of radionuclides and trace elements: IAEA-TECDOC-1360.

LAST, W., 2001, Textural analysis of lake sediments: Tracking Environmental Change Using Lake Sediments, Volume 2, eds. William M. Last and John P. Smol, Kluwer Academic Publishers, Boston.

KONERT, M. and VANDENBERGHE, J., 1997, Comparison of laser grain size analysis with pipette and sieve analysis: a solution for the underestimation of the clay fraction: Sedimentology, 44, 523-535.

LEWIS, D.W. and MCCONCHIE, D.M., 1994, Analytical Sedimentology: Chapman and Hill, New York, 197p.

MARRA, K., KEISER, L.J., SOREGHAN, G.S., ELWOOD MADDEN, M.E., and HALL, B., 2012, Proximal-distal trends in grain size and reactive surface area in warm semi-arid versus cold arid fluvial systems: In Review Geomorphology.

MCMANUS, J., 1988, Grain size determination and interpretation, ed. Maurice Tucker, Techniques in Sedimentology: Blackwell Scientific Publications, Oxford, 408.

MEHRA, O.P., and JACKSON, M.L.,1960, Iron oxide removal from soils and clays by a citrate–dithionite system buffered by sodium carbonate: Clays and Clay Mineralogy, 7, 317–327.

MOORE, D.M. AND REYNOLDS, R.C., JR., 1997, X-Ray Diffraction and the Identification and Analysis of Clay Minerals, 2nd Edition: Oxford University Press, New York, 378p.

MUGGLER, C.C., PAPE, T.H., BUURMAN, P., 1997, Laser grain-size determination in soil genetic studies 2. Clay content, clay formation, and aggregation in some brazilian oxisols: Soil Science, 162, 219-228.

SIMMONS, C.M., 1991, editor, Hazardous Waste Measurements: CRC Press, 307p.

SPERAZZA, M., MOORE, J.N., AND HENDRIX, M.S., 2004, High resolution particle size analysis of naturally occurring very fine-grained sediment through laser diffractometry: Journal of Sedimentary Research; 74, 736-743.

SYVITSKI, J. P. (ED.), 2007, Principles, methods and application of particle size analysis. Cambridge University Press, 368p.

VAASMA, T., 2008, Grain-size analysis of lacustrine sediments; a comparison of pre-treatment methods: Estonian Journal of Ecology: 57, 231-243.

3. SEM ANALYSIS OF QUARTZ MICROTEXTURES: EVIDENCE FOR TROPICAL GLACIATION DURING DEPOSITION OF THE PERMO-PENNSYLVANIAN CUTLER FORMATION, COLORADO

INTRODUCTION

For nearly 60 years, the Pennsylvanian-Permian Cutler Formation of southwestern Colorado has been interpreted to record warm-arid or warm-humid alluvial fan and braided-stream deposits shed from the ancestral Uncompahgre uplift (e.g., Cater, 1955, 1970; Elston and Shoemaker, 1960; Werner, 1974; Campbell, 1979; Shultz, 1984; Mack and Rasmussen, 1984; Dubiel et al., 2009). In contrast, Soreghan et al. (2009a) recently hypothesized a proglacial origin for the most proximal Cutler Formation, in large part on the basis of facies evidence (e.g., presence of dropstones, faceted clasts, loess, lacustrine strata, and common flood deposits). Furthermore, the Cutler Formation depositionally onlaps Unaweep Canyon, a paleolandform hypothesized to have been glacially carved during the late Paleozoic (Soreghan et al., 2007, 2008b). However, these hypotheses remain debated (eg. see Discussion and Replies - Hood 2009, Hood et al., 2009; Soreghan et al., 2009c) and require further testing.

Beginning over 40 years ago, Krinsley and Donahue (1968) and Krinsley and Doornkamp (1973) began applying Scanning Electron Microscopy (SEM) analysis of quartz microtextures to aid interpretation and study of depositional environments in Neogene (Quaternary) strata. Mahaney and Kalm (2000) and Mahaney et al. (2001) recognized quartz grain

microtextures such as curved grooves, straight grooves, deep troughs, and mechanically upturned plates that reflect fracture genesis via a high-pressure origin most consistent with glacial grinding. Many other authors have also recognized these same microtextures as evidence of glacial grinding (D'Orsay and van de Poll, 1985; Mahaney, 1995; Mahaney and Kalm 2000; Mahaney 2002; Van Hoesen and Orndorff, 2004; Curry et al., 2009; Strand and Immonen, 2010; Sweet and Soreghan, 2010; Deane, 2010; Kirschner and Anderson, 2011; Immonen, 2013). Mechanically upturned plates, crescentic gouges and arc-shaped steps have also been cited as distinctive of high-stress fracturing (D'Orsay and van de Poll, 1985; Mahaney, 1995; Mahaney and Kalm 2000; Mahaney 2002; Sweet and Soreghan, 2010; Kirshner and Anderson, 2011; Deane 2010; Immonen, 2013).

Although SEM microtextural analysis has proven useful in Neogene strata, application to ancient strata remains limited. Using SEM techniques, Mahaney and Andres (1996) found evidence for a glacial influence in modern Saharan sand dunes derived from Ordovician diamictite strata in Algeria. More recently, Sweet and Soreghan (2010) conducted an SEM microtextural study of alluvial facies within the Permo-Pennsylvanian Fountain Formation of central Colorado to further assess the feasibility of this technique in pre-Neogene strata. Sweet and Soreghan (2010) found that depositional microtextures persist and remain observable even in lithified strata, despite a diagenetic overprint. Extending these earlier studies, the purpose of this research is to 1) further assess the feasibility of applying SEM microtextural

analysis to assess depositional microtextures in ancient alluvial strata through the veil of diagenesis, and 2) assess whether or not the character or trends of microtextures preserved in the proximal Cutler Formation in particular shed light on possible depositional origins, especially discernment of a possible non-glacial from proglacial origin for these strata. The potential exists to apply microtextural analyses more widely to assess possible glacial influences on alluvial strata of equivocal derivation, and across the geologic time scale. Discerning the geologic record of glaciation is especially difficult for cases of upland and alpine glaciation, for which ice-contact strata are rarely if ever preserved. However, proximal alluvial deposits can be preserved, and subsequently analyzed using SEM microtextural analysis.

GEOLOGIC SETTING

Western North America during the Carboniferous-Permian was situated in western equatorial Pangaea, between approximately 0° and 10°N (Scotese, 1999). During the Late Carboniferous (Pennsylvanian), this region was affected by the Ancestral Rocky Mountains (ARM) orogeny, characterized by the formation of several intracratonic uplifts (Kluth and Coney, 1981; Kluth, 1986). In many cases, these uplifts were significantly denuded, resulting in erosion of all Phanerozoic strata and exposure of Precambrian granitic and gneissic basement; as a result, thick clastic wedges accumulated mantling many of these uplifts (Cater, 1955, 1970; Elston and Shoemaker, 1960; Werner, 1970). The Permo-Pennsylvanian Cutler Formation consists of first-

cycle arkosic sediments shed from the Uncompahgre uplift into the Paradox basin to the southwest (Campbell, 1979; Suttner and Dutta, 1986) (Fig. 3.1). The Cutler Formation depositionally onlaps Precambrian basement along the eastern margin of the basin, burying the Uncompahgre reverse fault such that no observable surface expression exists (Cater, 1955, 1970; White and Jacobson, 1983; Moore et al., 2008). Thus, the Cutler Formation records cessation of compressional deformation of the Uncompahgre uplift, and the subsequent subsidence of the uplift (Cater, 1970; Moore et al., 2008; Soreghan et al., 2012).

The proximal Cutler Formation has traditionally been interpreted as a "fanglomerate"/alluvial-fan unit deposited in a warm-arid climate (Werner, 1970; Mack and Rasmussen, 1984; Shultz, 1984; Suttner and Dutta, 1986; Dubiel et al., 2009). However, Campbell (1979, 1980) suggested that the large areal extent of the Cutler depositional system, together with the nature of the sedimentary structures record high discharge and thus a warm *humid* fan system. The presence of iron oxides (Werner, 1970), debris flow facies, local (distally) calcic rhizoconcretions (Mack and Rasmussen, 1984), and compositional and chemical immaturity (Suttner and Dutta, 1986) were cited in favor of the arid alluvial fan model. However, Shultz (1984) suggested the possibility of subaqueous deposition for some debris-flow facies. Soreghan et al. (2009a) significantly departed from earlier interpretations, hypothesizing that the proximal Cutler Formation deposited within 10 km of the Uncompahgre uplift represents deposition in predominantly lacustrine and

fluvial environments within a proglacial, and thus cold-wet setting. Furthermore, the Cutler Formation coincides with the southwestern mouth of modern Unaweep Canyon, hypothesized to be a largely exhumed Late Paleozoic glacially carved canyon formed coeval with the Cutler Formation (Soreghan et al., 2007, 2008b, 2009c). Soreghan et al. (2009a) also addressed the relative mineralogical and chemical immaturity of the Cutler Formation strata, suggesting that this immaturity, recorded to some degree in the relatively low chemical index of alteration (CIA) values, combined with facies evidence for a water-rich depositional system, is consistent with a possible cold-climate/proglacial origin.

The age of the Cutler Formation adjacent to the Uncompahgre uplift is poorly constrained in detail owing to the lack of datable material in the unit (Fig. 3.2). Correlations to formations in the more distal Paradox basin form the basis for the generalized Pennsylvanian-Permian age assigned to the proximal Cutler Formation (Mallory, 1972; Rascoe and Baars, 1972). Condon (1997) proposed that the base of the proximal Cutler Formation correlates to Upper Pennsylvanian (Gzhelian) carbonate strata in the Paradox basin, but Franczyk et al. (1995) suggested that the base of the Cutler Formation may be as old as Middle Pennsylvanian (Moscovian) on the basis of stratigraphic relationships 200 km to the southeast of the study region. The youngest Cutler strata inter-finger with lowest Permian marine carbonate strata in the Paradox basin (Bailey and Baars, 1972). The very gentle regional southwesterly dip (~4^{o}) of the most proximal Cutler Formation where it onlaps

Precambrian basement of the Uncompahgre uplift results in the exposure of progressively younger strata distally (Moore et al., 2008; Fig. 3.3). Furthermore, all of the Cutler strata exposed at the surface here record the youngest Cutler deposition in this region. An unknown thickness of older Cutler strata occur in the subsurface (e.g. Moore et al., 2008). Hence, the Cutler Formation exposed in study region could be entirely of early Permian age.

Soreghan et al. (2009a) recognized five major facies associations within ~10 km of the Cutler-Precambrian onlap (Fig. 3.3). Facies exposed within ~3 km of the Precambrian contact consist largely of debris flow and high-density turbidite facies interpreted to reflect subaqueous deposition in a lacustrine setting. Strata exposed more distally are interpreted to represent hyperconcentrated flood flow (HFF) deposits and upper-flow-regime fluvial deposition. The well-sorted siltstone facies in this more distal locality is volumetrically minor in the study area, but likely reflects an eolian origin (Soreghan et al., 2009a). The relationship between the lacustrine and fluvial facies in the proximal Cutler Formation remains unclear due to the limited and time-transgressive nature of the exposure. Because only the youngest strata in the proximal Cutler Formation crop out, it remains speculative whether lacustrine and fluvial environments coexisted, or if early lacustrine deposition yielded to later fluvial conditions with an indeterminate time gap between these systems (Soreghan et al., 2009a).

METHODS

A total of 15 samples, representing ~450 quartz grains (~30 quartz grains/sample) were analyzed from the proximal lacustrine, medial lacustrine and fluvial facies associations of Soreghan et al. (2009a) to ensure stratigraphic coverage of the Cutler Formation within 10 km of its onlap contact with Precambrian basement, and to determine if microtextural differences exist among these inferred facies associations (Fig. 3.3, 3.4). As with most units of this age, diagenetic alteration occurs locally, making it difficult to disaggregate samples without inducing new fractures. However, samples proximal to the uplift are remarkably friable and very weakly cemented with only minimal Fe-oxides and authigenic clays. More distally, samples contain only minor amounts of calcite cement as well as Fe-oxides and authigenic clays.

To eliminate iron-oxide cements, and induce disaggregation, samples were treated with the citrate-bicarbonate-dithionite (CBD) method to remove Fe oxides (Mehra and Jackson, 1960), and with sodium hexametaphosphate (dispersant) to facilitate further disaggregation. Samples were then treated with 1N HCl at 50^{o}C for 12 hours to remove any calcite cement coatings and to further encourage disaggregation. Samples with excessive coatings were treated with boiling HCl for 20 minutes. These HCl treatments do not affect quartz surface microtextures, as demonstrated in a before-and-after test of HCl pretreatment on artificially fractured quartz. The disaggregated samples were wet sieved, and the medium- to coarse-sand fractions (1.0 – 0.25 mm)

used for SEM analysis (following Mahaney, 2002). To prevent the introduction of laboratory-induced microtextures, samples were not sonicated. Use of a binocular microscope enabled identification and random selection of 20-40 quartz grains per sample for analysis (Mahaney et al., 1988).

Samples were mounted on aluminum SEM stubs and sputter coated with gold-palladium to prevent charging. A Zeiss 960 SEM set to 20 kV accelerating potential and a FEI Quanta 200 Environmental SEM were used for the analysis. Energy dispersive spectrum (EDS) analysis enabled verification of the mineralogy of each analyzed grain.

Each grain was inspected for the presence or absence of microtextures. Identification and classification of microtextures follows that outlined by Mahaney (2002; Table 3.1). Once a microtexture was documented, no attempt was made to quantify the abundance of that particular microtexture on a single grain. This approach aids objectivity, as no viable means exists to view the entire surface of a grain.The SEM enables viewing of only the top surface of a grain, and some surfaces remain obscured by diagenetic coatings. Grains exhibiting a diagenetic overprint sufficient to obscure any underlying texture precluded examination of primary (mechanical) microtextures and were thus excluded from analysis. Percent occurrences of each microtexture relative to the total number of grains in a sample were assessed after all grains were inspected. Samples were grouped based on the interpreted facies associations (Soreghan et al., 2009a) as 1) proximal lacustine, 2) medial lacustrine, and 3) fluvial, as well as

by two major depositional processes: debris flows and (combined) turbidity flows/hyperconcentrated flood flows. Histograms of microtextural frequency were used for initial examination of the raw data.

To further analyze the data, we sorted the microtextures into one of three groups designated as “high-stress,” “percussion,” or “polygenetic” (Sweet and Soreghan, 2010), based on inferred fracturing processes as reported in the literature (Campbell and Thompson, 1991: Mahaney and Kalm 2000; Mahaney, 2002). Curved grooves, straight grooves, deep troughs, and mechanically upturned plates are considered fractures produced by high-stress such as that expected to result from glacial grinding and crushing. V-shaped cracks and edge rounding are considered percussion fractures, produced largely during intergranular collisions during, e.g., saltation transport. Polygenetic fractures consist of fracture faces, subparallel linear fractures, conchoidal fractures, arc-shaped steps, linear steps, and breakage blocks, distinctive of neither high-stress nor percussion processes. This subdivision enables graphical analysis of the data using ternary plots in a semi-quantitative manner, following Sweet and Soreghan (2010).

To analyze the data quantitatively, we employed multidimensional scaling (nMDS), a non-parametric multivariate ordination technique (Kruskal and Wish 1978). The presence/absence data for all of the grains from a particular sample were averaged to obtain a score for each variable (i.e., microtexture; Table 3.1) for all samples. These continuous quantitative

variables, i.e., proportions of grains that display specific microtextural characteristics in each sample) were utilized for the nMDS technique. nMDS was performed using PAST 2.17b (Hammer et al., 2001) to determine if the samples grouped based on the previous facies associations delineated independently by Soreghan et al. (2009a), and also whether all samples, regardless of facies association, record glacial processes. The process of nMDS is iterative, and ultimately produces data configurations from a matrix of similarity or dissimilarity indices. The Euclidean similarity metric is the most common and was used in this study. The goal of the ordination is to approximate the original distances between points in a coordinate system of a few dimensions (axes). Using 18 dimensions (representing 18 microtextures in this case), is too many, so the data are simplified mathematically into 2 dimensions. A stress value is calculated for each iteration by comparing the ranked distances between the nMDS scores from the ordination and the original data. Lower stress values (~0.2 or less) equate to a closer agreement between the ordination and the original data (Hammer et al., 2001; Huntley, 2011). The stress value associated with the nMDS plots of facies associations and depositional processes reported by PAST for this study is 0.154, indicating a good agreement between the original data and the ordination. The ordination reduced the original multivariate data into a manageable number of variables without losing the real variation within the original data. Correlation coefficients were calculated between each variable and the nMDS scores. These are presented as vectors from the origin

(Hammer et al., 2001). By doing this, it was possible to interpret the relationship between the variables and the nMDS plot.

BURIAL HISTORY OF THE CUTLER FORMATION

The proximal Cutler Formation near Gateway, Colorado is a first-cycle arkosic sediment sourced directly from the crystalline (igneous-metamorphic) Precambrian basement of the adjacent Uncompahgre Plateau (former Uncompahgre Uplift of Pennsylvanian-Permian age). At its proximal-most contact, the Cutler Formation onlaps the Precambrian basement, burying several hundred meters of paleorelief (Moore et al., 2008; Soreghan et al., 2012). The burial depth for the Cutler Formation in this region approximates a maximum of ~1800 m, based on the maximum preserved overburden of ~600 m (from maps of Cater, 1955 and Eccles et al., 2013) and estimated maximum Cretaceous overburden of ~1200 m (McGookey et al., 1972). Additionally, Dutta and Suttner (1986) documented authigenic kaolinite, chlorite, smectite, iron-oxides, carbonate minerals and minor quartz within the Cutler Formation here, but no illite, consistent with a burial depth of less than ~2 km. Quartz cements are scarce in the Cutler Formation and were not found on any of the samples in this study. SEM analysis on the study samples indicate diagenetic products that include authigenic clays, iron-oxide cements, and localized carbonate cements. However, many diagenetic coatings are sufficiently thin that primary depositional microtextures remain visible beneath the coatings on most grains. Indeed, such coatings atop

textures provides assurance of the (Permian) antiquity of the microtextures and excludes the possibility of laboratory-induced microtextures.

RESULTS

Table 3.1 lists the 18 microtextural features recognized, and Figure 3.5 shows the raw-data histograms for microtextural occurrences within the proximal lacustrine, medial lacustrine, and fluvial facies associations. Precipitation features occur on nearly all samples in the study; thus this feature is not included in the statistical analyses. Visually, large differences in frequencies are apparent for some of the microtextural characteristics illustrated in the raw-data histograms, but it is difficult to assess patterns given the abundance of variables (Fig. 3.5). Quartz microtextures common to all facies are conchoidal fractures (45-61%) and subparallel linear fractures (41-52%). Microtextures that occur less commonly, but are similarly present in all facies are v-shaped cracks (15-19%) and mechanically upturned plates (16-21%). Other microtextures appear to be more distinctive of particular facies, as explained below.

Facies Trends

The proximal lacustrine facies of the Cutler Formation onlaps Precambrian crystalline basement of the modern Uncompahgre Plateau and thus is the most proximal facies exposed today (Soreghan et al., 2009a). Samples chosen from this facies association consist of internally massive (i.e.

unstructured) granule conglomerate and massive matrix-supported boulder- to cobble diamictite, interpreted as subaqueous mass-flow deposits (Soreghan et al., 2009a). Examination of the raw SEM microtextural data (Fig. 3.5, 3.6, 3.7, 3.8) indicates that occurrences of arc-shaped steps, linear steps, deep troughs, and curved grooves (19%-26%) within the proximal facies association are nearly double those of the medial lacustrine or fluvial associations (5%-9%). Additionally, fracture faces (ff, 30%) and abrasion features (af, 13%) are more common in this facies association than in either the medial lacustrine (ff 8% ab 2%) or fluvial associations (ff 6% ab 2%).

The medial lacustrine facies crops out within 1-3 km of the onlap contact with Precambrian basement (Soreghan et al., 2009a). Samples chosen from this facies association consist of crudely stratified, trough cross-stratified, and graded granule conglomerate, interpreted as the deposits of subaqueous mass-flow origin and traction flow in a lacustrine Gilbert-type delta. Examination of the raw SEM microtextural data (Fig. 3.5, 3.9) indicates that sharp angular features (32%) and straight grooves (27%) are more common in this facies than in either the proximal lacustrine or fluvial facies associations (saf 11%-16% and sg 16-20%, respectively).

The fluvial facies association crops out at a distance of 3-10 km from the Precambrian basement contact and consists of horizontal and (subordinate) trough cross-stratified granule conglomerate and minor very coarse-grained sandstone, interpreted as the products of hyperconcentrated flood flows and traction flow in a fluvial system (Soreghan et al., 2009a).

Examination of the raw SEM microtextural data from this facies association (Figs. 3.5, 3.9) indicates that edge rounding (39%) is most common in this facies than in either lacustrine facies (9% - 22%).

Depositional Process Trends

Grouping samples on the basis of inferred depositional processes, i.e., 1) debris flows, and 2) turbidity-, and hyperconcentrated-flood flows shows trends similar to the facies association groupings outlined above (Fig. 3.5). Both groups exhibit similar abundances (~50%) of subparallel linear fractures, and conchoidal fractures. Similar to both groups, but not as common (~18%) are arc-shaped steps, straight grooves, mechanically upturned plates, and v-shaped cracks. However, fracture faces, linear steps, breakage blocks, crescentic gouges, curved grooves, deep troughs, abrasion features and dissolution etching are more common (10-27%) on grains in the debris flow facies relative to grains in the turbidity flow/hyperconcentrated flood flow facies, relative to their occurrences (2-8%) in the other facies. However, edge rounding and adhering particles (36% - 37%) are nearly three times as common in the turbidite samples relative to samples from the debris flow facies (8%).

Semi-Quantitative Analysis: Textural Groupings

To enable initial graphical analysis of the data, we grouped the textures using the “high-stress,” “percussion,” and “polygenetic” groupings

reflecting inferred fracture genesis, following Sweet and Soreghan (2010). Figure 3.9 illustrates the resultant ternary diagram with fracture types on the 3 apices. Using this approach, high-stress fractures are more common in the proximal facies, whereas percussion fractures are more common in the distal facies.

Quantitative Analysis: nMDS Plot

Figure 3.10 shows the vector for each variable (correlation coefficient between each variable and the nMDS scores) affecting the sample locations on the nMDS plot to illustrate how each microtexture affected the sample position in 2D space. Results for the nMDS of the facies associations indicate that textures from proximal lacustrine samples form a statistically distinct region, defined by those samples with the greatest incidences of fracture faces, abrasion features, mechanically upturned plates, sharp angular features, conchoidal fractures, and subparallel linear fractures. The medial lacustrine and fluvial samples plot in a space affected primarily by edge rounding and adhering particles (Fig. 3.11). Results for the nMDS of the depositional processes also reveal distinct groupings (Fig. 3.12), with samples from debris flow deposits plotting in a separate space than samples from the turbidites and hyperconcentrated flood flows.

DISCUSSION

Microtextural frequency data has historically been displayed in raw histograms to infer relationships between sample groups (Fig. 3.5 ; e.g., Campbell and Thompson 1991; Mahaney 2002; Mahaney and Kalm 2000). However, it is difficult to evaluate significant differences between samples visually, as there are so many microtexture types depicted on these histograms. For the Pennsylvanian-Permian Fountain Formation, a unit of similar age and diagenetic history as the Cutler Formation, Sweet and Soreghan (2010) sorted microtextures into one of three groups (detailed above). They then plotted the data using a ternary plot of fracture types, and used this approach to demonstrate that the majority of the Fountain Formation samples plotted between data published from Quaternary glacial sediments, characterized by abundant high-stress fractures, and those from Devonian fluvial sandstone characterized by percussion fractures. This result reinforced their hypothesis of a glacial/proglacial influence on the Fountain Formation strata.

Microtextural analysis is plagued by the issue of equifinality, wherein different processes operating in various environments can ultimately produce the same texture(s) (e.g. Brown, 1973). However, more recent research has documented that certain microtextures are distinctive of high-stress fracturing imparted by glacial grinding. Curved grooves, straight grooves, and deep troughs are documented more commonly on glacially derived grains than any other microtexture (D'Orsay and van de Poll, 1985; Mahaney, 1995; Mahaney

and Kalm, 2000; Mahaney, 2002; Van Hoesen and Orndorff, 2004; Curry et al., 2009; Strand and Immonen, 2010; Sweet and Soreghan, 2010; Deane, 2010; Kirschner and Anderson, 2011; Immonen, 2013). Mechanically upturned plates, crescentic gouges, and arc-shaped steps are also cited as evidence of high-stress fracturing (D'Orsay and van de Poll, 1985; Mahaney, 1995; Mahaney and Kalm, 2000; Mahaney, 2002; Sweet and Soreghan, 2010; Kirshner and Anderson, 2011; Deane 2010; Immonen, 2013).

For example, Van Hoesen and Orndorff (2004) employed microtextural analysis of known glacial and nonglacial clasts of varying age and lithology to document an abundance of high-stress fractures (curved grooves, straight grooves, and deep troughs) on clasts formed in glacial settings, and a combination of percussion- and high-stress fractures in clasts derived from a proglacial setting. Krishner and Anderson (2011) similarly documented an abundance of high-stress textures (curved grooves, straight grooves, deep troughs, and mechanically upturned plates) on quartz grains from Pliocene sediments of the northern Antarctic Peninsula to infer a transition to more extreme glacial conditions at that time. Similarly, Immonen (2013) used the abundance of high-stress microtextures (arc-shaped steps, curved grooves, crescentic gouges, and deep troughs) on ice-rafted quartz grains in Paleocene marine strata from the Arctic Ocean to infer ephemeral polar glaciations during times of previously documented global warmth. Additionally, Deane (2010) compared microtextures (arc-shaped steps, curved grooves, straight grooves) on quartz grains from known glacial

deposits to quartz grains from deposits of suspected glacial origin. The results showed both data sets were statistically indistinguishable using microtextural analysis, leading Deane (2010) to infer a glacial origin for both.

On the basis of this growing body of literature, together with the presence of prevalent high-stress microtextures (curved grooves, straight grooves, deep troughs, and mechanically upturned plates) documented in our samples, we infer a glacial-proglacial origin for the proximal Cutler Formation. The nMDS analysis confirms quantitatively that high-stress fractures are more significant in the proximal lacustrine samples inferred to record proglacial lacustrine deposition. In contrast, percussion fractures are more common in the distal samples, inferred to record fluvial deposition (Fig. 3.12). The medial lacustrine and fluvial samples are primarily from turbidites and hyperconcentrated flood flow deposits, respectively and we infer that the percussion fractures have partially overprinted some of the high-stress fractures in the medial and distal facies, with the occurrence of percussion fractures increasing with transport distance. The persistence of glacial microtextures in the study area is consistent with the relatively short transport distance (<10 km). Mahaney and Kalm (1996, 2000), documented similar results in their study of known glaciofluvial quartz grains from the Venezuelan Andes, Estonia, and Latvia. V-shape cracks and edge-rounding were found to overprint glacially-induced microtextures with transport distances from 1 km up to 100 km.

Previous environmental interpretations for the Cutler Formation posited deposition in either a hot-arid alluvial fan system (e.g., Werner,1970; Mack and Rasmussen,1984; Schultz, 1985; Suttner and Dutta, 1986; Dubiel et al., 1996, 2009) or a hot-humid alluvial fan environment (Campbell, 1979, 1980). Unfortunately, no comprehensive and systematic treatments of quartz microtextures from these modern depositional settings and climates exist with which to make actualistic comparison with the Cutler Formation microtextural results. However, Table 3.2 lists microtextures common in these environments, as compiled from various previous studies, and provides some basis for comparison with the Cutler Formation data.

The Table 3.2 data compilation reveals useful trends. If deposition occurred in a hot-arid fan, depositional processes should include mass flows proximally and traction stream flow distally, produced through infrequent storm events (Mather and Hartley, 2005). Expected microtextures might thus include an abundance of fracture faces common in mass-wasted deposits, and v-shaped percussion fractures reflecting common saltation transport in traction stream flow (Table 3.2; Mahaney, 2002). Additionally, the common occurrence of eolian activity in (especially distal parts of) hot-arid fan systems (e.g. Blair and McPherson, 1992), should produce edge rounding, specifically bulbous edges and abrasion features (Alireza et al., 2009; Mahaney, 2002; Hodel et al., 1988), and grain pitting common to frosted, eolian-transported sand (Mahaney, 2002). Studies of these types of systems show an abundance of eolian grains throughout the system and significant abrasion

microtextures even if very little transport occurred (Hodel et al., 1988; Costa et al., 2013). However, quartz sand from the Cutler Formation of the study region lack features indicative of eolian processes, and v-shaped percussion fractures and fracture faces are comparatively rare.

Quartz grains from a semi-arid climate would also be expected to have abundant dissolution etching (Wang et al., 1994). Quartz dissolution is accelerated during dry season weathering because evaporation drives increased cation concentrations of soluble components such as Na, K, Ca, and Mg in the pore fluids, leading to clay mineral precipitation. The resultant clay mineral precipitation removes silica from pore fluids and thus drives residual water toward silica undersaturation, increasing quartz dissolution rates (Dove and Nix, 1997; Wang et al., 1994). It is therefore the seasonal wetting and drying that drives the increased rates of quartz dissolution. (Dove and Crerar, 1990; Wang et al., 1994; Dove and Nix, 1997). Quartz surfaces in first-cycle fluvial sediments derived from granite weathering in a modern semi-arid region (Oklahoma) exhibit intense dissolution etching that obscures mechanical microtextures that may have been present (Keiser et al., 2013). In contrast, mechanically produced microtextures occur on the majority of the quartz grains studied in the Cutler Formation samples, and although dissolution etching textures occur, these textures do not obliterate underlying mechanical textures.

Although quartz is considered highly resistant to chemical weathering (White and Brantley, 1995), weathering rates increase in hot-humid climates

where conditions favor abundant vegetation (Dove and Crear, 1990; Berger et al., 1994). Studies of mineral dissolution in modern humid-tropical environments show intense breakdown of quartz grains with abundant solution pits and silica precipitation along the edges of these pits (Doornkamp, 1974). A humid climate would support abundant vegetation that would in turn lead to the formation of organic-rich fluids that increase quartz dissolution rates by up to a factor of 2.5 (e.g. Howard et al., 1995; Blake and Walter, 1999). These rates were observed during laboratory experiments on quartz in near-neutral organic acid solutions of oxalate and citrate (0.5 - 20mM) at 70^{o}C and are attributed to the effects of an increased ionic strength (I = 0.35) in pore fluids, which increases quartz dissolution rates (Dove and Crear, 1990; Berger et al., 1994). Intense chemical weathering of quartz would ultimately produce quartz grains lacking mechanical microtextures due to the intense dissolution of the original grain.

In summary, review of common quartz textures and weathering regimes documented in granitoid weathering systems in modern climates and associated (alluvial-fluvial) depositional environments show an association of microtextures common to each environment (Table 3.2). Quartz grains from hot humid alluvial fan environments generally exhibit dissolution features, clay precipitation, abundant v-shaped percussion cracks, edge rounding, and fracture faces. Extreme dissolution, v-shaped percussion cracks, abrasion features, bulbous edges, abundant edge rounding, and fracture faces are common on grains from hot arid to semi-arid desert fans. In contrast, cold

humid proglacial fans have quartz grains exhibiting some dissolution features and clay precipitation, but abundant evidence for mechanical weathering that includes curved grooves, straight grooves, mechanically upturned plates, deep troughs, v-shaped percussion cracks, edge rounding, and fracture faces. Based on this analysis, it is unlikely the quartz grains of the proximal Cutler Formation reflect deposition in a hot-humid, hot-arid, or semi-arid alluvial fan environment.

The results of the nMDS plots (Fig. 3.11, 3.12) reinforce the findings that the pattern of high-stress fractures are more abundant in the proximal lacustrine setting, as indicated initially by the histogram plots (Fig. 3.5) of the raw data, as well as the ternary plot (Fig. 3.9). Figure 3.9 shows that proximal samples plot closer to the high-stress apex of the ternary plot and distal fluvial samples plot closer to the percussion apex. Percussion fractures, more abundant distally, are expected to increase with transport distance *a priori*, owing to the longer duration of grain entrainment and consequent saltation in the fluvial system. Similar results from the qualitative, semi-quantitative, and quantitative microtextural data indicate that the samples group by facies. More fundamentally, quartz grains from all facies exhibit microtextures most indicative of the mechanical fracturing common in glacial environments, notably curved grooves, straight grooves, deep troughs, and mechanically upturned plates. This, together with the lack of intense dissolution features, is most consistent with the proglacial lacustrine interpretation for the proximal Cutler Formation proposed by Soreghan et al.(2009a).

CONCLUSIONS

The Cutler Formation proximal to the (paleo) Uncompahgre uplift has been variously interpreted as the result of alluvial fan-fluvial processes in a warm, non-glacial system, or lacustrine-fluvial processes in a cold proglacial system (Werner, 1970; Campbell (1979, 1980); Mack and Rasmussen, 1984; Shultz, 1984; Suttner and Dutta, 1986; Dubiel et al., 2009; Soreghan et al., 2009a). Analysis of microtextures on quartz grains from this unit indicates that microtextures distinctive of high-stress features such as curved grooves, straight grooves, deep troughs, and mechanically upturned plates predominate, and signs of chemical dissolution more typical of warm non-glacial systems are comparatively minor. Quantitative analyses of the results further indicate that high-stress features are especially common in the most proximal facies, with percussion-induced fractures such as v-shaped cracks more common distally. Previous work in modern and recent glacial and proglacial depositional systems indicates that high-stress fractures such as curved grooves, straight grooves, deep troughs, and mechanically upturned plates are particularly characteristic of the high-intensity physical weathering common in glacial systems. Accordingly, the common occurrence of these types of microtextures in the proximal Cutler Formation is consistent with the hypothesis of upland glaciation in the Uncompahgre highland during late Pennsylvanian and early Permian time (Soreghan et al., 2008a; Soreghan et al. 2008b; Soreghan et al., 2009a; Sweet and Soreghan, 2008; Sweet and Soreghan, 2010).

SEM microtextural analysis is a useful tool for the study of ancient depositional environments despite the abundance of precipitation features inherent to sediment in the “deep-time” sedimentary record. Furthermore, multiple approaches to data analysis that move beyond visual inspection of raw data histograms, to semi-quantitative classification of textures using ternary diagrams, as well as quantitative statistical techniques such as the non-parametric multivariate ordination technique, nMDS, provide quantitatively robust results that significantly augment the historically qualitative nature of quartz microtextural analysis.

ACKNOWLEDGEMENTS

Funding for this research was provided by the National Science Foundation (EAR-0746042 and ANT-0442639), the Petroleum Research Fund of the American Chemical Society (ACS-PRF 52114-ND8), the USGS EdMap program (G11AC20217 and G12AC20266), and the University of Oklahoma School of Geology and Geophysics. Any opinions, findings, and conclusions or recommendations expressed in this material are those of the author(s) and do not necessarily reflect the views of the funding agencies. We gratefully acknowledge technical support from various individuals at the University of Oklahoma, specifically G. Stowe, and J. Jernigan (Petroleum Engineering laboratory), P. Larson (Microbiology), and R. Terry (Psychology). We also thank J.W. Huntley and M. Kowalewski for guidance on statistical analyses.

Table 3.1: Microtextures used for SEM analysis of quartz grains. (Mahaney, 2002; Sweet and Soreghan, 2010)

Quartz Microtextures	
abrasion features (af)	edge rounding (er)
adhering particles (ap)	fracture faces (ff)
arc-shaped steps (as)	linear steps (ls)
breakage blocks (bb)	mech-upturned plates (mup)
conchoidal fractures (cf)	precipitation features (pf)
crescentic gouges (crg)	sharp angular features (saf)
curved grooves (cg)	straight grooves (sg)
deep troughs (dt)	subparallel linear fractures (sf)
dissolution etching (de)	v-shaped percussion cracks (vc)

Table 3.2: Quartz microtextures related to climate and depositional environment. SEM photos illustrate key microtextural features.

CLIMATE	HOT HUMID	HOT ARID / SEMI-ARID	COLD HUMID
DEPOSITIONAL ENVIRONMENT	WET FAN	DESERT FAN	PROGLACIAL FAN
QUARTZ MICROTEXTURES	Dissolution Clay Precipitation Angular grains V-shaped cracks Edge rounding Fracture faces	Extreme dissolution V-shaped cracks Abrasion features Bulbous edges Edge rounding Fracture faces	Minor dissolution Clay precipitation Curved grooves Straight grooves Mechanically up-plates Deep troughs V-shaped cracks Edge rounding Fracture faces
SEM PHOTOS	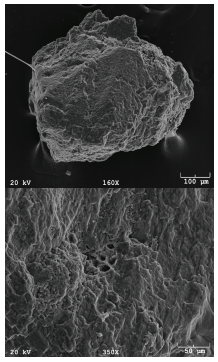	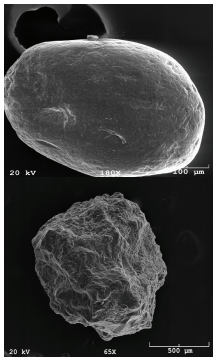	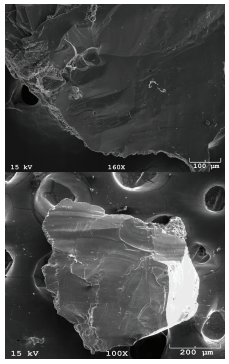
REFERENCES	Blake and Walter, 1999 Pye and Mazzullo, 1994 Scarciglia et al., 2005 Doornkamp, 1974 Little et al., 1978	Howard et al., 1995 Wang et al., 1994 Dove and Crerar, 1990 Cooke, 1979 Magee et al., 1988	D'Orsay and Van de Poll, 1985 Mahaney and Kalm, 2000 Mahaney, 2002 Sweet and Soreghan, 2010 Kirshner and Anderson, 2011 Deane, 2010 Immonen, 2013

Figure 3.1: Location map modified from Soreghan et al. 2009a showing the late Paleozoic Uncompahgre uplift considered part of the Ancestral Rocky Mountains. Study area is shown by the box. The cross section A-A' is shown in Fig. 3.3 and Fig. 3.4.

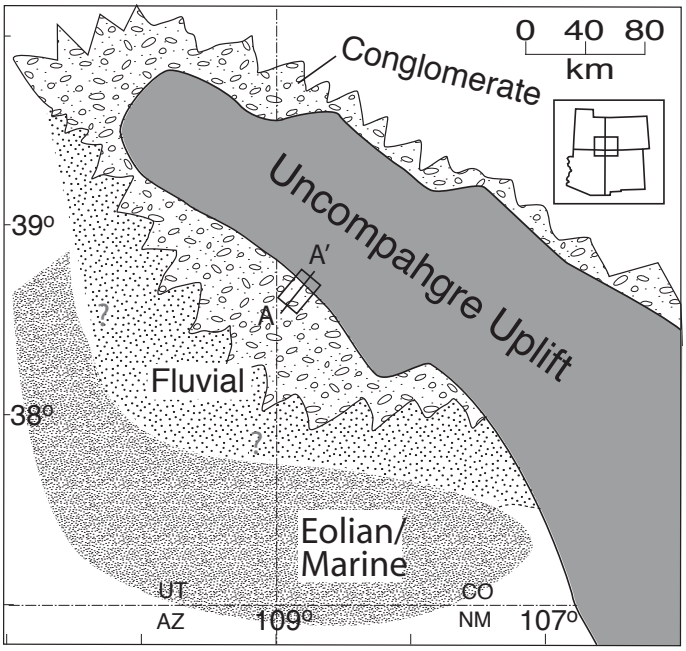
0 40 80
km
Conglomerate
Uncompahgre Uplift
39º
A'
A
?
Fluvial
38º
?
Eolian/
Marine
UT
AZ
CO
NM
109º
107º

Figure 3.2: Pennsylvanian-Early Permian stratigraphy of the Cutler Formation study region (near Gateway, Colorado), after Sweet and Soreghan 2010.

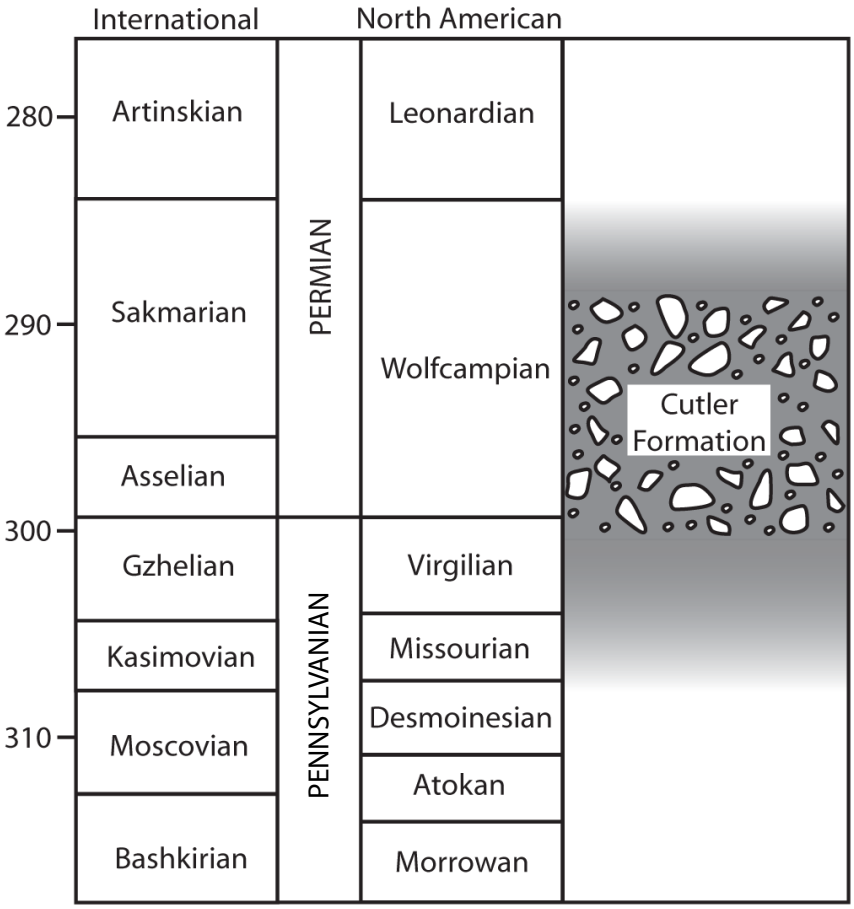
International
North American
280
290
300
310
Artinskian
Sakmarian
Asselian
Gzhelian
Kasimovian
Moscovian
Bashkirian
PERMIAN
PENNSYLVANIAN
Leonardian
Wolfcampian
Virgilian
Missourian
Desmoinesian
Atokan
Morrowan
Cutler
Formation

Figure 3.3: A) Line drawing of the relationship between the Uncompahgre Uplift, Unaweep Canyon, and the Cutler Formation near Gateway, CO. B) Detailed location map illustrating measured section locations (III through XII, shown in Fig. 3.4), sample locations (black dots, Fig. 3.4), and facies associations (of Soreghan et al., 2009a).

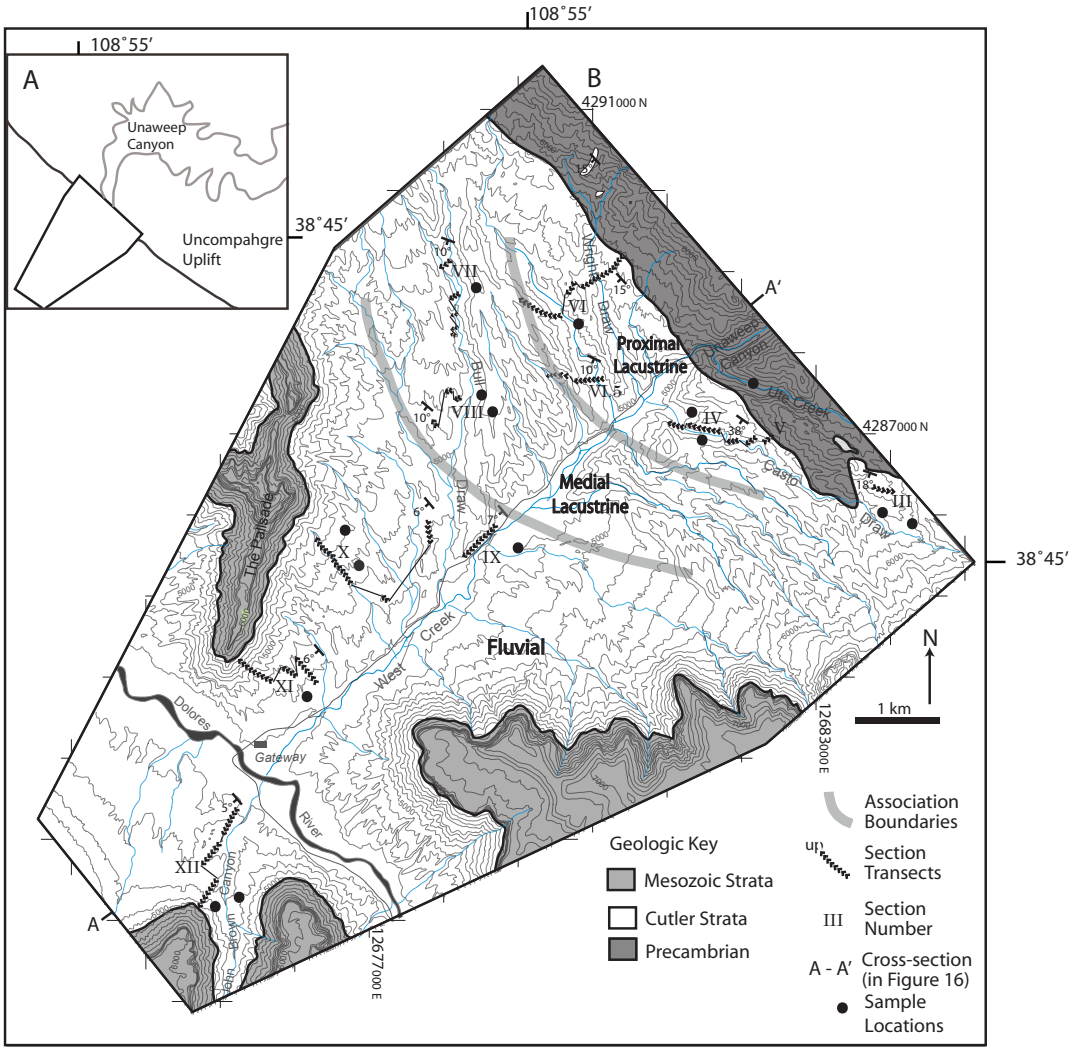
108°55′
108°55′
A
Unaweep
Canyon
Uncompahgre
Uplift
38°45′
B
4291000 N
A′
Proximal
Lacustrine
Medial
Lacustrine
Fluvial
Wright
Draw
Bull
Draw
Dario
Draw
Unaweep
Canyon
Little Creek
4287000 N
38°45′
The Palisade
West
Creek
Dolores
River
Gateway
Brown
Canyon
John
Canyon
12683000 E
12677000 E
N
1 km
Geologic Key
Mesozoic Strata
Cutler Strata
Precambrian
Association
Boundaries
Section
Transects
Section
Number
Cross-section
(in Figure 16)
Sample
Locations

Figure 3.4: Cross section (A-A' from Fig. 3.3B) of the study area with stratigraphic column locations and annotations of facies associations. Stratigraphic positions of samples collected for quartz microtextural analysis are shown with black squares. Db/Dc = Boulder to cobble diamictite, Gr = Conglomerate, S = Sandstone (map modified from Soreghan et al., 2009a).

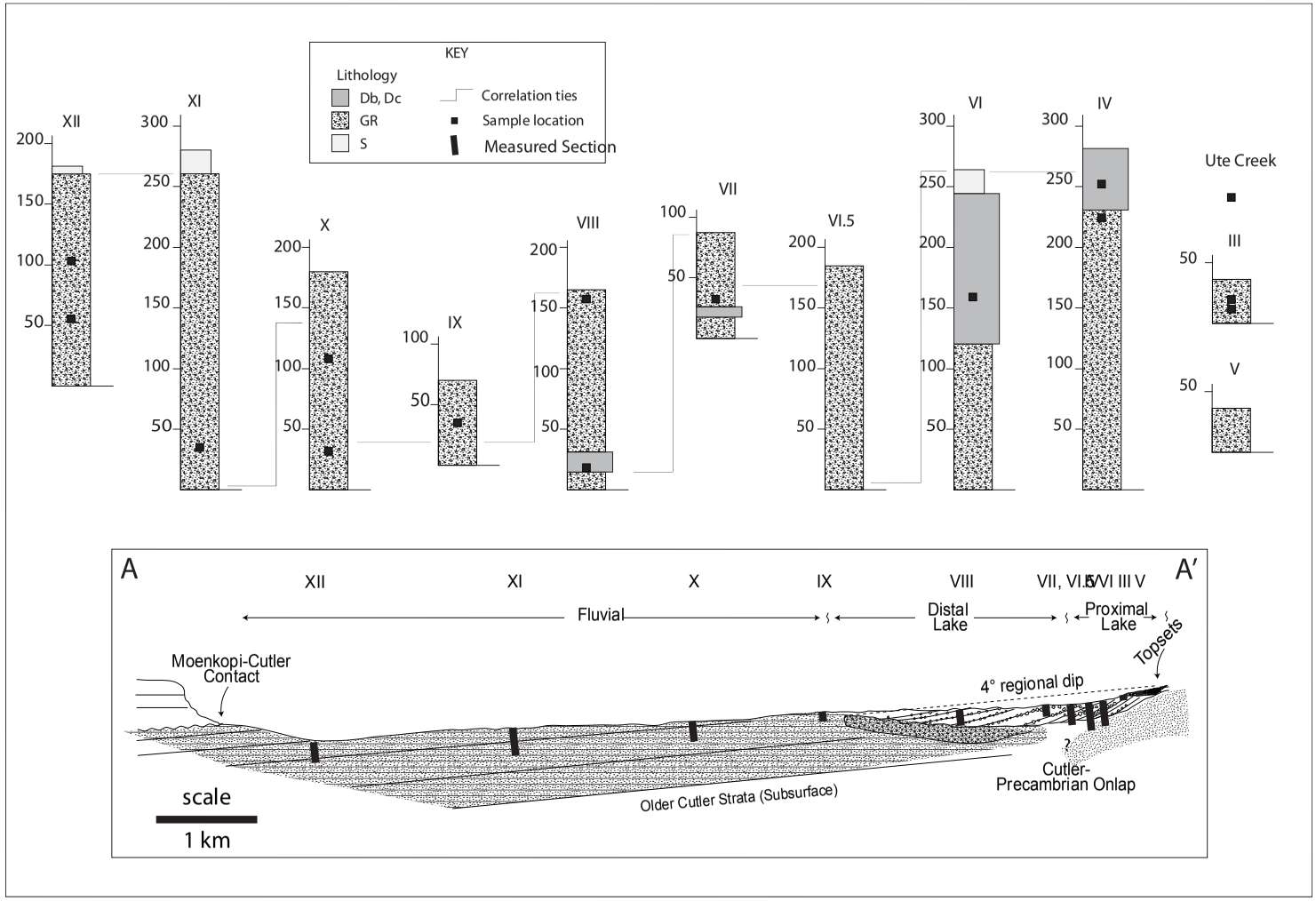
KEY
Lithology
Db, Dc
GR
S
Correlation ties
Sample location
Measured Section
XII
XI
X
IX
VIII
VII
VI.5
VI
IV
III
V
Ute Creek
A
A′
Fluvial
Distal Lake
Proximal Lake
Moenkopi-Cutler Contact
Toposets
4° regional dip
Older Cutler Strata (Subsurface)
Cutler-Precambrian Onlap
scale
1 km

Figure 3.5: Frequency histograms of SEM microtexture frequencies of quartz microtextures from the proximal lacustrine, medial lacustrine, and fluvial facies associations of the Cutler Formation as well as the turbidity flow/ hyperconcentrated flood flow and debris flow depositional processes. Frequency represents the total number of grains in each sample exhibiting each microtexture relative to the total grains in the sample.

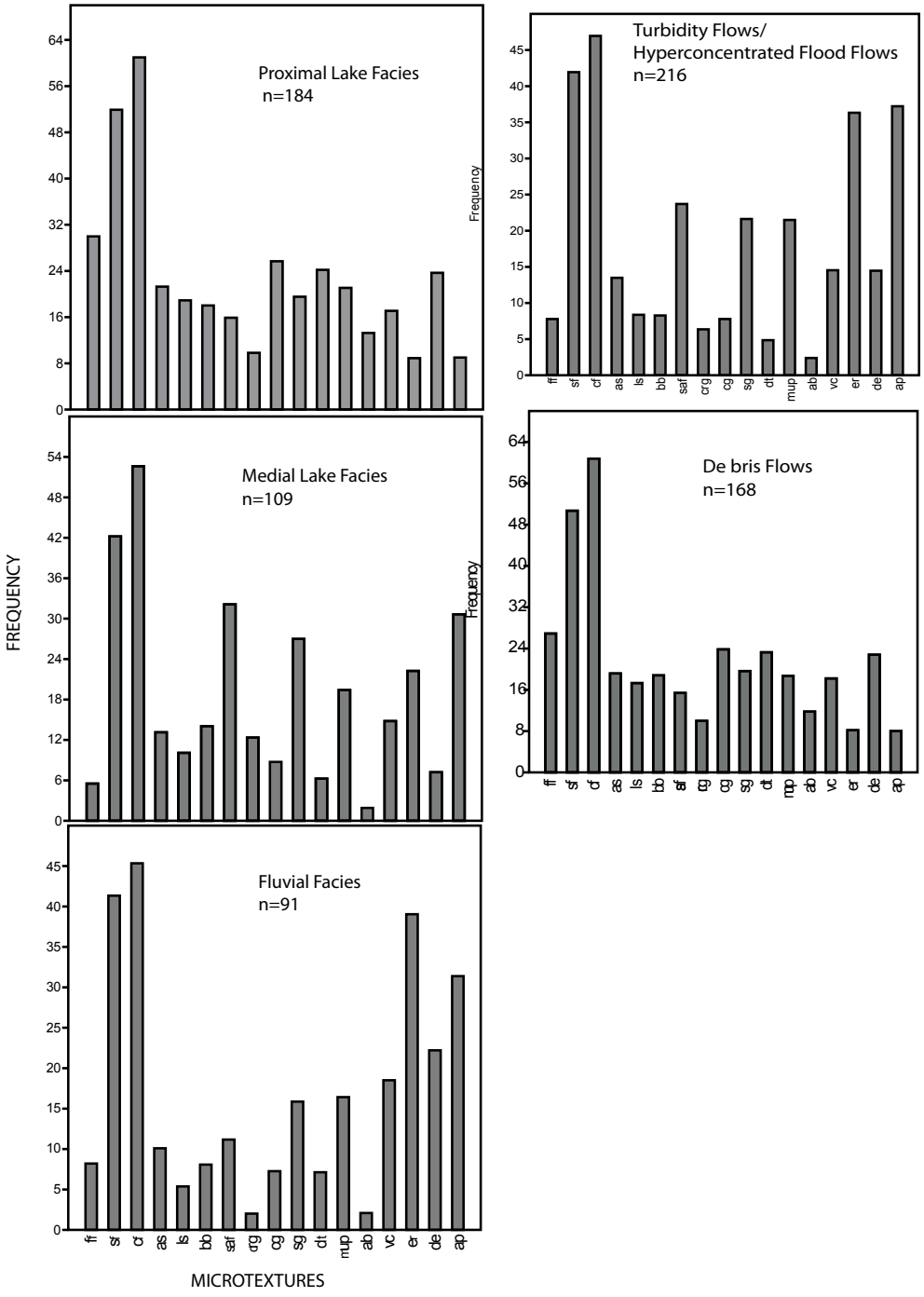
Proximal Lake Facies
n=184
Turbidity Flows/
Hyperconcentrated Flood Flows
n=216
Medial Lake Facies
n=109
De bris Flows
n=168
Fluvial Facies
n=91
FREQUENCY
Frequency
MICROTEXTURES
ff
sf
cf
as
ls
bb
saf
crg
cg
sg
dt
mup
ab
vc
er
de
ap

Figure 3.6: SEM images of selected quartz grains from the proximal lacustrine facies in the Cutler Formation. **A)** Angular quartz grain displays numerous high-stress fractures such as a straight groove (sg), crescentic gouge (crg), and mechanically upturned plate (mup). Subparallel linear fractures (sf), conchoidal fracture (cf), adhering particles (ap), and precipitation features (pf) are also present. **B)** Angular quartz grain displaying a deep trough (dt) and straight groove (sg) as well as subparallel linear fractures (sf), conchoidal fractures (cf), and precipitation features (pf). **C)** Quartz grain with abundant precipitation superimposed on a curved groove (cg), mechanically-upturned plate (mup), and deep troughs (dt).

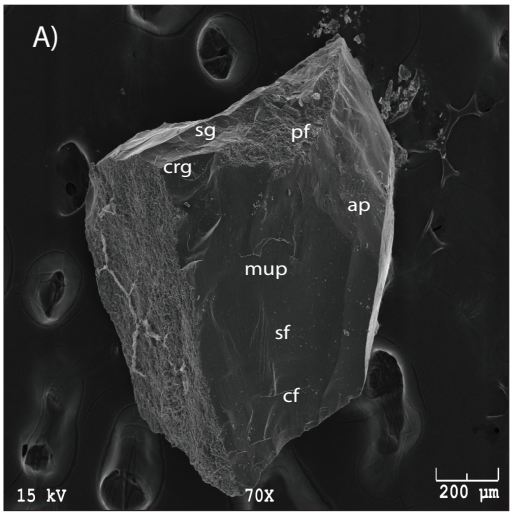
A)
sg
pf
crg
ap
mup
sf
cf
15 kV
70X
200 µm

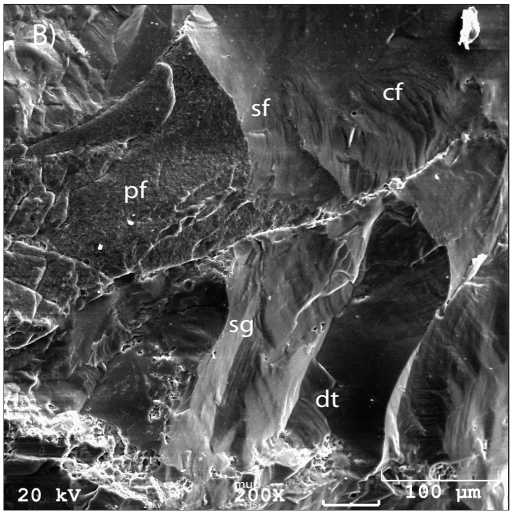
B)
sf
cf
pf
sg
dt
20 kV
200x
100 µm

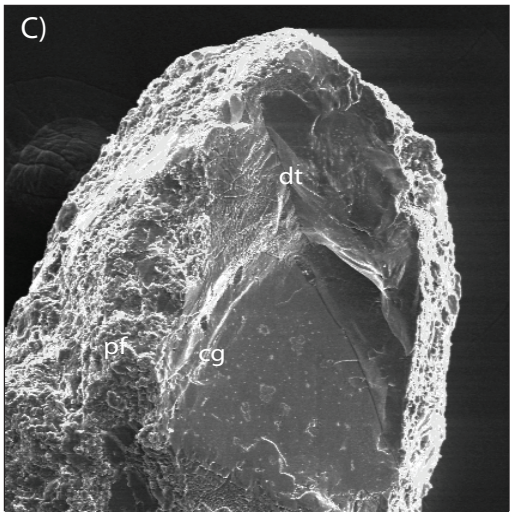
C)
dt
pf
cg

Figure 3.7: SEM images of selected quartz grains from the medial facies in the Cutler Formation. **A)** A straight groove (sg) is shown covered in precipitation features (pf) on a slightly rounded quartz grain. **B)** Mechanically-upturned plate (mup), adhering particles (ap), and linear steps (ls) are present on this quartz grain surface. **C)** A pronounced curved groove (cg) is displayed on this quartz grain as well as a crescentic gouge (crg), subparallel linear fractures (sf). Edge rounding (er) is present as well.

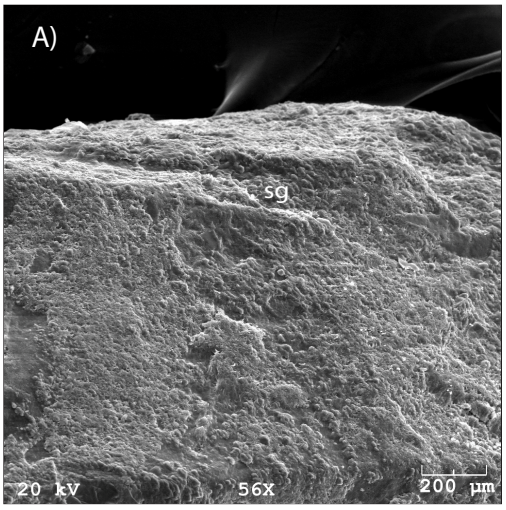
A)
sg
20 kV
56x
200 µm

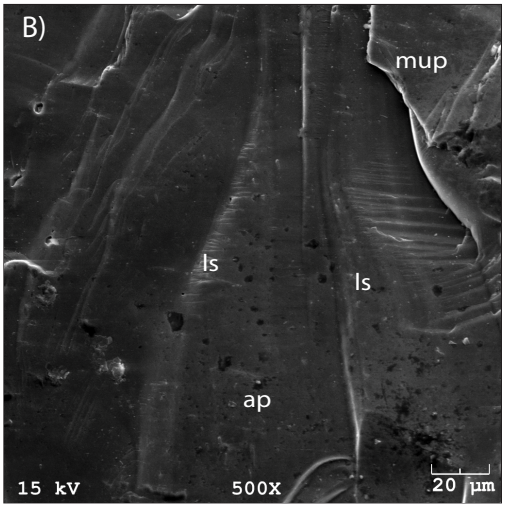
B)
mup
ls
ls
ap
15 kV
500x
20 µm

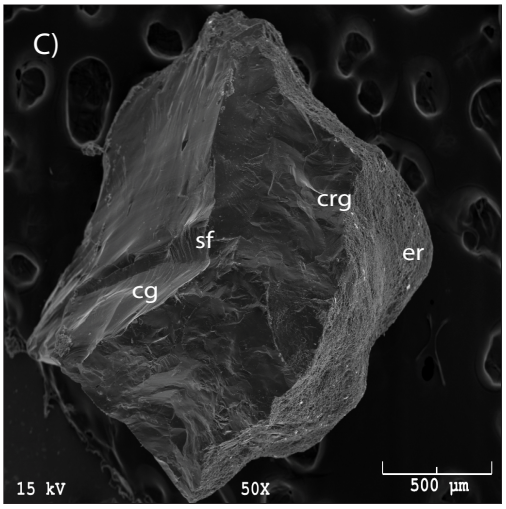
C)
crg
sf
er
cg
15 kV
50x
500 µm

Figure 3.8: SEM images of selected quartz grains from the fluvial facies in the Cutler Formation. **A)** This grain displays a straight groove (sg) and subparallel linear fractures (sf). **B)** This grain has been rounded but a deep trough (dt), straight groove (sg), and crescentic gouge (crg) can still be seen. **C)** Straight groove (sg), adhering particles (ap), dissolution etching (de), and conchoidal fracture (cf) are present.

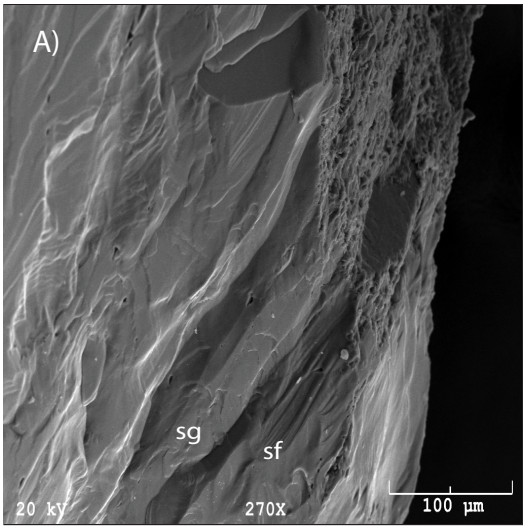
A)
sg
sf
20 kV
270x
100 µm

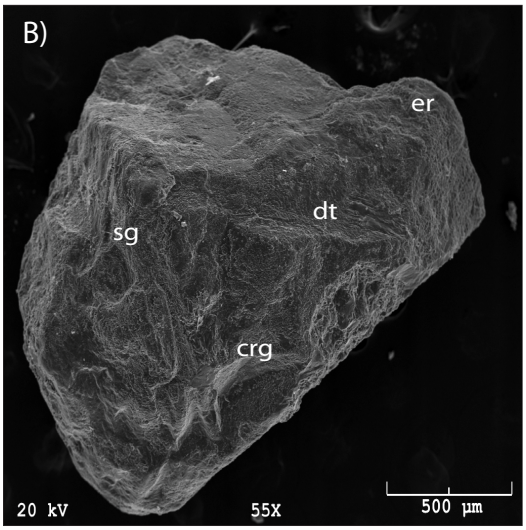
B)
er
dt
sg
crg
20 kV
55x
500 µm

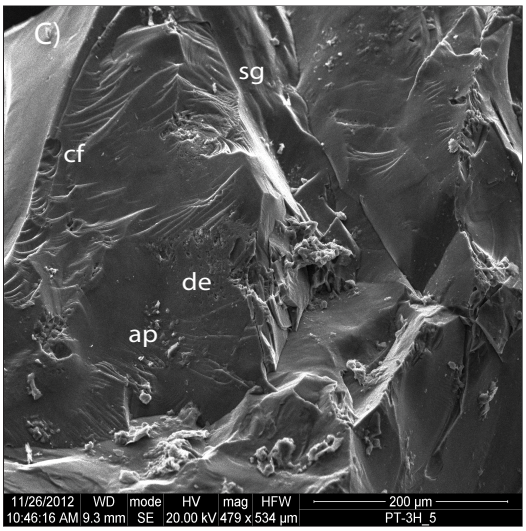
C)
sg
cf
de
ap
11/26/2012 WD mode HV mag HFW
10:46:16 AM 9.3 mm SE 20.00 kV 479 x 534 µm
200 µm
PT-3H_5

Figure 3.9: Relative abundances of polygenetic, high-stress and percussion fractures (following definition of Sweet and Soreghan, 2010) on quartz grains from the proximal lacustrine, medial lacustrine, and fluvial facies associations of the Cutler Formation. High-stress fractures are considered to be straight and curved grooves, deep troughs, and mechanically upturned plates. V-shaped cracks, edge rounding, and dissolution etching are considered to be percussion fractures. Polygenetic fractures are fracture faces, subparallel linear fractures, conchoidal fracture, arc-shaped steps, linear steps, and breakage blocks. High-stress fractures are more abundant in the proximal lacustrine facies whereas percussion fractures are more abundant in the fluvial facies.

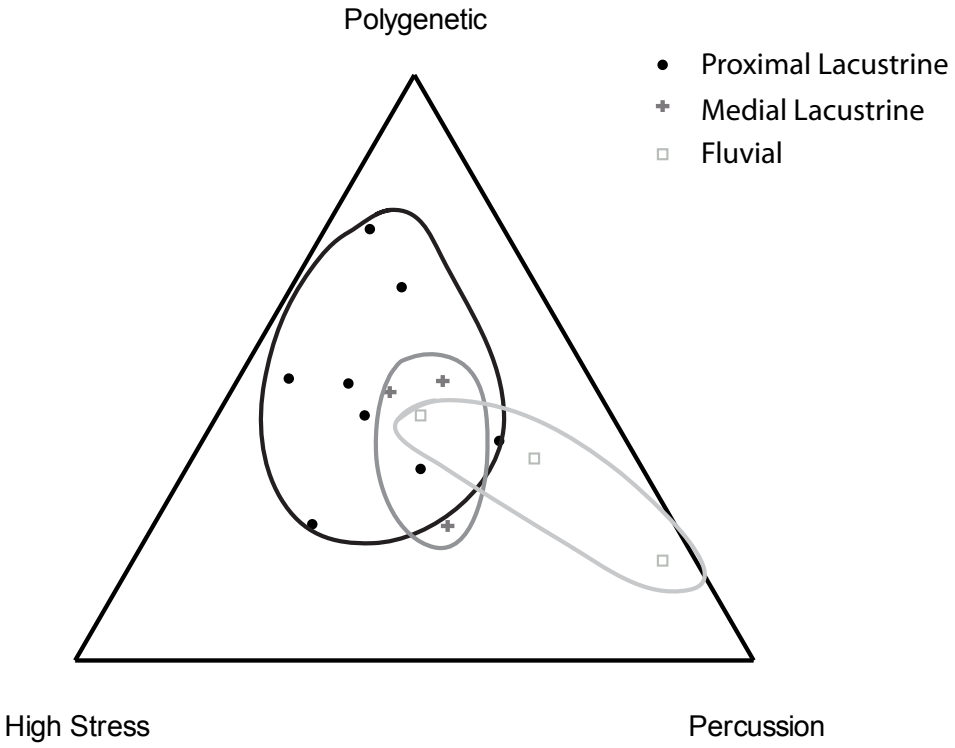
Polygenetic
Proximal Lacustrine
Medial Lacustrine
Fluvial
High Stress
Percussion

Figure 3.10: Plot of nMDS loading relating microtextures to dimension 1 and 2 (18 microtextural variable were reduced to 2 dimensions using nMDS). Correlation coefficients were calculated between each variable (microtexture) and the nMDS scores. They are presented as vectors from the origin. See Table 3.1 for an explanation of the abbreviations. The length and direction of each vector relative to the other vectors determines how the microtextures relate to dimensions 1 and 2 of the nMDS plots.

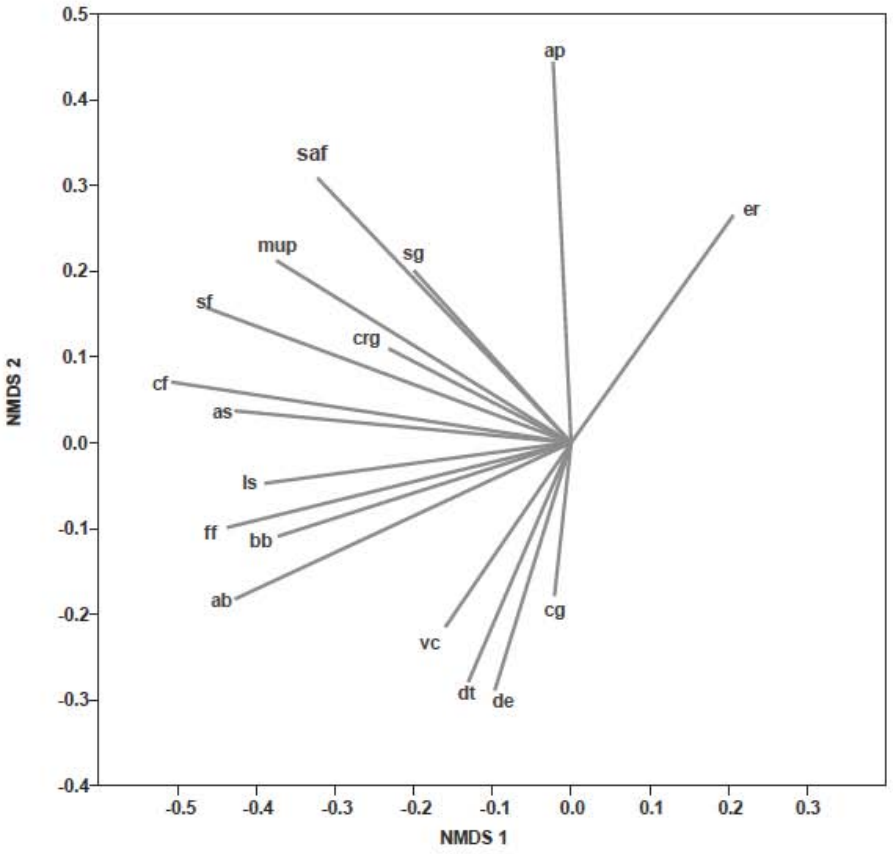
0.5
0.4
0.3
0.2
0.1
0.0
-0.1
-0.2
-0.3
-0.4
NMDS 2
-0.5
-0.4
-0.3
-0.2
-0.1
0.0
0.1
0.2
0.3
NMDS 1
ap
saf
er
mup
sg
sf
crg
cf
as
ls
ff
bb
ab
cg
vc
dt
de

Figure 3.11: nMDS plot for quartz grain microtextures from the Cutler Formation facies associations: grain textures from the proximal lacustrine, medial lacustrine, and fluvial. The proximal lacustrine plots in a space distinctive from those of the other two facies associations.

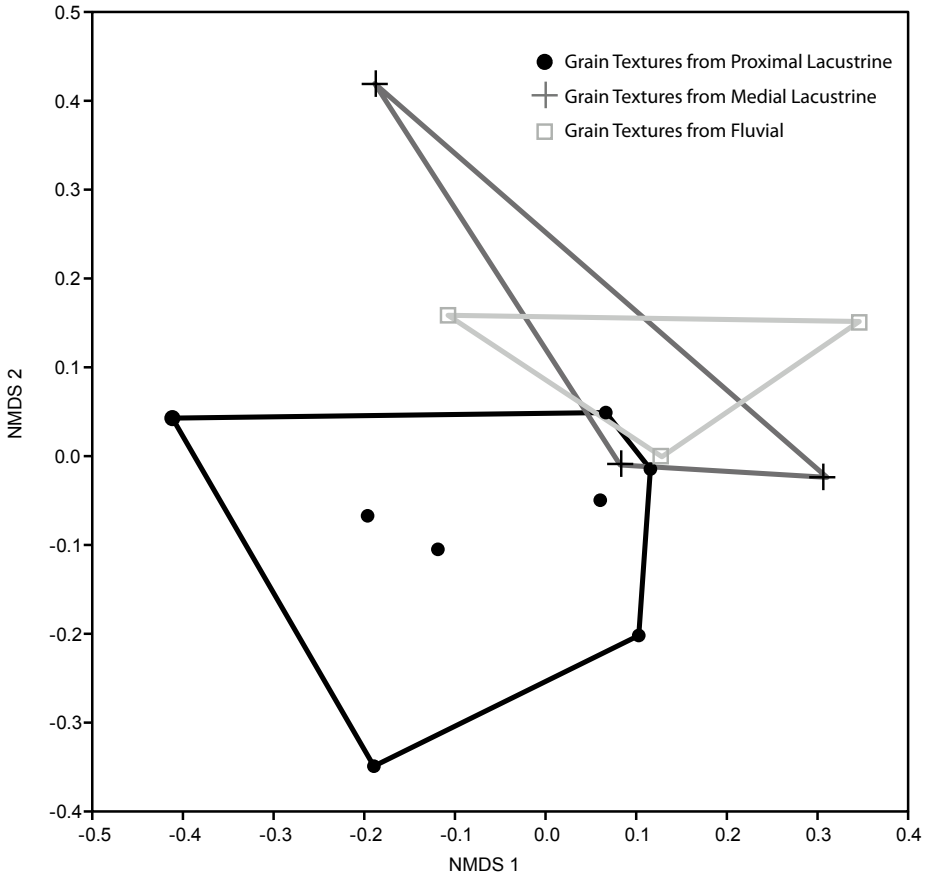
Grain Textures from Proximal Lacustrine
Grain Textures from Medial Lacustrine
Grain Textures from Fluvial
NMDS 2
NMDS 1
0.5
0.4
0.3
0.2
0.1
0.0
-0.1
-0.2
-0.3
-0.4
-0.5
-0.4
-0.3
-0.2
-0.1
0.0
0.1
0.2
0.3
0.4

Figure 3.12: nMDS plot for quartz grain microtextures from the Cutler Formation by depositional processes: debris flows and turbidity flows/ hyperconcentrated flood flows. Grain textures from debris flows plot in a separate space from the turbidity flows/hyperconcentrated flood flows.

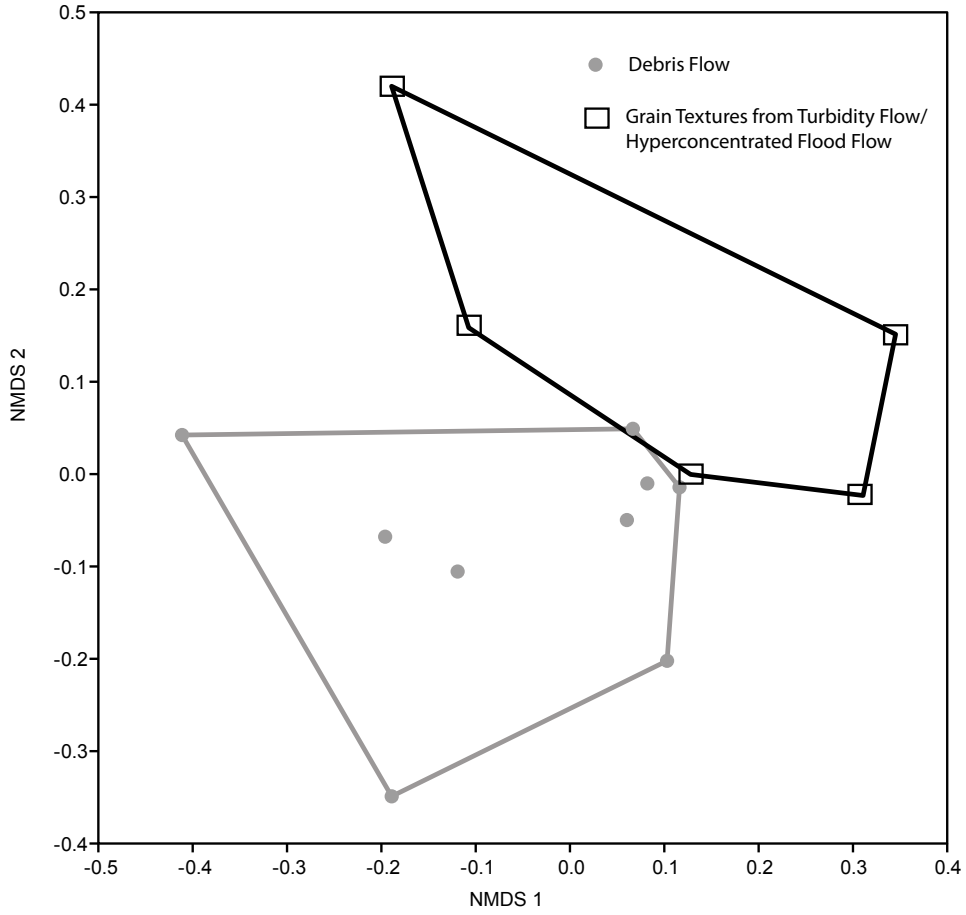
Debris Flow
Grain Textures from Turbidity Flow/
Hyperconcentrated Flood Flow
NMDS 2
NMDS 1
0.5
0.4
0.3
0.2
0.1
0.0
-0.1
-0.2
-0.3
-0.4
-0.5
-0.4
-0.3
-0.2
-0.1
0.0
0.1
0.2
0.3
0.4

REFERENCES

BAILEY, R. JR and BAARS, D.L., 1972, Permian System: Rocky Mountain Association of Geologists, Geologic Atlas of the Rocky Mountain Region, USA Rocky Mountain Association of Geologists, Denver, Colorado, 143-165.

BERGER, G., CADORE, E., SCHOTT, J., and DOVE, P.M., 1994, Dissolution rate of quartz in lead and sodium electrolyte solutions between 25^{o}C and 300^{o}C: Effect of the nature of surface complexes and reaction affinity: Geochimica et Cosmochimica Acta, 58(2), 541-551.

BLAKE, R.E. and WALTER, L.M., 1999, Kinetics of feldspar and quartz dissolution at 70-80^{o}C and near-neutral pH: Effects of organic acids and NaCl: Geochimica et Cosmochimica Acta: 63(13/14), 2043-2059.

BLAIR, T.C., and MCPHERSON, J.G, 1992, The Trollheim alluvial fan and facies model revisited. Geological Society of America Bulletin, 104(6), 762-769.

BLISSENBACH, E., 1954, Geology of alluvial fans in semiarid regions. Geological Society of America Bulletin, 65(2), 175-190.

BROWN, J.E., 1973, Depositional histories of sand grains from surface textures: Nature 242, 396-398.

CAMPBELL, J.A., 1979, Lower Permian depositional system, northern Uncompahgre basin, in Baars, D.L., ed., Permianland Field Symposium, Four Corners Geological Society, Guidebook 9, 13-21.

CAMPBELL, J.A.,1980,Lower Permian depositional systems and Wolfcampian paleogeography, Uncompahgre basin, eastern Utah and southwestern Colorado, in Fouch, T.D., and Magathan, E.R., eds., Paleozoic Paleogeography of West-Central United States, Society for Sedimentary Geology, Rocky Mountain Section, 327–340.

CAMPBELL, S. and THOMPSON, I.C.,1991, The palaeoenvironmental history of late Pleistocene deposits at Moel Tryfan, North Wales: evidence from Scanning Electron Microscopy (SEM): Proceedings of the Geologists' Association, 102(2), 123-134.

CATER, F.W., JR., 1955, Geology of the Gateway quadrangle, Colorado: U.S. Geological Survey Quadrangle Map GQ-55.

CATER, F.W., 1970, Geology of the salt anticline region in southwestern Colorado: U.S. Geological Survey Professional Paper, 637p.

CONDON, S.M., 1997, Geology of the Pennsylvanian and Permian Cutler Group and Permian Kaibab Limestone in the Paradox Basin, southeastern Utah and southwestern Colorado: U.S. Geological Survey, Bulletin 2000, 46p.

COOKE, R.U., 2007, Laboratory simulation of salt weathering processes in arid environments: Earth Surface Processes and Landforms, 4(4), 347-359.

COSTA, P.J.M., ANDRADE, C., MAHANEY, W.C., MARQUES DA SILVA, F., FREIRE, P., FREITAS, M.C., JANARDO, C., OLIVEIRA, M.A., SILVA, and T., LOPES, V., 2013, Aeolian microtextures in silica spheres induced in wind tunnel experiment: Comparison with aeolian quartz: Geomorphology, 180-181, 120-129.

CURRY, A.M., PORTER, P.R., IRVINE-FYNN, T.D.L., REES, G., SANDS, and T.B., PUTTICK, J., 2009, Quantitative particle size, microtextural and outline shape analysis of glacigenic sediment reworked by paraglacial debris flows: Earth Surface Processes and Landforms: 34, 48-62.

DEANE, SARAH M., 2010, Quartz grain microtextures and sediment provenance: Using scanning electron microscopy to characterize tropical highland sediments from Costa Rica and the Dominican Republic: M.S.Thesis, University of Tennessee, Knoxville, Tennessee, 123p.

DOORNKAMP, J.C.,1974, Tropical weathering and the ultra-microscopic characteristics of regolith quartz on Dartmoor: Geografiska Annaler. Series A, Physical Geography, 56(1/2), 73-82.

D'ORSAY, A.M., and VAN DE POLL, H.W.,1985, Quartz grains surface textures: Evidence for middle Carboniferous glacial sediment input to the Parrsboro Formation of Nova Scotia: Geology, 13, 285–287.

DOVE, P.M. and CRERAR, D.A., 1990, Kinetics of quartz dissolution in electrolyte solutions using a hydrothermal mixed flow reactor: Geochemica et Cosmechimica Acta, 54, 955-969.

DOVE, P.M. and NIX, C.J., 1997, The influence of alkaline earth cations, magnesium, calcium, and barium on the dissolution kinetics of quartz: Geochimica et Cosmochimica Acta: 61(16), 3329-3340.

DUBIEL R.F., HUNTOON, J.E., CONDON, S.M, and STANESCO, J.D., 1996, Permian deposystems, paleogeography, and paleoclimate of the Paradox basin and vicinity, in Longman, M.W., and Sonnenfeld, M.D., eds., Paleozoic Systems of the Rocky Mountain Region: SEPM, Rocky Mountain Section, 427-444.

DUBIEL, R. F., HUNTOON, J. E., STANESCO, J. D., and CONDON, S.M., 2009, Cutler Group alluvial, eolian, and marine deposystems: Permian facies relations and climatic variability in the Paradox Basin. The Paradox Basin revisited: New developments in petroleum systems and basin analysis: Denver, Colorado, Rocky Mountain Association of Geologists Special Publication, 265-308.

ECCLES, T.M., SOREGHAN, G.S., KAPLAN, S.A., PATRICK, K.D., and SWEET D.E., in press, Geologic Map of the Unaweep Canyon Area, Delta 30' X 60' Quadrangle, Mesa County, Colorado. Colorado Geologic Survey Open-File Report, 1 sheet, scale 1:48,000.

ELSTON, D.P., and SHOEMAKER, E.M., 1960, Late Paleozoic and early Mesozoic structural history of the Uncompahgre front, in Four Corners Geological Society [Guidebook], Geology of the Paradox Basin Fold and Fault Belt, 47-55.

FRANCZYK, K.J., CLARK, G., BREW, D.C., and PITMAN, J.K., 1995, Chart showing lithology, mineralogy, and paleontology of the Pennsylvanian Hermosa Group at Hermosa Mountain, La Plata County, Colorado: U.S. Geological Survey, Miscellaneous Investigations, Map I-2555.

HAMMER, H. and DAT, R., 2001, PAST: paleontological statistics software package for education and data analysis. Palaeontology Electron 4: http:// palaeo-electronica.org/2011/past/issue1 01.htm

HODEL, K.L., REIMNITZ, E., and BARNES, P.W., 1988, Microtextures of quartz grains from modern terrestrial and subaqueous environments, north slope Alaska: Journal of Sedimentary Petrology, 58(1), 24-32.

HOOD, W.C., 2009a, An exhumed Late Paleozoic canyon in the Rocky Mountains: A discussion: The Journal of Geology, 117(2), 210-214.

HOOD, W.C., COLE, R.D., and ASLAN, A., 2009b, Anomalous cold in the Pangaean tropics: Comment: Geology, 37(6), 192.

HOWARD, J.L., AMOS, D.F., and DANIELS, W.L.,1995, Micromorphology and dissolution of quartz sand in some exceptionally ancient soils: Sedimentary Geology: 105, 51-62.

HUNTLEY, J.W., 2011, Exploratory multivariate techniques and their utility for understanding ancient ecosystems. In M. Laflamme et al., eds., Quantifying the Evolution of Early Life: Springer, Netherlands, 23-48.

IMMONEN, N., 2013, Surface microtextures of ice-rafted quartz grains revealing glacial ice in the Cenezoic Arctic: Palaeogeography, Palaeoclimatology, Palaeoecology, 374, 293-302.

KARIMI, A., KHADEMI, H., KEHL, M., and JALALIAN, A., 2009, Distribution, lithology and provenance of peridesert loess deposits in northeastern Iran: Geoderma, 148, 3–4, 241-250.

KEISER, L.J., SOREGHAN, G.S., MARRA, K., and ELWOOD-MADDEN, M.E., Climate differences inferred from modern and Permian weathering products in proximal alluvial sediments of an exhumed Permian granitic highland, Wichita Mountains (Oklahoma), to be submitted to Palaeogeography, Palaeoclimatology, Palaeoecology August, 2013.

KIRSHNER, A.E. and ANDERSON, J.B., 2011, Cenezoic glacial history of the northern Antarctic Peninsula: A micromorphological investigation of quartz sand grains, Tectonic, Climate, and Cryospheric Evolution of the Antarctic Peninsula: Special Publication 063.

KLUTH, C.F., 1986, Plate tectonics of the Ancestral Rocky Mountains, in Peterson, J.A, ed., Paleotectonics and sedimentation in the Rocky Mountain region, United States: American Association of Petroleum Geologists Memoir 41, 353-369.

KLUTH, C.F., and CONEY, P.J., 1981, Plate tectonics of the ancestral Rocky Mountains: Geology, 9, 10–15.

KRINSLEY, D.H., and DONAHUE, J., 1968, Environmental interpretation of sand grain surface textures by electron microscopy: Geological Society of America, Bulletin, 79, 743–748.

KRINSLEY, D.H., and DOORNKAMP, J.C., 1973. Atlas of Sand Grain Surface Textures: Cambridge, U.K., Cambridge University Press, 91p.

KRINSLEY, D., and TAKAHASHI, T., 1962, Surface textures of sand grains an application of electron microscopy, glaciation: Science, 138(3546), 1262-1264.

KRUSKAL, J.B., and WISH, M., 1978, Multidimensional Scaling. Sage University Paper Series on Quantiative Applications in the Social Sciences, Sage Publications, London, 93p.

LITTLE, I. P., ARMITAGE, T. M., and GILKES, R.J.,1978, Weathering of quartz in dune sands under subtropical conditions in eastern Australia: Geoderma, 20(3), 225-237.

MACK, G.H., and RASMUSSEN, K.A.,1984, Alluvial-fan sedimentation of the Cutler Formation (Permo-Pennsylvanian) near Gateway, Colorado: Geological Society of America Bulletin, 95, 109-116.

MAGEE, A.W., BULL, P.A., and GOUDIE, A.S., 1988, Chemical textures on quartz grains: An experimental approach using salts: Earth Surface Processes and Landforms, 13, 665-676.

MAHANEY, W.C.,1995, Pleistocence and Holocene glacier thickness, transport histories and dynamics inferred from SEM microtextures on quartz particles: Boreas, 24p.

MAHANEY, W.C., 2002, Atlas of Sand Grain Surface Textures and Applications: Oxford, U.K., Oxford University Press, 256p.

MAHANEY, W.C., and ANDRES, W., 1996, Scanning electron microscopy of quartz sand from the north-central Saharan desert of Algeria: Zeitschrift fur Geomorphologie, N.F. Supplement-Bd.103, 179-192.

MAHANEY, W.C. and KALM, V., 2000, Comparative SEM study of oriented till blocks, glacial grains and Devonian sands in Estonia and Latvia: Boreas, 29, 35–51.

MAHANEY, W.C., STEWART,A., and KALM, V., 2001, Quantification of SEM microtextures useful in sedimentary environmental discrimination: Boreas, 30, 165–171.

MALLORY, W.W., 1972, Pennsylvanian arkose and the Ancestral Rocky Mountains, in Mallory, W.W., ed., Geologic Atlas of the Rocky Mountain Region: Rocky Mountain Association of Geologists, Denver, CO 131–132.

MATHER, A. and HARTLEY, A., 2005, Flow events on hyper-arid alluvial fan: Quebrada Tambores, Salar de Atacama, northern Chile, in Alluvial Fans: Geomorphology, Sedimentology, and Dynamics, A.M. Harvey, A.E. Mather, and M. Stokes, eds.: Geological Society of London, Special Publication 251, 9p.

MCGOOKEY, D.P, HAUN, J.D., HALE, L.A., GOODELL, H.G., MCCUBBIN, D.G., WEIMER, R.J., and WULF, G.R., 1972, in Cretaceous System,W.W. Mallory, ed: Geologic Atlas of the Rocky Mountain Region, Rocky Mountain Association of Geologists, Denver, 331 p.

MEHRA, O.P., and JACKSON, M.L., 1960, Iron oxide removal from soils and clays by a citrate–dithionite system buffered by sodium carbonate: Clays and Clay Mineralogy, 7, 317–327.

MOORE, K.D., SOREGHAN, G.S., and SWEET, D.E., 2008, Stratigraphic and structural relations in the proximal Cutler Formation of the Paradox basin: Implications for timing of movement on the Uncompahgre fault: The Mountain Geologist, 45, 49–68.

PYE, K. and MAZZULLO, J.,1995, Effects of tropical weathering on quartz grain shape: An example from northeastern Australia: Journal of Sedimentary Research, 64(3), 500-507

RASCOE, B., J.R., and BAARS, D.L., 1972, Permian System: in Geologic Atlas of the RockyMountain Region; edited by Mallory, W.W., Rocky Mountain Association of Geologists, Denver, Colorado, 177-189.

SCARCIGLIA, F., LE PERA, E., and CRITELLI, S., 2005, Weathering and pedogenesis in the Sila Grande Massif (Calabria, South Italy): From field scale to micromorphology: Catena, 61(1), 1-29.

SCHULTZ, A.W., 1984, Subaerial debris-flow deposition in the upper Paleozoic Cutler Formation, western Colorado: Journal of Sedimentary Petrology, 54, 759-772.

SCOTESE, C.R., 1999 PALEOMAP animations, paleogeography: Arlington, University of Texas, Department of Geology PALEOMAP Project, 48 leaves.

SOREGHAN, G.S., SWEET, D.E., MARRA, K.R., EBLE, C.F., SOREGHAN, M.J., ELMORE, R.D., KAPLAN, S.A., and BLUM, M.D., 2007, An exhumed late Paleozoic landscape in the Rocky Mountains: Journal of Geology, 115, 473-481.

SOREGHAN, G.S., SOREGHAN, M.J., and HAMILTON, M.A., 2008a, Origin and paleoclimatic significance of tropical silt in the late Paleozoic icehouse: Palaeogeography, Palaeoclimatology, Palaeoecology, 268, 234–259.

SOREGHAN, G.S., SOREGHAN, M.J., POULSEN, C.J., YOUNG, R.A., EBLE, C.F., SWEET, D.E., and DAVOGUSTTO, O.C., 2008b, Anomalous cold in the Pangaean tropics: Geology, 36, 659–662.

SOREGHAN, G.S., SOREGHAN, M.J., MOORE, K.D., and SWEET, D.E., 2009a, Hot fan or cold outwash? Hypothesized proglacial deposition in the upper Paleozoic Cutler Formation, western tropical Pangaea: Journal of Sedimentary Research, 79, 495-522.

SOREGHAN, G.S., SOREGHAN, M.J., POULSEN, C.J., YOUNG, R.A., EBLE, C.F., SWEET, D.E., and DAVOGUSTTO, O.C., 2009b, Anomalous cold in the Pangaean tropics: Reply to Discussion: Geology, 37, 215–220.

SOREGHAN, G.S., SWEET, D.E., MARRA, K.R., EBLE, C.F., SOREGHAN, M.J., ELMORE, R.D., KAPLAN, S.A., and BLUM, M.D., 2009c, An exhumed late Paleozoic canyon in the Rocky Mountains: Reply to Discussion: Journal of Geology, 117(2), 215-220.

SOREGHAN, G.S., KELLER, G.R., GILBERT, M.C., CHASE, C.G., and SWEET, D.E., 2012, Load-induced subsidence of the Ancestral Rocky Mountains recorded by preservation of Permian landscapes: Geosphere, 8(3), 654-668.

STRAND, K. and IMMONEN, N., 2010, Dynamics of the Barents-Kara ice sheet as revealed by quartz sand grain microtextures of the late Pleistocene Arctic Ocean sediments: Quaternary Science Reviews, 29, 3583-3589.

SUTTNER, L.J., and DUTTA, P.K.,1986, Alluvial sandstone composition and paleoclimate, I framework mineralogy: Journal of Sedimentary Petrology, 56, 329–345.

SWEET, D.E., and SOREGHAN, G.S., 2010, Application of quartz sand microtextural analysis to infer cold-climate weathering in the equatorial Fountain Formation (Pennsylvanian-Permian, Colorado): Journal of Sedimentary Research, 80, 1-7.

SWEET, D.E., and SOREGHAN, G.S., 2010, Late Paleozoic tectonics and paleogeography of the Ancestral Front Range: structural, stratigraphic and sedimentological evidence from the Fountain Formation (Manitou Springs, Colorado): Geological Society of America, Bulletin, 122, 575-594.

VAN HOESSEN, J.G. and ORNDORFF, R.L., 2004, A comparative SEM study of the micromorphology of glacial and nonglacial clasts with varying age and lithology: Canadian Journal of Earth Science, 41, 1123-1139.

WANG, Y., NAHON, D., and MERINO, E., 1994, Dynamic model of the genesis of calcretes replacing silicate rocks in semi-arid regions: Geochimica et Cosmochimica Acta., 58, 5131-5145.

WERNER, W.G., 1974, Petrology of the Cutler Formation (Pennsylvanian-Permian) near Gateway, Colorado, and Fishers Towers, Utah: Journal of Sedimentary Petrology, 44, 292-298.

WHITE, A. F. and BRANTLEY, S. L., 1995, Chemical weathering rates of silicate minerals: an overview. Chemical Weathering Rates of Silicate Minerals, 31,1-22.

WHITE, M. A., and JACOBSON, M. I.,1983, Structures associated with the southwest margin of the ancestral Uncompahgre Uplift. Northern Paradox basin-Uncompahgre uplift: Grand Junction Geological Society Guidebook, 33-39.

4. A COMPARISON OF MODERN AND PERMIAN WEATHERING IN ALLUVIAL SEDIMENTS OF THE WICHITA MOUNTAINS (OKLAHOMA): EVIDENCE FOR A WETTER CLIMATE IN THE EARLY PERMIAN

INTRODUCTION

Climate is a major control on physical and chemical weathering of siliciclastic sediments (e.g. Twidale and Romani, 2005; Taylor and Eggleton, 2010). Other factors such as provenance, transport, denudation rate, exposure time, drainage basin relief and biological influences also affect weathering (e.g., White and Blum, 1995; Brown and Ransom, 1996; Riebe et al., 2004). Hence, inferring climate from weathering signals preserved in ancient systems is challenging. Modern and ancient sediments weathered from the Wichita Mountains (Oklahoma), however, offer a near-unique opportunity to contrast weathering signals in fluvial sediments from both the modern and the Permian, and thus refine paleoclimatic inferences for the latter relative to the former. The Wichita Mountains, composed of Cambrian granite, form part of an Early Permian paleo-landscape presently undergoing exhumation for the first time since Permian burial (Gilbert, 1982, Soreghan et al., 2012). These granitic mountains are releasing sediment into modern streams that drain the uplands. Analogously, the Lower Permian (Leonardian/ Artinskian) Post Oak Conglomerate proximal to the mountains records drainage systems of similar size (drainage basin area and relief) as the modern, and that emanated from the same granitic bedrock source. Few studies have explored climatic records from Permian strata proximal to the

Wichita uplift. This study examines sediments within a modern stream draining the Wichita Mountains to 1) document geochemical and textural weathering signals in a modern granitic terrane under warm-temperate semi-arid climate conditions, and 2) compare these to weathering signals preserved in an ancient system bearing the same provenance and drainage basin controls (non-climatic factors). Results shed light on weathering processes in general, and clarify the upland-proximal Permian climate of this region of western equatorial Pangaea by comparison to the weathering signals archived in the modern and recent climate system here.

GEOLOGIC SETTING

Paleozoic History (Wichita-Anadarko System)

The (modern) Wichita Mountains of southwestern Oklahoma form part of an inverted rift system termed the Southern Oklahoma Aulacogen, which formed during the Cambrian (Hoffman et al., 1974; Gilbert 1983; Keller et al., 1983; Fig. 4.1). An early Cambrian rifting event resulted in bimodal volcanism (basaltic and rhyolitic) accompanied by the intrusion of Cambrian granite, and followed by the accumulation of 4-5 km of Lower and Middle Paleozoic strata during post-rift subsidence (Powell and Phelps, 1977; Brewer et al., 1983; Donovan, 1982; Gilbert, 1982, 1983). Subsequently, crustal shortening associated with the Ancestral Rocky Mountains orogeny occurred in the Pennsylvanian, and resulted in inversion of the old rift, and creation of the Wichita uplift and adjacent Anadarko (foreland) basin (Brewer et al., 1983).

As the Anadarko basin subsided, 4-5 km of Pennsylvanian sediment accumulated in the basin, eroded primarily from the adjacent uplift; clast compositions of these strata shift from carbonate-dominated low in the section to entirely crystalline basement- (granite) derived through time, recording an inverted stratigraphy reflecting the progressive unroofing of the uplift. By Early Permian time, the Wichita uplift began subsiding, and was ultimately buried by Permian strata (e.g. the Hennessey Shale; Fig. 4.1), sourced primarily from distal regions (Stith, 1968; Gilbert, 1983; Soreghan et al., 2012). During this Early Permian phase the Post Oak Conglomerate, which interfingers with the Hennessey Shale distally, was deposited by streams draining the (weathered) Wichita uplands. Winkler et al. (1999) used apatite fission-track data to document that burial depth of the Wichita uplift was between 800 m and 1.5 km. Today, the Post Oak Conglomerate sourced from the granite of the Wichita uplift is exposed at the surface, and together with the Hennessey Shale onlaps the relief preserved on the Cambrian igneous basement. Indeed, both surface mapping and subsurface data (Ham et al., 1964) demonstrate up to 1 km of Permian strata onlapping the Wichita uplift, providing evidence that the current relief on the Cambrian basement represents a paleo-landscape that dates from Permian time (Gilbert, 1982). The Wichita Mountains thus form a rare example of a Permian paleo-landscape currently undergoing exhumation (Gilbert, 1982, 1989).

In addition to these fundamental mapping relationships, there are several additional lines of evidence supporting the inference of a Permian age

for this landscape. This includes widespread karst developed on Lower Paleozoic carbonate strata along the north flank of the Wichita Mountains (Slick Hills; Fig. 4.1). The karst is dated as Lower Permian on the basis of vertebrate fossils within the cave fill (Donovan et al., 2001). Spheroidally weathered granitic boulders forming a tor-type topography (Gilbert, 1982, 1989) protrude through Permian strata that do not exhibit spheroidal weathering south of the Wichita Mountains, indicating that the weathering that produced the tor-type topography formed prior to burial by Permian sediment (Gilbert, 1982).

Finally, paleomagnetic studies provide further evidence for the Permian age of surface weathering in the Wichita Mountains. The red (oxidized) color of the granite at the surface today contrasts greatly with the gray (reduced) color of granite at depth (Hamilton, 2011; Price, 1998). The red color reflects a chemical remagnetization event (~ 25 m) associated with weathering and oxidation that occurred during Early Permian time, prior to the deposition of the Post Oak Conglomerate (Hamilton, 2011).

The Permian Post Oak Conglomerate

The Lower Permian Post Oak Conglomerate mantles the Wichita paleouplift, extending on average 20 km from the core of the Wichita Mountains (Fig. 4.1), and is estimated to reach thicknesses of 120 -180 m (Chase, 1954; Al-Shaieb et al., 1980) locally, although the thickness is not well constrained owing to a lack of large vertical exposures. The Post Oak

Conglomerate interfingers distally with Lower Permian redbeds of the Hennessey Shale, Garber Sandstone, and Wellington Formation, and this interfingering provides indirect age control for the Post Oak Conglomerate (Chase, 1954; Al Shaieb et al., 1980; Havens, 1983; Donovan and Ragland, 1986; Figure 4.5). Al-Shaieb et al. (1980) documented assemblages of features, such as presence of erosional bases, internally massive bedding, cut-and-fill structures, inferred mud flow deposits, and abrupt vertical and lateral changes in grain-size to posit the presence of discontinuous fluvial channel deposits in the Post Oak Conglomerate, separated by siltstone and mudstone (interfluve) strata distally. Aerial views of the study region reveal topographic highs consisting of Post Oak Conglomerate, which have been interpreted to be the remnants of these channels (Gilbert, 1982; Fig. 4.4). Using petrographic and grain-size data from the Post Oak Conglomerate, Stone (1977) recognized four paleochannels that drained the Wichita uplift during the Permian. Clast lithology varies from carbonate to rhyolitic to granitic depending on location, as the clast lithology reflects the source area from which each channel originated. The average clast size decreases distally, and abrupt grain-size changes occur vertically and laterally (Stone, 1977). Much of the most proximal Post Oak Conglomerate contains large well-rounded granitic clasts (>30 cm) in internally massive, poorly sorted deposits.

The Post Oak Conglomerate is locally famous for the occurrence of distinctive, remarkably well-rounded clasts. The presence of such rounding,

despite the well-documented minimal transport distance, is inferred to reflect the action of spheroidal weathering during the Permian (Gilbert, 1982). The presence of tor topography and streams choked with well-rounded boulders on Mount Scott today provide additional evidence that support the action of Permian spheroidal weathering as the cause for the rounding (Gilbert, 1982). The Wichita Mountains landscape currently undergoing exhumation was shaped by a relatively long period of spheroidal weathering based on the size and abundance of spheroidally weathered clasts in the Post Oak Conglomerate, and subsequent transport of the weathered grus during the Early Permian (Al-Shaieb et al, 1980; Gilbert, 1982).

Paleoclimate

Interpretations for the paleoclimate of the greater study region during Early Permian time generally posit semi-arid to arid conditions (Al-Shaieb et al., 1980; Miller et al., 1996; Kessler et al., 2001; Tabor and Montanez, 2002; Tabor and Montanez, 2004; Tabor and Poulsen, 2008; Pack, 2010). For example, Miller et al. (1996) used Wolfcampian (Asselian-Sakmarian) paleosols in northeastern Kansas to infer a semi-arid, seasonal climate based on the presence of abundant Vertisols and Calcisols. Using oxygen isotopes, clay mineralogy, and paleosol types, Tabor and Montanez (2002, 2004) documented a shift from more humid conditions to more arid conditions across the Pennsylvanian-Permian boundary in north-central Texas and southern Oklahoma. The presence of abundant loessite as well as loess-

hosted paleosols with calcic and vertic features in northeastern New Mexico led Kessler et al., (2001) to infer arid to semiarid and seasonal conditions during the late Wolcampian (Sakmarian) to early Leonardian (Artinskian) as well. Few data exist for the immediate regions surrounding the Wichita Mountains (ancient Wichita uplift), aside from documentation of presumably semi-arid-type calcareous paleosols (Calcisols) in relatively distal facies of the Post Oak Conglomerate along the northern flank of the Wichita Mountains (Fig. 4.1; Al-Shaieb, 1980). However, the Post Oak Conglomerate in this region contains abundant clasts of Lower Paleozoic limestone, calling into question any climatic significance of calcareous paleosols here, as the limestone clasts provide an abundant local source for $CaCO_3$. Furthermore, a more dynamic view of the paleoclimate through the Early Permian has been suggested, punctuated by alternating warmer and cooler phases at a higher frequency than previously recognized (Montanez et al., 2007; Retallack, 2013).

Cenozoic History (The Wichita Mountains)

The modern Wichita Mountains formed as this area of the Midcontinent was broadly warped during the late Mesozoic to Paleogene, likely associated with evolution of the Rio Grande Rift (Winkler et al., 1999; Eaton, 2008). This broad warping resulted in erosion of the Mesozoic, and now Permian cover, and thus the partial exhumation that produced the modern landscape of the Wichita Mountains. Denudation of the Wichita Mountains began in the

Paleogene (~55-25 Ma; Winkler et al., 1999) during which the climate of the Midcontinent is thought to have been semi-arid to arid (Terry, 2001). The modern Blue Beaver Creek drains the granitic knobs on the southern flank of the exhumed paleolandscape (Table 4.3). A hydrologic station downstream on Blue Beaver Creek recorded an average discharge (~30 years of data) of .04 m^3/s in July (lowest flow month) to 1.1 m^3/s in May (highest flow month) (Mast and Turk, 1999). The study region today has a mean annual precipitation of 770 mm/yr and a mean annual temperature of 20^oC (Mast and Turk, 1999). Hence, the modern climate is considered to be warm temperate using the Köeppen climate classification (Mast and Turk, 1999; Kottek et al., 2006). The Blue Beaver Creek drainage lies entirely on the Mount Scott Granite and therefore drains the same granite that sourced the Permian drainage of the Post Oak Conglomerate in the study area of the southern flank of the Wichita Mountains, making this an ideal site for comparison of weathering in these modern and ancient systems.

METHODS

This study targets two systems (Fig. 4.2): a modern stream (Blue Beaver Creek) and an ancient fluvial system of the Post Oak Conglomerate (identified by Stone, 1977) sourced from the same granite and of approximately the same size as the modern system.. Minor rhyolite is also present but bears a geochemical signature that mimics that of the granite. Assessment of the size for the Permian drainage basin follows the

interpretation of Stone (1977), who inferred the drainage basin size on the basis of mineralogic and grain-size dispersal patterns determined by petrographic analysis of over 100 thin sections from the Post Oak Conglomerate. The proximal (~5-7 km) portion of Blue Beaver Creek is on restricted wildlife refuge land and therefore minimally affected by anthropogenic activity. In modern Blue Beaver Creek, 500 g samples (10) were collected along a ~7 km transect at 1000 m intervals, beginning at the headwaters on the Wichita Mountains Wildlife Refuge (Fig. 4.2). These samples were wet-sieved to separate the silt + clay (<63 μm), sand, and gravel fractions. The sand and gravel fractions were air-dried and weighed. The mud fraction was processed to remove carbonate, organic matter, and iron oxides. The carbonate was removed using buffered acetic acid with a pH of 4.7 for 12 hours at 50^{o}C. Following this, the samples were treated with 30% H_2O_2 and heated for 12 hours at 50^{o}C to remove organics. Finally the samples were treated with the citrate-bicarbonate-dithionite (CBD) method (Mehra and Jackson, 1960; Janitsky, 1986) to remove iron oxides. The chemically treated mud fraction was subsequently freeze-dried and weighed.

The type section of the Permian Post Oak Conglomerate (Stone, 1977) was measured and logged (Figs. 4.2, 4.5) to detail the depositional facies and thus aid in assessment of the depositional processes. Owing to the limited number and vertical extent of outcrop exposures across the study area, sampling within the Permian system (Post Oak Conglomerate) was limited to 5 samples, three from a proximal location and 2 from a distal location ~5 km

from the proximal location. At each location, 500 g samples were collected from the unaltered matrix within the Post Oak Conglomerate. The Permian samples are weakly carbonate cemented and were therefore disaggregated using 1N HCl at 50^{o}C for 12 hours. Prior to this treatment, an experiment was performed to determine the effects of HCl compared with buffered acetic acid dissolution on the whole-rock geochemistry. The results indicated insignificant differences in the major oxides used in this study between the two treatments. Following the chemical treatments, the samples were wet sieved to separate the mud, sand, and gravel fractions. The mud, sand and gravel fractions were air-dried and weighed for grain-size analysis.

The modern and Permian mud fractions of the samples were analyzed for the mineralogy of the <63 μm size fraction using bulk quantitative XRD techniques. Mud samples were powdered and mounted onto glass slides carefully to ensure random orientation of the crystal axes. ClaySim was used to approximate mineralogy from the XRD results. Major element geochemistry of the pretreated mud fraction was determined from X--ray fluorescence (XRF) analysis performed by an outside lab (ALS Chemex). Grain-size analysis of the mud fraction was performed using a Beckman Coulter LS 200 laser particle size analyzer (LPSA). Grain mounts were prepared of the sand fractions for both the modern and Permian samples. Polished thin sections were prepared for samples of unaltered matrix from the Post Oak Conglomerate to analyze the textures and cements.

A number of granite clasts of pebble size from the Post Oak Conglomerate were collected for weathering rind analysis using scanning electron microscopy (SEM) analysis. Granite clasts from the modern stream (Blue Beaver Creek) where it drains the Mount Scott Granite do not exhibit weathering rinds and therefore analysis of these clasts was unwarranted. The Permian clasts were cut to obtain a ~ 2.5 cm cross section and polished using Emory paper. An ion mill was used to further polish the samples prior to SEM analysis. Energy dispersive spectrum (EDS) analysis was utilized to determine the chemical and mineral composition of the rind and core of each clast. Photomicrographs of the clasts allowed for qualitative analysis of the weathering features present in the rinds.

RESULTS

Exposures of the Post Oak Conglomerate are limited in the Wichita Mountains. The Permian Post Oak conglomerate crops out only in small 2-3 m vertical sections in a few areas around the granitic remnants of the Wichita Mountains. The most vertically extensive exposure is the type section, which consists of a well-exposed section 16 m thick and with 200 m of lateral extent (Boulder Park area; Figs. 4.2, 4.5), described below.

Lithofacies

Cobble to Boulder Conglomerate

The most common lithofacies is very poorly sorted clast- to matrix-supported cobble- to boulder conglomerate (10-40 cm clasts). Clasts consist of well-rounded to sub-rounded granite and rhyolite with no imbrication present. Bedding thicknesses vary laterally from ~ 30 cm- 4 m and include both clast-supported and matrix-supported textures. The matrix consists of angular coarse sand- to gravel-sized material in varying proportions, with minor mudstone. Thin, laterally discontinuous lenses of coarse sandstone and granule conglomerate occur locally, and commonly exhibit crude stratification. Gradational to diffuse contacts occur within the upper granule conglomerate units.

Granule Conglomerate

Internally massive to crudely stratified and graded granule conglomerate caps the massive cobble to boulder conglomerate units with bed thicknesses ranging from 40 cm to 3 m, and contain numerous out-sized floating clasts of up to 20 cm diameter. The massive granule conglomerate beds are laterally discontinuous. Weak internal horizontal stratification associated with upwardly fining sequences occurs locally. The granule conglomerate is interbedded with cobble lenses near the top of the section.

Other features

Color mottling that includes both oxidized (red-brown) and reduced (gray-green) hues occurs at the tops of some beds. The mottling is confined to laterally continuous intervals across most of the exposed section. Most of the mottled granule conglomerate and coarse sandstone units additionally exhibit a blocky fracturing pattern, wherein the fractures are randomly oriented, producing equant blocks generally 2-5 cm across. Clay coats are visible locally on fracture surfaces. Additionally, subvertical, downwardly tapering traces (2-5 cm width) exhibiting reduced colors also occur locally.

Interpretation

Stone (1977) interpreted the Post Oak Conglomerate as a fluvial deposit in general on the basis of the lenticular geometry of individual beds, and occurrence of local cross-bedding and cut-and-fill structures in distal sections. Although the presence of these facies characteristics are consistent with a fluvial system, the facies documented in the type section suggest a predominance of hyperconcentrated flood flows (HFFs), which are flows intermediate in sediment/water ratio between stream flow and debris flow (Smith and Lowe, 1991; Jiongxin, 2004; Hartley et al., 2005). Evidence for HFF processes include the abundance of outsized floating cobbles within granule conglomerate beds, a lack of cross-stratification, poor sorting and internally massive beds that exhibit crude horizontal stratification, and local normal grading (Smith and Lowe, 1991). HFF deposits form as a result of

rapid deposition under conditions of high water discharge and a high-sediment load (e.g., Smith 1986).

In addition to the depositional facies, features indicative of pedogenesis also occur locally, such as oxidized (red) - reduced (gray-green) color mottling inferred to reflect alternating wetting and drying, downward tapering reduced zones recording brief landscape stability, clay coats indicative of clay formation and illuviation, and blocky fracturing interpreted to record ped formation (Kraus, 1996; Retallack, 2001). These characteristics are present in laterally continuous intervals consistent with pedogenesis, but the lack of horizonation suggests only incipient pedogenesis, consistent with Protosol (Mack et al., 1993, or Entisol (Soil Survey Staff, 2013) formation (Fig. 4.5, 4.6). These immature paleosols reflect very little time for development, which is consistent with facies evidence showing this is an active area of the depositional system.

Grain-size Analysis and Mineralogy

Figure 4.7 illustrates the major differences between the modern and Permian samples in terms of grain size and mineralogy. Whereas the grain size distribution of the modern sediment samples (n = 4) averages 3% mud, 64% sand, and 33% gravel, the Permian sediment samples (n = 4) average 12% mud, 68% sand, and 20% gravel, and thus a large difference in the mud (<63 μm) fraction. Within the mud fraction, the average mode for the modern

samples is medium silt (29.8 μm), whereas the average of the modes for the Permian samples is very fine silt (7.1 μm)

In addition to the significant differences in bulk grain-size distributions between the modern and Permian samples, semi-quantitative analysis of the bulk mud fractions reveal large differences in mineralogy. Whereas the modern muds contain ~35% clay minerals, the mud fractions from the Permian samples contain 65% clay minerals. Bulk quantitative XRD results suggest the clays in the modern samples comprise, in order of abundance, ferrihydrite, kaolinite and chlorite, whereas those in the Permian samples consist of kaolinite, chlorite, magnetite, and hematite. Within the mud fractions of both the modern and Permian samples, primary minerals comprise, in order of relative abundance, quartz, k-feldspar, plagioclase, amphibole and pyroxene.

Weathering Rinds

Clasts from the Post Oak Conglomerate were collected to document textures and alteration within the weathering rinds and cores. The weathering rinds of all examined clasts (n= 3) exhibit pervasive microfracturing and clay formation clearly visible using SEM analysis (Fig. 4.8), and extensive fracturing also occurs in the clast cores (Fig. 4.8). Precipitation of Fe- and Ti-oxides, as well as kaolinite and other clays is abundant in the rind and is also abundant in the many fractures in the cores of the clasts.

Geochemistry

The geochemistry of the mud fraction is useful for determining degree of alteration in the modern and Permian samples, using established weathering indices. Controlling for grain-size by examining only the mud fraction enables better comparison between the modern and Permian samples (Nesbitt et al., 1996). Bedrock samples were analyzed using whole-rock geochemistry. The major-element (oxide) weight percents for mud samples from a wide variety of modern river systems in the world with felsic source terranes (Table 4.2; Van de Kamp, 2010) are also used as comparisons for the samples in this study. Although the source terranes for these published data are felsic, the comparison is not directly equivalent with the Blue Beaver and Post Oak samples because the bedrock is not identical to the granitic bedrock in the Wichita Mountains. Table 4.2 lists the major-element (oxide) weight percents for the granitic bedrock, sediment from modern Blue Beaver Creek, matrix from the Post Oak Conglomerate, and mud from fluvial systems of other modern climates from the data of Van de Kamp (2010).

Figure 4.9 illustrates averages of the major oxides (SiO_2, K_2O, Al_2O_3, Na_2O) for each system. The amount of silica loss in the Permian samples is significantly higher than the silica loss documented in the modern samples when compared to the silica content in the granitic bedrock. The bedrock exhibits the highest percentage of K_2O. All other samples have similar percentages of K_2O that are lower than values in the bedrock. Most

significantly, the Post Oak Conglomerate exhibits substantially more (>2 times) Al_2O_3 relative to the bedrock and modern sediment samples, and has values similar to those documented in fluvial sediments of modern tropical settings.

Chemical index of alteration (CIA) values were calculated using molar proportions of the major oxide weight percents (Table 4.2, Fig. 4.9). As defined by Nesbitt and Young (1996), the CIA = $[Al_2O_3/(Al_2O_3+CaO+Na_2O+K_2O)]*100$, where CaO is silicate-bound. Acidification of the samples prior to geochemical analysis ensures elimination of any carbonate-bound CaO. The bedrock from published data was not acidified prior to geochemical analyses, such that trace carbonate phases could artificially alter the CIA to lower values. Typical values for unweathered granite average ~50, whereas a value of 100 would represent essentially complete weathering to a kaolinitic composition (Nesbitt and Young, 1996). The bedrock in the Eastern Wichita Mountains is composed of the Mount Scott Granite, Quanah Granite, Medicine Park Granite, Rush Lake Granite, Saddle Mountain Granite, Davidson Metarhyolite, Carlton Rhyolite, Rhyolite Xenoliths, and the Wichita Granite Group. All bedrock samples have CIA values of 56-58 (Price, 1998), suggesting that some weathering has occurred in the bedrock samples. The highest CIA values, averaging ~ 81, (Table 4.2, Fig. 4.9) characterize the Post Oak Conglomerate mud fraction, and the published data for modern sediment samples from the Amazon, Penang Island, and Malaysian sites of Van de Kamp (2010), (Table 4.2, Fig. 4.9). The Wichita Mountains samples

are also plotted on an ACNK (Al_2O_3, CaO + Na_2O, and K_2O) diagram to illustrate weathering trends (Nesbitt et al., 1996; Yang et al., 2004; Fig. 4.11). The modern samples from Blue Beaver Creek show a slight departure from the bedrock values, whereas the samples from the Post Oak Conglomerate plot significantly apart from the bedrock samples, shifted toward the Al_2O_3 apex.

DISCUSSION

Spheroidal Weathering of the Permian Granitic Landscape

The Wichita Mountains exhibit a classic tor topography (Gilbert, 1982) consisting of abundant residual boulder streams and stacks of boulders, both of which reflect prolonged spheroidal weathering. Tor topography is common and well-developed in tropical regions as the characteristic granitic upland (Twidale and Romani, 2005; Fletcher et al., 2006). Where tor topography occurs in other climates such as the deserts of the American Southwest, it is thought to reflect inheritance from formerly humid climates, such as occurred during the the late Tertiary (Oberlander, 1972; Twidale and Romani, 2005; Strudley, 2006). Spheroidal weathering is driven by fracture-controlled subsurface weathering, which allows water to infiltrate the bedrock such that the bedrock is in constant contact with moisture, followed by chemical weathering (hydrolysis and oxidation) in the shallow subsurface through interactions between the oxidized groundwater and the host rock (Oberlander, 1972; Pope et al., 1995; Twidale and Romani, 2005; Dixon et al., 2009; Hall,

2012). The shape and size of the resultant corestones depends on the duration of uninterrupted subsurface weathering by oxygenated water, which implies spheroidal weathering occurs near the surface (Pope et al., 1995; Twidale, 2005; Dixon et al., 2009; Hall, 2012). Fletcher et al. (2006) inferred that pore-fluid oxygen concentration is the limiting factor in spheroidal weathering, owing to the necessity of production of Fe oxides and consequent precipitation of ferric minerals, which causes strain and thus promotes continued rock fracturing. Hence, spheroidal weathering must occur in the near-surface environment, as part of regolith formation.

The near-surface process of spheroidal weathering is one of the most common mechanisms of weathering granite to a saprolite (Dixon et al., 2009). Steady-state denudation and weathering advance rates are required for the continued spheroidal weathering process. If erosion outpaces weathering, the amount of time that rock interacts with non-equilibrated pore fluids is short, making it unlikely that significant spheroidal or chemical weathering will occur. If weathering outpaces erosion, a regolith mantle will form, resulting in progressive decrease in the rate of chemical weathering (Twidale, 2005; Riebe et al., 2004; Fletcher et al., 2006; Dixon et al., 2009). The Post Oak Conglomerate is a remnant of spheroidally weathered soil profiles as evidenced by the abundant cobble-sized corestones, abundant clay, and tor-type topography prevalent in the Wichita Mountains today.

Diagenetic alteration could have further influenced the chemistry of the Post Oak Conglomerate. However, both the Post Oak Conglomerate and the

underlying fractured granitic paleolandscape that it mantles would have been equally affected by such diagenetic alteration. Differences in chemistry between the Permian sediments and the sediment of the modern Blue Beaver Creek thus reflect differences in the weathering intensity of the Permian relative to modern climates.

Weathering Signatures in the Post Oak Conglomerate Relative to Weathering Signatures in Modern Stream Sediments

All data collected, including macroscopic facies analysis, sediment textures, SEM analysis of weathering rinds, and sediment geochemistry show systematic differences in both depostional regimes and alteration between the modern and ancient fluvial environments. The modern stream exhibits low discharge throughout the year (.04 m^3/s - 1.1 m^3/s) and therefore boulders and cobbles are uncommon in the stream.

A key initial difference between the sediments of the Post Oak Conglomerate and those of the modern stream is the proportion of mud. Stream competency as assessed by common clast sizes present in the Post Oak Conglomerate relative to the modern streams is addressed by Price (1998) who noted that the modern drainages transport sediment of primarily sand to gravel sizes, whereas the Post Oak Conglomerate includes common cobble to boulder sizes within a matrix of abundant clay (Fig. 4.6, 4.7). Utilizing the mud fraction as a means to assess weathering regimes relies on the idea that the mud fraction in fluvial deposits reflects the soil weathering

profile forming concurrent with deposition (Nesbitt et al.,1996). Therefore, this fraction faithfully records weathering signals related in large part to climate. The abundance of clay-size particles and clay minerals in the mud fraction of the Post Oak Conglomerate as determined by petrographic, grain-size, and XRD analysis implies that significantly more weathering occurred in the Permian relative to what is occurring in the modern fluvial system. Temperature and water are both key to the hydrolysis weathering reactions that drive clay mineral production, but the presence of water is the primary factor. High volumes of water combined with steady-state erosion and weathering drove production of the significantly greater amount of clay found in the Post Oak Conglomerate.

The geochemical data also reflect this increased clay production. A cross plot of K_2O + Na_2O versus SiO_2 highlights the amount of feldspar weathering that occurred during the Permian, and indicates that feldspar weathering is much less important in the modern system relative to the Permian system (Fig 4.10). The abundant clay-size sediment signifies increased rates of hydrolysis and therefore more weathering driven by more water-rock interaction than what occurs in the modern and recent climate system of the region. This conclusion is also echoed by Nichols (1968) findings of clay mineral formation in Wichita Mountains granite.

The chemical index of alteration (CIA) is a well-established weathering indicator, widely applied to assess weathering in both modern and ancient soil profiles, as well as fluvial deposits (e.g., Goldberg, 2010; Singh, 2010;

Bahlburg and Dabrinzki, 2011; Bastida et al., 2013). The CIA of the mud fraction (average 62, n=6; Table 4.2, Fig. 4.9) from sediments of Blue Beaver Creek indicates relatively minor to moderate chemical weathering is taking place in the modern drainage basin. However, the CIA of the mud fraction of the Post Oak Conglomerate, which averages 81 (n=5), suggests significant amounts of chemical weathering occurred during the deposition of the Post Oak Conglomerate (Table 4.2, Fig. 4.9). Additionally, samples from surface exposures of the bedrock exhibit a higher CIA value (~57; n=9) than expected for unweathered bedrock (~50) suggesting substantial weathering has occurred in the Permian (Table 4.2; Nesbitt et al., 1996; Price, 1998). Finally, the depositional facies of the Post Oak Conglomerate, dominated by HFF deposits, reflects an abundance of both water and sediment in the system, which contrasts with the generally limited water availability today.

Comparative Analysis with Other Modern Climates

As a comparison exercise, muds from modern stream sediments draining generally felsic systems and representing a variety of climates were plotted on an ACNK (Al_2O_3, $CaO + Na_2O$, and K_2O) diagram to determine possible similarities between those known climates and the Permian samples (Fig. 4.11). These modern streams plot in locations on the ACNK diagram that reflect the amount of weathering that occurs in those climates (Fig. 4.11). High amounts of Al_2O_3 in the mud fraction indicates abundant weathering in the tropical climates, e.g. the Amazon, Malaysia, and Penang Island samples;

notably, the samples from the Permian Post Oak Conglomerate plot near the samples from these tropical regions. These results imply that the Post Oak Conglomerate records a significant degree of weathering, comparable to modern wet-tropical regions (~2000 - 4000 mm/yr MAP; Fig. 4.11, 4.12). Additionally, the modern sediments from Blue Beaver Creek plot in close proximity to other modern fluvial sediment samples from regions in the temperate semi-arid climate zone (~500 - 1500 mm/yr MAP; Fig. 4.11, 4.12) which agrees with the climate in the Wichita Mountains today.

It is widely recognized that a large-scale aridification occurred in general from Pennsylvanian through Permian time in equatorial Pangea (e.g. Tabor and Poulsen, 2008). For the region of the Wichita Mountains specifically, humid conditions in the earliest Permian are inferred from speleothem records of Permian caves (Woodhead et al, 2010). However, by Post Oak time (Leonardian) and later (Early Guadalupian), interpretations have suggested generally semi-arid to (increasingly) arid conditions (e.g. Chase 1954; Al-Shaieb et al., 1980; Benison et al., 2001, Sweet et al., 2012; Foster, 2013). Our findings indicate tropical wet conditions recorded by the Post Oak Conglomerate. It is likely that effective moisture fluctuated greatly as the Permian progressed and that the long-term aridification trend was punctuated by wetter spikes, perhaps associated with CO_2 fluctuations (e.g. Retallack, 2013; Fig. 4.3), which are documented for Permian time (e.g., Montañez et al., 2007).

A final factor critical in influencing weathering is biological factors, especially activity of plants, which is linked to climate regime but also reflects evolution in the case of Permian relative to the modern environment. Weathering in the Wichita Mountains today is influenced by a modern vascular land plant community that includes angiosperms and more importantly, grasses. In contrast, the Permian plant community was limited to pre-angiosperm and no grasses (DiMichele et al., 2009). Hence, all other factors equal, the ability of plants to enhance weathering in the modern plant ecosystem should enhance weathering today relative to the Permian. Our observations indicate that Permian weathering was more intense than today suggesting the role of climate, and specifically water availability, played a much bigger influence on weathering in the Permian relative to the modern system.

CONCLUSIONS

The Permian paleo-landscape of the Wichita Mountains provides a unique setting to document geochemical and textural weathering signals in a modern granitic terrane and compare these to weathering signals preserved in the Permian system bearing the same provenance and drainage basin controls. This provides a means to better assess climate controls on weathering in the ancient system by comparison with the known modern (and recent) climate system. Significant amounts of clay, high percentages of Al_2O_3 in the mud fraction, spheroidal weathering, thick weathering rinds, and

hyperconcentrated flood flow deposits are more prominent in the Permian Post Oak Conglomerate relative to fluvial sediments from the modern Blue Beaver Creek, with relatively minimal amounts of weathering in the latter. These results indicate that the climate, and particularly effective moisture during deposition of the Post Oak Conglomerate differed significantly from the temperate semi-arid climate prevailing today. Specifically, the increased weathering recorded by the Post Oak Conglomerate records weathering under climate conditions that were much wetter than those of the modern and recent. Furthermore, CIA values of muds from modern tropical climates are very similar to CIA values of muds from the Permian Post Oak Conglomerate, and much higher than CIA values of the muds from the modern Blue Beaver Creek, further supporting the interpretation of wetter conditions during deposition of the Post Oak Conglomerate.

ACKNOWLEDGEMENTS

This research was conducted with partial support from the National Science Foundation (EAR-0746042 and ANT-0442639), student research grants awarded to L. Keiser from SEPM and Sigma Xi, and the University of Oklahoma School of Geology and Geophysics. Any opinions, findings, and conclusions or recommendations expressed in this material are those of the author(s) and do not necessarily reflect the views of the National Science Foundation. We are extremely grateful to Dr. Charles Gilbert, Professor Emeritus, School of Geology and Geophysics, University of Oklahoma, for many fruitful discussions on the geology of the Wichita Mountains. We would like to thank Alison Stumpf and Earl Manning for their assistance with fieldwork. We are grateful for the help of the Wichita Mountains Wildlife Refuge personnel, specifically Mr. Rupert, who assisted in securing permits (Permit # 21670-10-019 and # 21670-11-018) for sample collection. Thanks to Jeremy Jernigan and Gary Stowe with the OU Petroleum Engineering Department for their help with the SEM.

Table 4.1: Attributes of modern and Permian drainages

Table 1: Attributes of modern and Permian drainages

	Modern Blue Beaver Creek	Ancient Post Oak Conglomerate
source rock	granite	granite
basin area	42 km^2	30 - 50 km^2
basin relief	320 m	300 - 350 m
MAP	770 mm/yr	?
MAT	16 °C	?
climate	temperate	?

Blue Beaver Creek data from Mast and Turk, 1999
MAP - mean annual precipitation
MAT - mean annual temperature

Table 4.2: Geochemistry of major-element oxides

		SiO_2	Al_2O_3	K_2O	Na_2O	CIA
		%	%	%	%	
Bedrock	Mt Scott Granite	72.79	12.28	4.20	0.46	57.01
	Quanah Granite	75.60	11.80	4.75	0.16	56.79
	Medicine Park Granite	75.60	11.90	4.61	0.21	57.21
	Rush Lake Granite	74.40	11.85	4.67	0.26	56.20
	Saddle Mountain Granite	72.77	12.57	4.35	0.46	58.05
	Davidson Metarhyolite	73.90	13.60	4.31	0.33	65.87
	Rholite Xenoliths	76.35	12.25	4.72	0.19	57.92
	Carlton Rhyolite	75.55	12.37	4.46	0.33	61.38
	Wichita Granite Group	77.60	11.40	4.11	0.33	58.34
Blue Beaver Creek	Blue Beaver 6	70.40	10.10	2.77	0.02	62.21
	Blue Beaver 9	68.30	9.89	3.04	0.03	59.55
	Blue Beaver 12	68.30	9.71	2.93	0.03	58.17
	Blue Beaver 13	65.10	10.60	3.01	0.03	59.76
	Blue Beaver 15	63.80	11.90	3.63	0.03	59.16
	Blue Beaver 16	66.70	11.80	2.63	0.02	72.48
Post Oak Conglomerate	Post Oak Quetone Pt 1	42.10	20.40	2.39	0.04	79.84
	Post Oak Quetone Pt 2	50.70	22.50	3.18	0.06	76.84
	Post Oak Quetone Pt 3	57.10	21.50	4.42	0.03	76.81
	Post Oak Boulder Park 1	56.00	25.70	3.19	0.03	84.23
	Post Oak Boulder Park 2	54.40	27.10	2.57	0.02	87.79
Modern Tropical	Amazon Deep Sea Fan	51.00	19.00	2.60	0.01	83.70
	Malaysia Peninsula	55.37	25.97	2.44	0.01	89.43
	Penang Island	54.17	23.21	3.06	0.02	83.13
Modern Temperate	Llano TX	61.78	12.87	3.28	0.04	66.48
	Massif-Central France	58.71	15.18	3.39	0.03	70.51
	Georgia-Alabama	65.77	14.39	3.34	0.02	74.18
Modern Arid Semi-Arid	Mineral Mtns	60.27	16.18	3.44	0.04	62.50
	Shawave Mtns	55.92	17.89	2.95	0.04	68.23
	Southern California	49.26	15.19	2.72	0.03	64.61
UCC	Upper Continental Crust	66.00	15.20	3.40	0.06	56.93

Modern stream geochemistry from other climates is from Van de Kamp (2010). Penn-Permian geochemistry from proximal first cycle arkosic sediment is from Cullers (1994). Average upper continental crust (UCC) is shown for reference (Taylor and Mclennan, 1985).

Figure 4.1: Location map of the Wichita Mountains illustrating regional geology, faults, study area, and the relationship between the Permian Post Oak Conglomerate and Wichita Mountains bedrock.

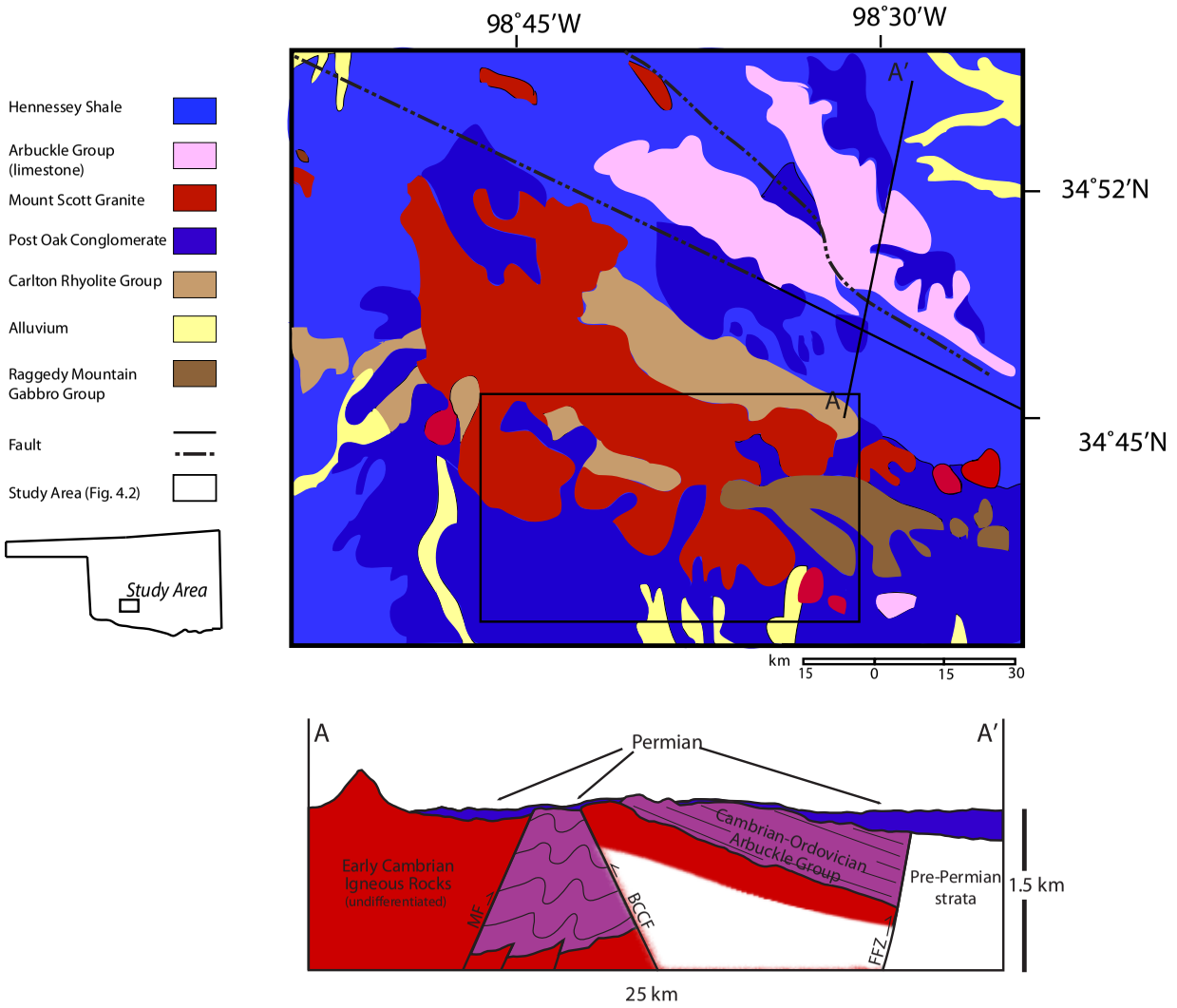
98°45′W
98°30′W
34°52′N
34°45′N
A
A′
Hennessey Shale
Arbuckle Group (limestone)
Mount Scott Granite
Post Oak Conglomerate
Carlton Rhyolite Group
Alluvium
Raggedy Mountain Gabbro Group
Fault
Study Area (Fig. 4.2)
Study Area
km
15
0
15
30
Permian
Cambrian-Ordovician Arbuckle Group
Early Cambrian Igneous Rocks (undifferentiated)
Pre-Permian strata
MF
BCCF
FFZ
1.5 km
25 km

Figure 4.2: Location map of the Wichita Mountains study area including the bedrock geology (Havens, 1983), the modern Blue Beaver Creek and hypothesized Permian Post Oak stream channels (Stone, 1977), measured section and sample locations.

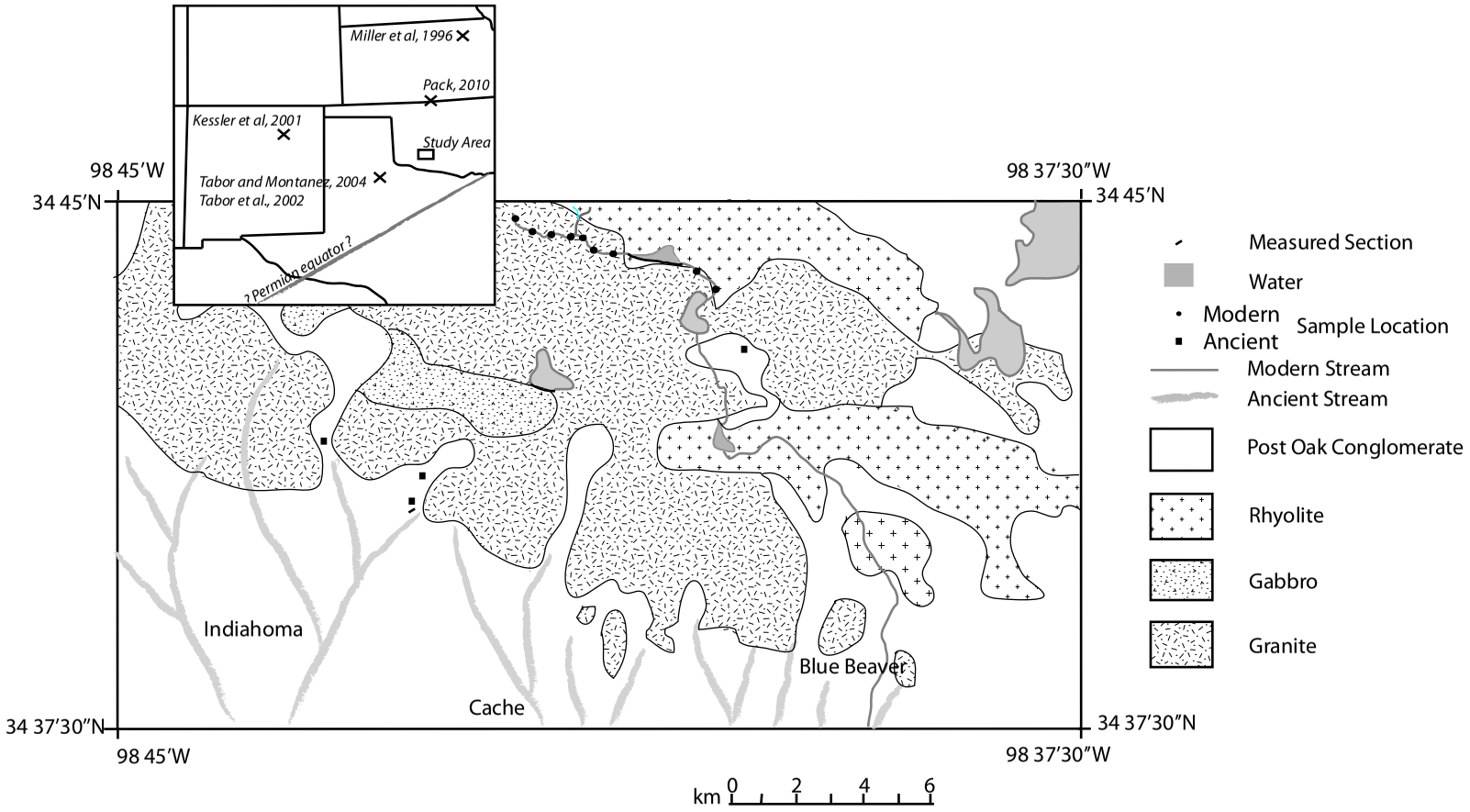
Miller et al, 1996
Pack, 2010
Kessler et al, 2001
Study Area
Tabor and Montanez, 2004
Tabor et al., 2002
?Permian equator?
98 45′W
98 37′30″W
34 45′N
34 37′30″N
Indiahoma
Cache
Blue Beaver
km 0 2 4 6
Measured Section
Water
Modern
Ancient
Sample Location
Modern Stream
Ancient Stream
Post Oak Conglomerate
Rhyolite
Gabbro
Granite

Figure 4.3: Stratigraphy and timescale for the southern Oklahoma region illustrating the interfingering of the Permian Hennessey Shale and the Post Oak Conglomerate during Leonardian (Artinskian) time (modified from Pack, 2010). Shaded areas are inferred times of increased paleoprecipitation (Retallack, 2013)

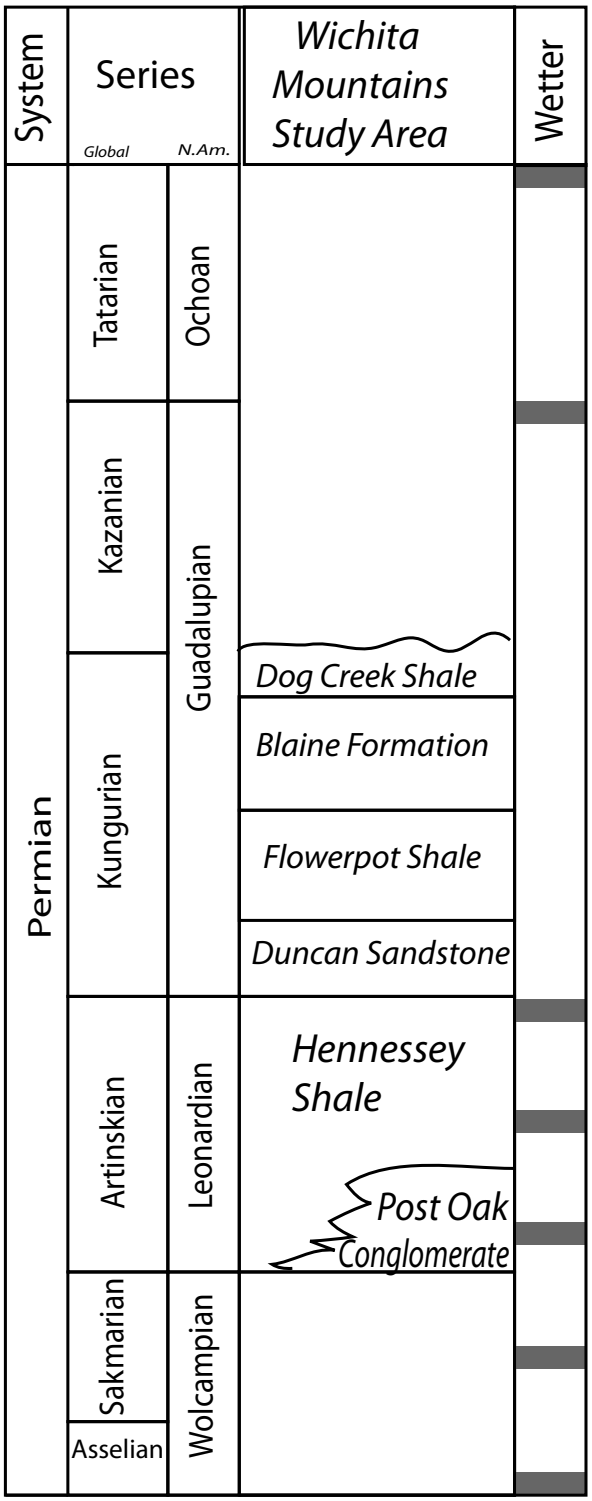
System
Series
Global
N.Am.
Wichita Mountains Study Area
Wetter
Permian
Tatarian
Ochoan
Kazanian
Guadalupian
Kungurian
Dog Creek Shale
Blaine Formation
Flowerpot Shale
Duncan Sandstone
Artinskian
Leonardian
Hennessey Shale
Post Oak Conglomerate
Sakmarian
Wolcampian
Asselian
Increased paleoprecipitation (Retallack, 2013)

Figure 4.4: Aerial photograph of Post Oak Conglomerate. The topographic highs outlined in red are remnants of the Permian channels (Gilbert, 1982).

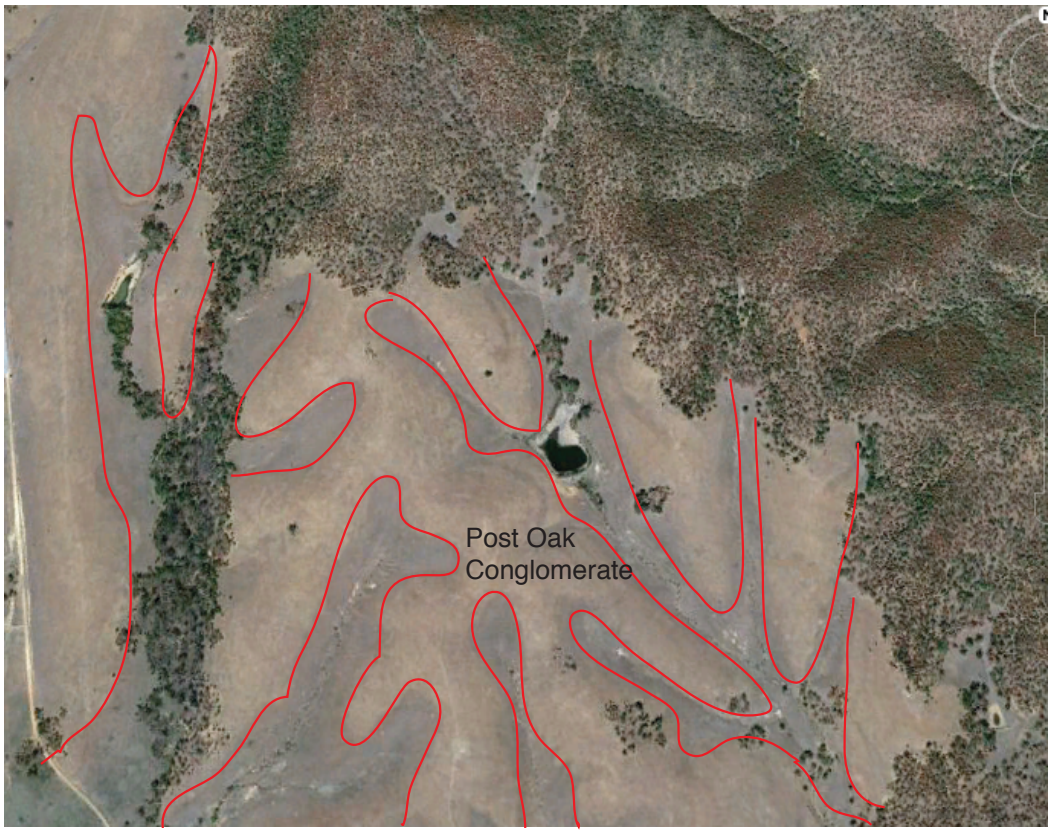
Post Oak
Conglomerate

Figure 4.5: Measured section log of the Boulder Park outcrop (~16 m) for the Post Oak Conglomerate. Thick deposits of granule to boulder conglomerate predominate, with crude horizontal stratification in some units. A) Lateral gradation (over ~4 m) from crudely stratified granule conglomerate to internally massive coarse sand with floating boulders and cobbles. B) Lateral continuity of possible paleosol horizons in 3 units.

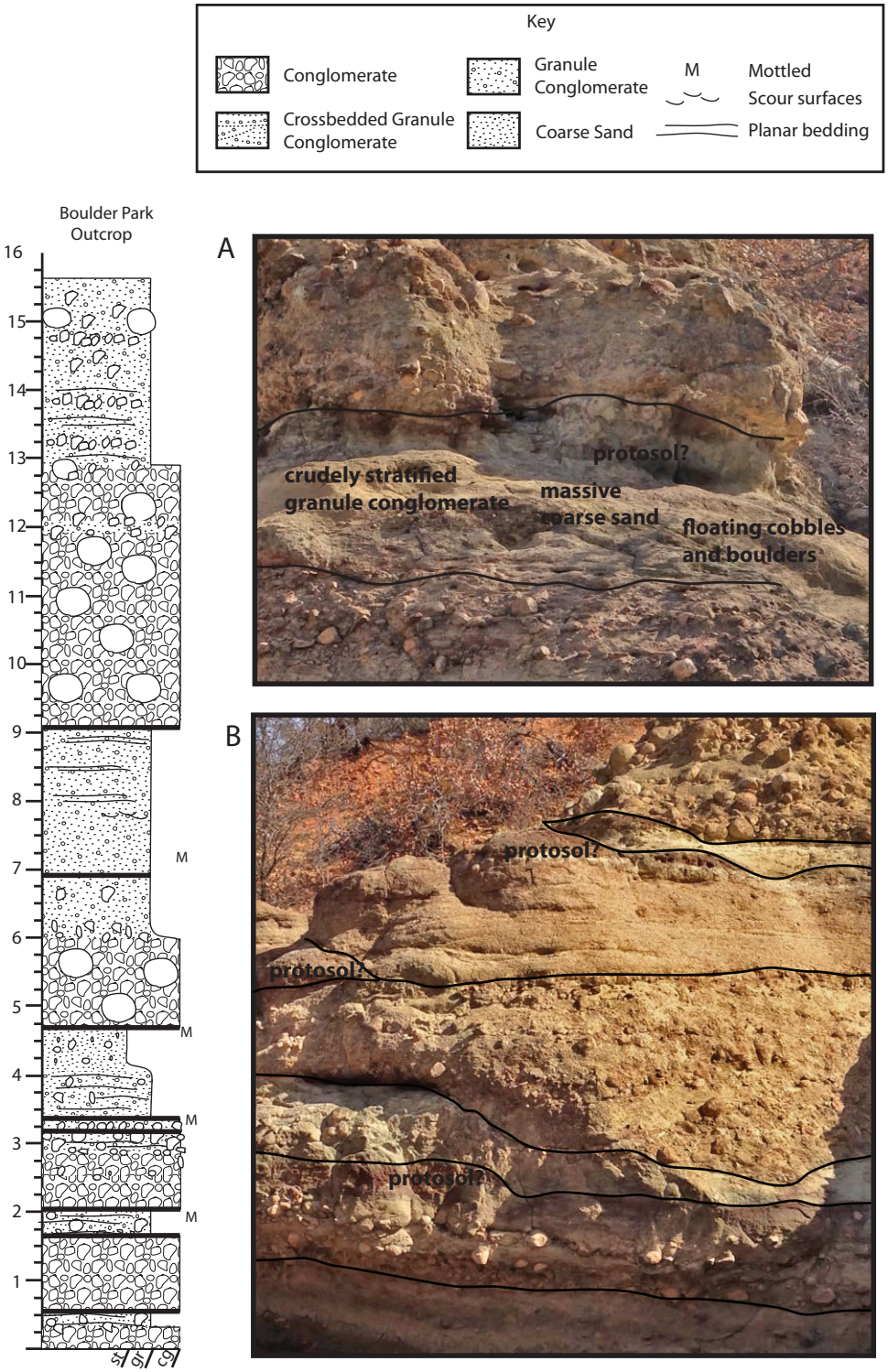
Key
Conglomerate
Granule Conglomerate
M
Mottled
Scour surfaces
Crossbedded Granule Conglomerate
Coarse Sand
Planar bedding
Boulder Park Outcrop
16
15
14
13
12
11
10
9
8
7
6
5
4
3
2
1
M
M
M
M
A
crudely stratified granule conglomerate
massive coarse sand
protosol?
floating cobbles and boulders
B
protosol?
protosol?
protosol?

Figure 4.6: Facies Images of the Post Oak Conglomerate. A.) Inferred root trace defining pedogenic alteration within a relatively fine-grained interval. Whereas the surrounding matrix exhibits a red-brown (oxidized) color, the root trace exhibits reduced colors and a downwardly tapering geometry. B.) Lateral continuity of a paleosol horizon at the Boulder Park Outcrop C.) Blocky texture present in one of the inferred paleosol horizons D.) Clay coats in the same horizon as C E.) Diffuse top in horizon inferred to be a hyper-concentrated flood flow (HFF) F.) The top of the image shows another laterally continuous inferred paleosol horizon. The remaining deposits in the image are coarse sand with local floating out-sized clasts G.) An example of a spheroidally weathered cobble with a thick weathering rind still present.

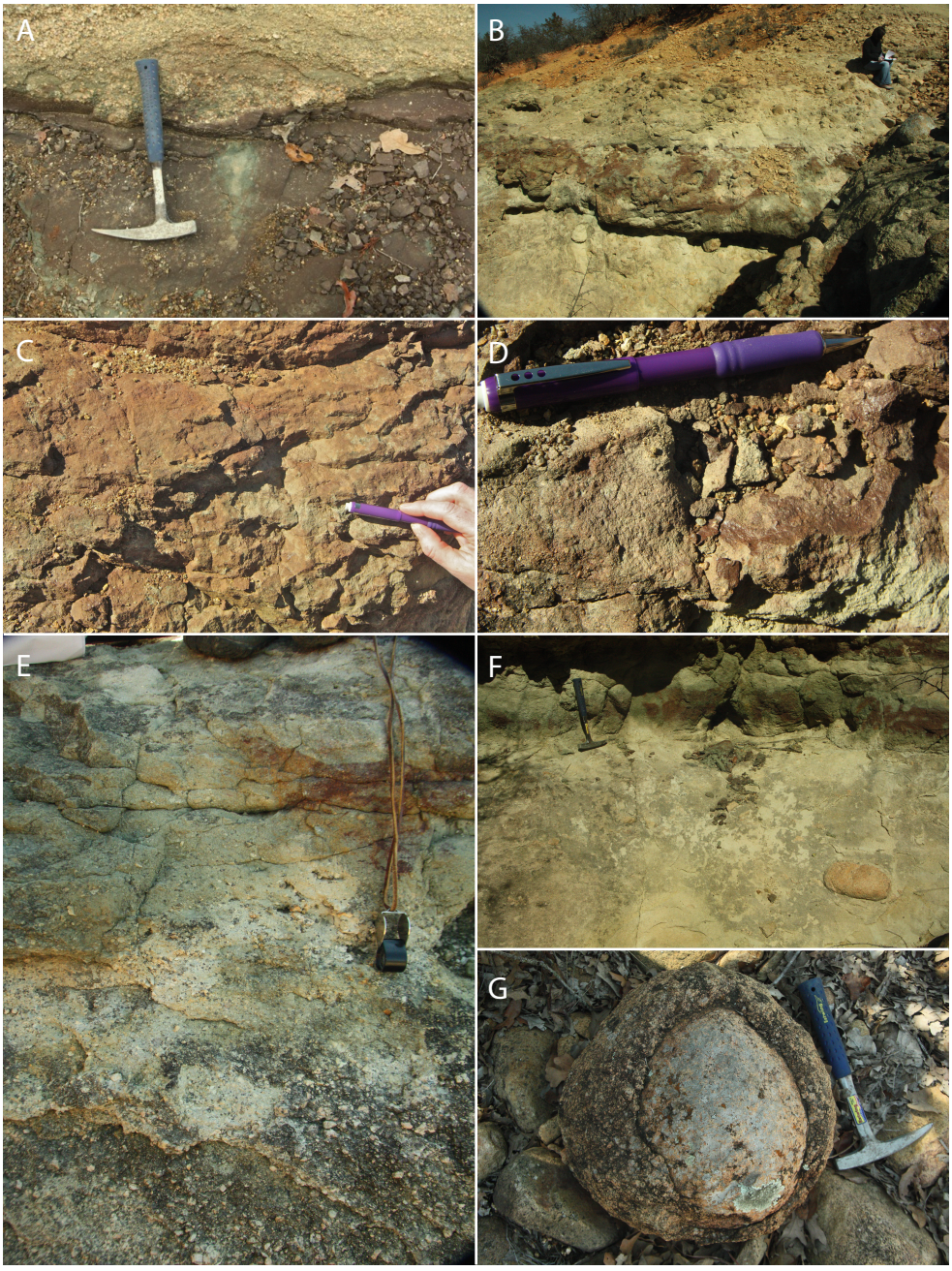
A
B
C
D
E
F
G

Figure 4.7: Bulk quantitative XRD analysis was used to determine the percentage of primary minerals and clay minerals in the modern and Permian samples (<63 μm). The percent clay in the Permian samples is nearly double that of the modern samples. Grain-size analysis of both the modern (n=5) and Permian sediment (n=5) reveals an average of 12% mud in the Permian and 3% mud in the modern. LPSA results for the <63 μm fraction of the samples indicates the average mode for the Permian samples is 7.1 μm while the average mode for the modern samples is 29.8 μm.

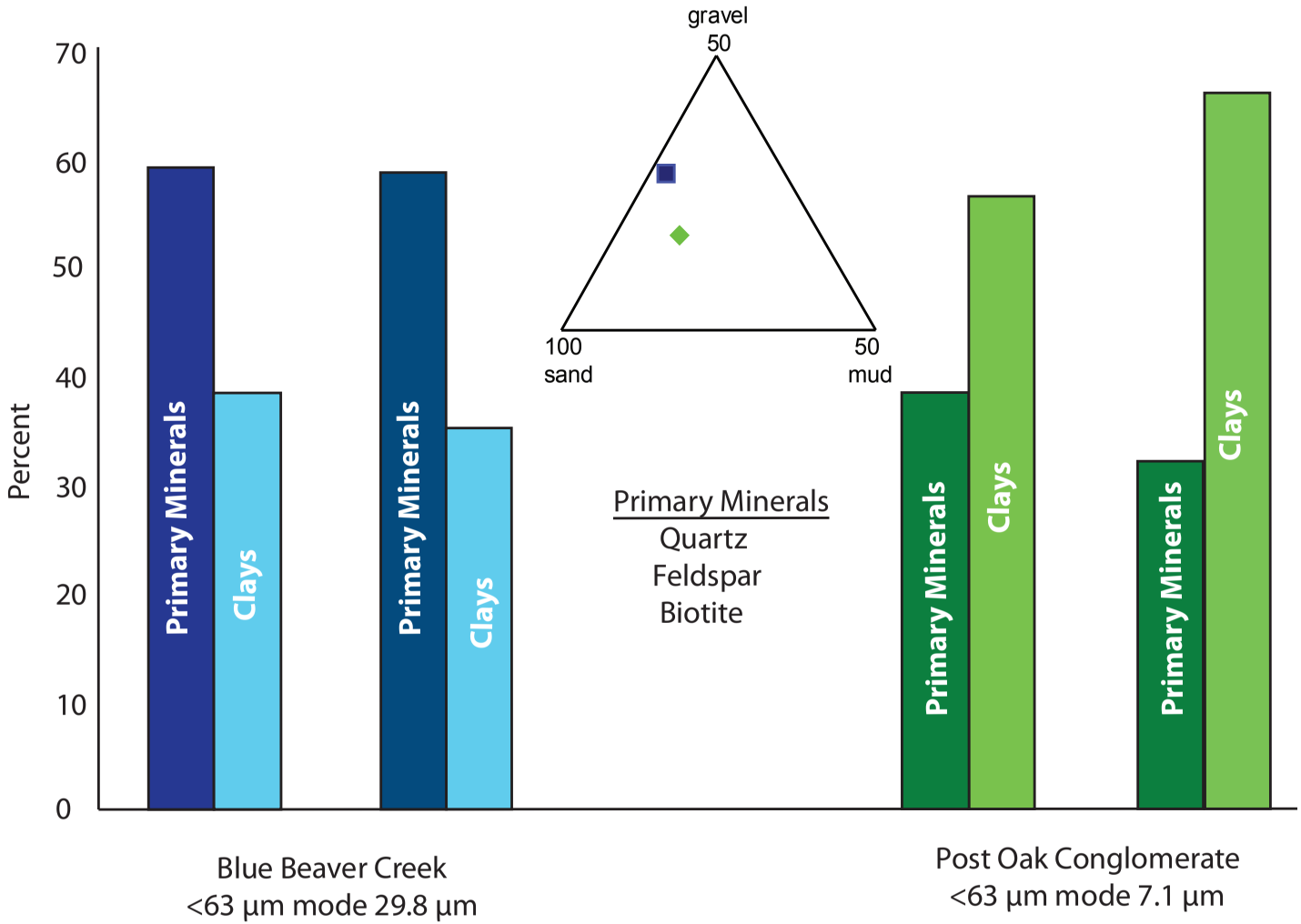
gravel
50
100
sand
50
mud
Percent
70
60
50
40
30
20
10
0
Primary Minerals
Clays
Primary Minerals
Clays
Primary Minerals
Clays
Primary Minerals
Clays
Primary Minerals
Quartz
Feldspar
Biotite
Blue Beaver Creek
<63 µm mode 29.8 µm
Post Oak Conglomerate
<63 µm mode 7.1 µm

Figure 4.8: Analyses of weathered rinds and cores of clasts extracted from the Permian Post Oak Conglomerate. A) Image of the cut clast prior to ion milling showing the thickness of the rind (3 mm - arrow). B) SEM back-scattered electron image (magnification 1000X) of clay found in fractures of the core. C) SEM image of the boundary between the rind and core with extensive weathering and clay formation in the rind and abundant fracturing in the core with clay formation. D) SEM BSE image (magnification 200x) showing abundant microfracturing that permeates the rind, and penetrates the core of the clast. The fracturing and clay formation illustrates how fluids can readily enter the granitic bedrock.

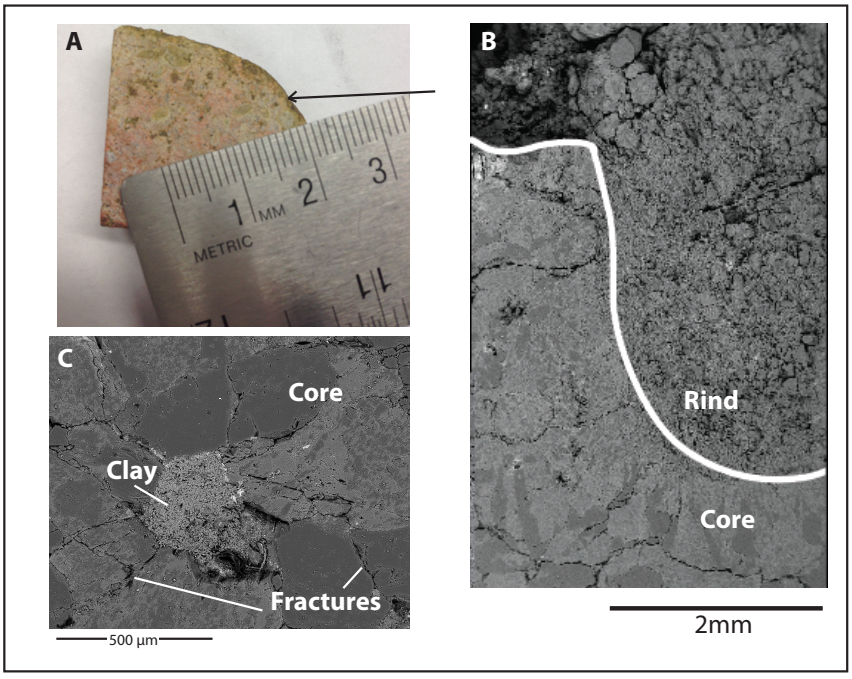
A
B
C
Core
Clay
Fractures
500 µm
Rind
Core
2mm

Figure 4.9: Graphs of selected major-element oxides from bulk geochemical analyses. The results are averaged for samples from the bedrock (from Price 1998), modern sediment of Blue Beaver Creek, and matrix from the Post Oak Conglomerate. Results are also shown for various felsic-sourced sediment from alluvial systems in modern semi-arid to arid, modern temperate, and modern tropical climates documented by Van De Kamp et al., 2010. UCC is the average composition of the upper continental crust value of Taylor and McLellan (1985).

K_2O
5.0
4.5
4.0
3.5
3.0
2.5
2.0
1.5
1.0
0.5
0
Bedrock
Blue
Beaver
Post Oak
Arid
Temperate
Tropical
Modern
UCC
CIA
90
80
70
60
50
40
30
20
10
0
SiO_2
80
70
60
50
40
30
20
10
0
Al_2O_3
25
20
15
10
5
0

Figure 4.10: Cross-plot of K_2O + Na_2O versus SiO_2 from XRF analysis of the mud fraction for the modern sediment (Blue Beaver Creek), the Permian sediment (matrix of the Post Oak Conglomerate), and bedrock (granites from the Wichita Mountains listed in Table 4.2)(Price, 1998). Beginning with a felsic (granitic) source, weathering increases towards the upper right corner on this plot. Relative to the (essentially unweathered) bedrock, the sediment from the Permian Post Oak Conglomerate exhibits substantially more weathering than the sediment from modern Blue Beaver Creek, despite sharing the same bedrock source.

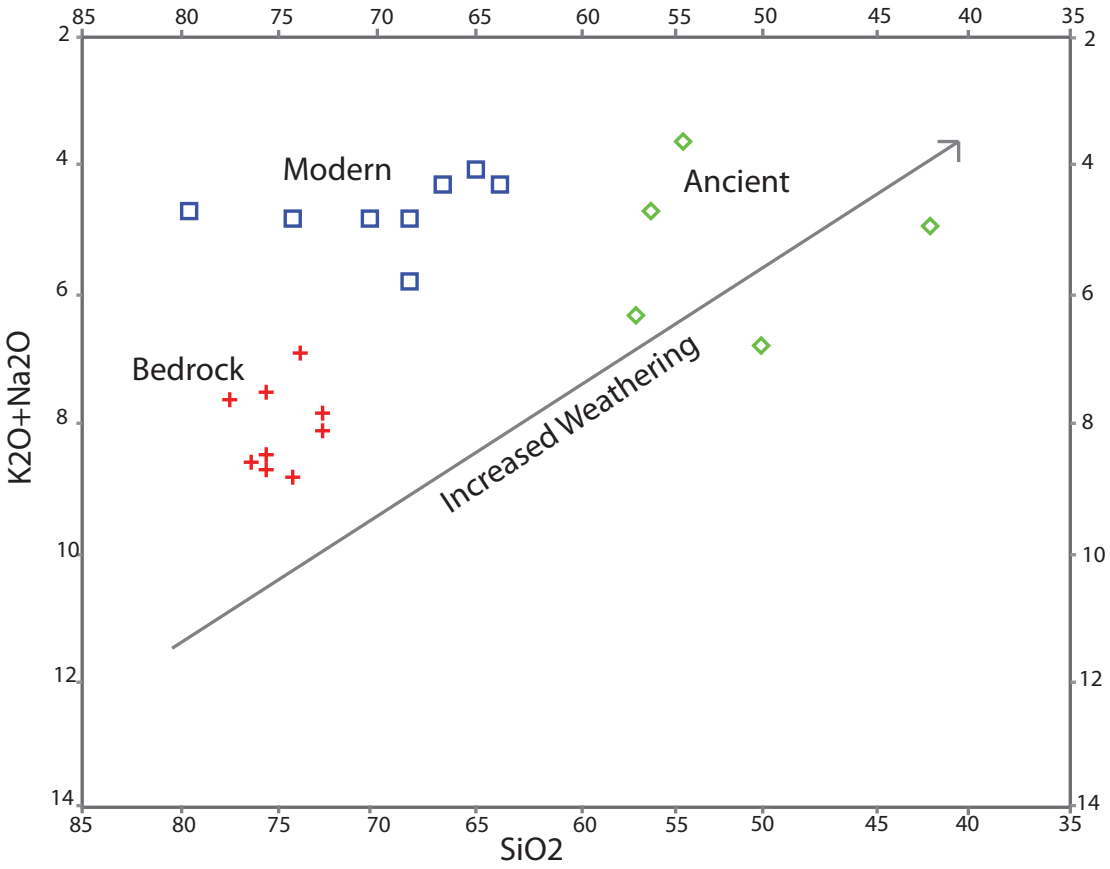
85
80
75
70
65
60
55
50
45
40
35
2
4
6
8
10
12
14
K2O+Na2O
SiO2
Modern
Ancient
Bedrock
Increased Weathering

Figure 4.11: A.) ACNK (Al_2O_3, CaO + Na_2O, and K_2O) diagram meant to illustrate weathering intensity (Nesbitt and Young, 1996). The bedrock (granites from the Wichita Mountains listed in Table 4.2 (Price, 1998) falls very near the feldspar join at 50%. The modern sediment shows slightly more Al_2O_3 concentrations and less CaO and Na_2O concentrations, consistent with more weathering. The Post Oak Conglomerate exhibits an even higher concentration of Al_2O_3 and much less K_2O, CaO, and Na_2O than the modern sediment, consistent with more intense weathering than the modern sediment. K = kaolinite, Gi= gibbsite, Chl= chlorite, Pl= plagioclase, Ks= K-feldspar, A= Al_2O_3, K=K_2O, CN=CaO+Na_2O. B) ACNK diagram upper apex only. Modern sediment samples collected from fluvial systems draining generally felsic terranes in a variety of climate systems (from Van De Kamp, 2010) are plotted as a comparison (Table 4.2, Fig. 4.12A). Bulk composition of the Upper Continental Crust (UCC) is from Taylor and McLellan (1985).

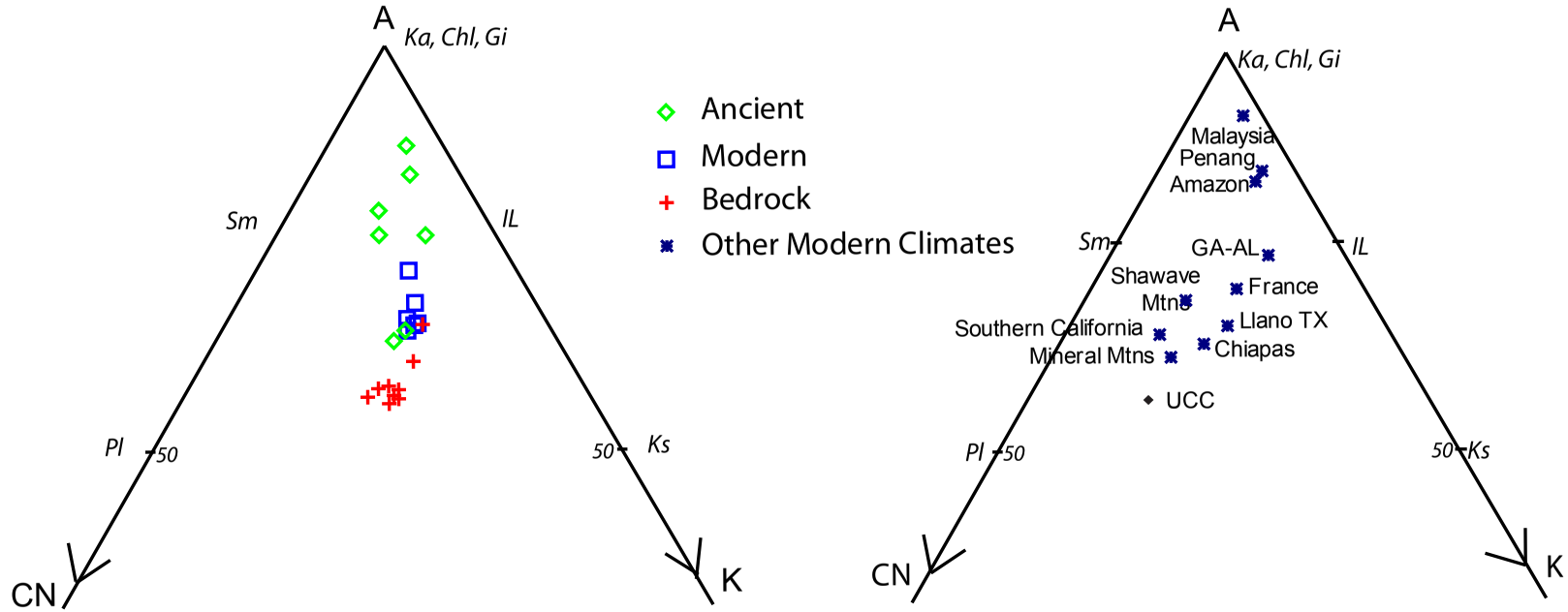
A
Ka, Chl, Gi
Sm
IL
Pl
50
50
Ks
CN
K
Ancient
Modern
Bedrock
Other Modern Climates
A
Ka, Chl, Gi
Malaysia
Penang
Amazon
Sm
GA-AL
IL
Shawave
Mtns
France
Southern California
Llano TX
Mineral Mtns
Chiapas
UCC
Pl
50
50
Ks
CN
K

Figure 4.12: a) Mean annual precipitation (MAP) versus mean annual temperature (MAT) for a variety of fluvial sediments collected from a range of modern climates from Van De Kamp (2010) and Lydolph (1985). The modern climate of the Wichita Mountains is also plotted for comparison. b) Groupings are circled on the ANCK diagram from figure 4.11. The groupings reflect the 3 climates zones illustrated on the MAP and MAT diagram (a). The Post Oak Conglomerate plots in the tropical climate zone on the ACNK diagram (Fig. 4.11) and therefore can be plotted on the MAP/MAT plot. A range of MAP and MAT and not exact numbers is all that can be reasonably interpreted from this method.

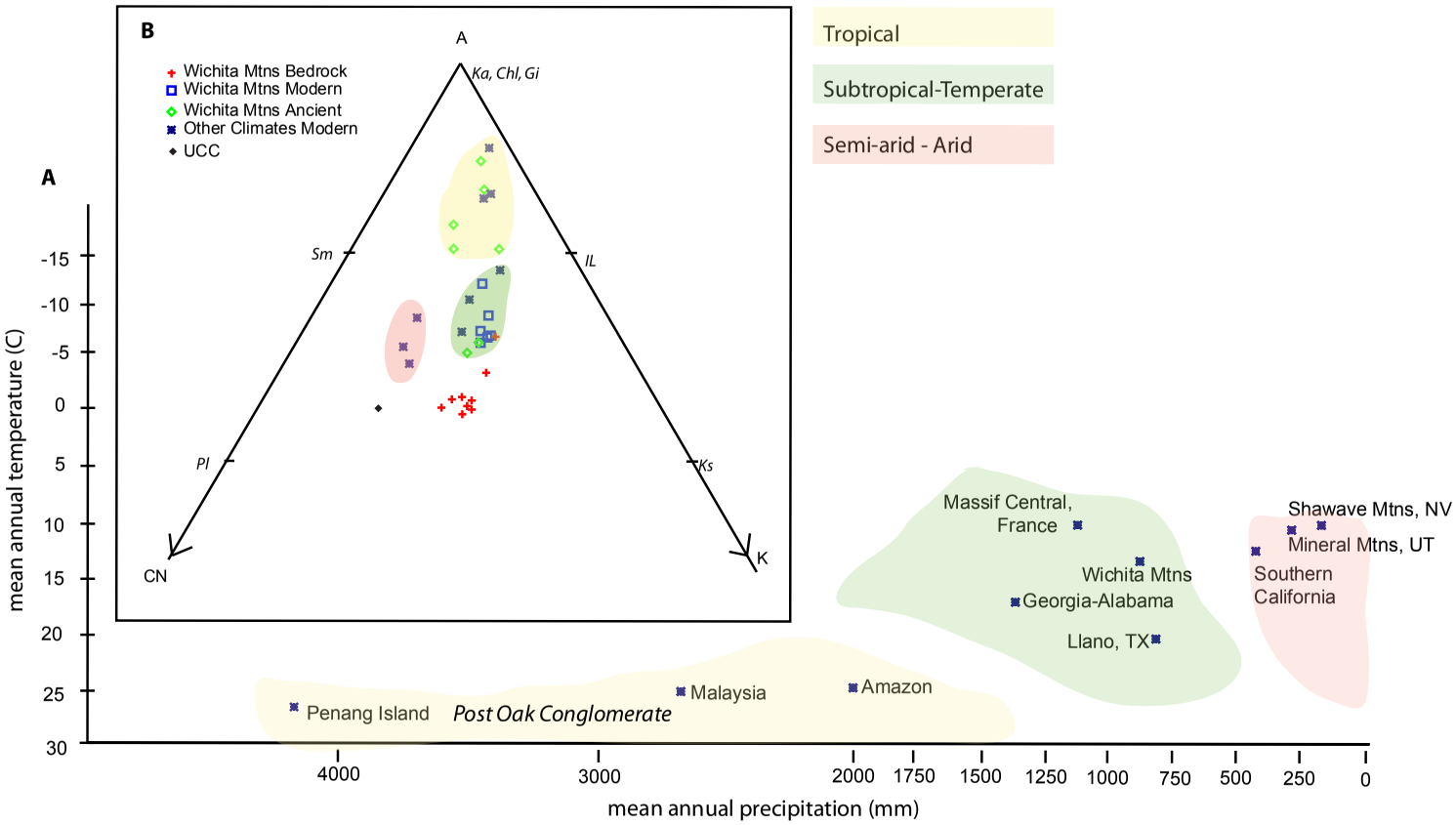
B
A
Ka, Chl, Gi
Wichita Mtns Bedrock
Wichita Mtns Modern
Wichita Mtns Ancient
Other Climates Modern
UCC
Sm
IL
Pl
Ks
CN
K
A
mean annual temperature (C)
-15
-10
-5
0
5
10
15
20
25
30
4000
3000
2000
1750
1500
1250
1000
750
500
250
0
mean annual precipitation (mm)
Tropical
Subtropical-Temperate
Semi-arid - Arid
Massif Central, France
Wichita Mtns
Georgia-Alabama
Llano, TX
Shawave Mtns, NV
Mineral Mtns, UT
Southern California
Malaysia
Amazon
Penang Island
Post Oak Conglomerate

REFERENCES

AL-SHAIEB, Z., HANSON, R.E., DONOVAN, N.R., and SHELTON, J.W., 1980, Petrology and Diagenesis of Sandstones in the Post Oak Formation (Permian) Southwestern Oklahoma: Journal of Sedimentary Petrology, 50(1), 43-50.

BAHLBURG, H., and DOBRZINSKI, 2011, A review of the Chemical Index of Alteration (CIA) and its application to the study of Neoproterozoic glacial deposits and climate transitions. Geological Society, London, Memoir, 36(1), 81-92.

BASTIDA, J., OSCAR, M.C., SANCHO, C., and MUNOZ, A., 2013, Environmental changes during the Upper Pleistocene-Holocene in Mediterranean Northeast Spain as recorded by the mineralogy and geochemistry of alluvial records: Quaternary International, http://dx.doi.org/10.1016/j.quaint.2013.02.041.

BENISON, K. C., and GOLDSTEIN, R. H., 2001, Evaporites and siliciclastics of the Permian Nippewalla Group of Kansas, USA: a case for non-marine deposition in saline lakes and saline pans: Sedimentology, 48(1), 165-188.

BREWER, J.A., GOOD, R., OLIVER, J.E., BROWN, L.D., and KAUFMAN, S., 1983, COCORP profiling across the Southern Oklahoma aulacogen, overthrusting of the Wichita Mountains and compression with the Anadarko Basin: Geology, 11, 109-114.

BROWN, K. M., and RANSOM, B., 1996, Porosity corrections for smectite-rich sediments: Impact on studies of compaction, fluid generation, and tectonic history: Geology, 24(9), 843-846.

CHASE, GERALD W., 1954, Permian conglomerate around Wichita Mountains, Oklahoma: AAPG Bulletin-American Association of Petroleum Geologist Bulletin, 38(9), 2028-2035.

DIXON, J.L., HEIMSATH, A.M., and AMUNDSON, R., 2009, The critical role of climate and saprolite weathering in landscape evolution: Earth Surface Processes and Landforms, 34,1507-1521.

DONOVAN, R.N.,1982, Permian paleokarst features, in Gilbert, C.A. and R.N. Donovan, eds., Geology of the Eastern Wichita Mountains, southwestern Oklahoma; Geological Survey of Oklahoma, Guidebook 22, 65-77.

DONOVAN, R. N. and RAGLAND, D. A., 1986, Paleozoic Stratigraphy of the Slick Hills, Southwestern Oklahoma, in Donovan, R.N. (editor) The Slick Hills of southwestern Oklahoma, Fragments of an aulacogen? Oklahoma Geological Survey, Guidebook 24, 13-16.

DONOVAN, R.N., COLLINS, K., and BRIDGES, S.D., 2001, Permian Sedimentation and Diagenesis on the Northern Margin of the Wichita Uplift, in Johnson, K.S. (ed.), Pennsylvanian and Permian geology and petroleum in the southern Midcontinent, 1998 Symposium: Oklahoma Geological Survey Circular 104, 171-184.

EATON, G.P., 2008, Epeirogeny in the Southern Rocky Mountains region evidence and origin: Geosphere, 4, 764-784.

FLETCHER, R.C.,BUSS, H.L., and BRANTLEY, S.L., 2006, A spheroidal weathering model coupling porewater chemistry to soil thickness during steady-state denudation: Earth and Planetary Science Letters, 244, 444-457.

FOSTER, 2013, Environments and provenance of redbeds of the Dog Creek Shale (Midcontinent): Implications for Middle Permian paleoclimate in Western Pangaea: M.S. Thesis, University of Oklahoma, Norman, Oklahoma, 112p.

GILBERT, M.C., 1982, Geologic setting of the Eastern Wichita Mountains, with a brief discussion of unresolved problems, in Gilbert, M.C., and R.N. Donovan, eds., Geology of the Eastern Wichita Mountains Southwestern Oklahoma: Oklahoma Geological Survey, Guidebook 21,1-30.

GILBERT, M.C., 1983, Timing and chemistry of igneous events associated with the southern Oklahoma aulacogen: Tectonophysics, 94, 439-455.

GOLDBERG, K. and HUMAYUN, M., 2010, The applicability of the chemical index of alteration as a paleoclimatic indicator: An example from the Perman of the Parana Basin, Brazil: Palaeogeography, Palaeoclimatology, Palaeoecology, 293, 175-183.

HALL, K., THORN, C., and SUMNER, P., 2012, On the persistence of ‘weathering’: Geomorphology, 149, 1-10.

HAM, W.E., DENISON, R.E., and MERRITT, C.A., 1964, Basement rocks and structural evolution of southern Oklahoma: American Association of Petroleum Geologists, 1, 36-55.

HAMILTON, E.M., 2011, Paleomagnetic and Petrological Investigation of Long Mountain Granite, Wichita Mountains, Oklahoma: M.S. Thesis, University of Oklahoma, Norman, Oklahoma, 123p.

HARTLEY, A.J., MATHER, A.E., JOLLEY, E., and TURNER, P., 2005, Climatic controls on alluvial-fan activity, Coastal Cordillera, northern Chile in Alluvial Fans: Geomorphology, Sedimentology, Dynamics, Geological Society, London, Special Publication, 251, 95-115.

HAVENS, J.S., 1983, Reconnaissance of ground water in vicinity of Wichita Mountains Southwestern Oklahoma: Oklahoma Geological Survey Circular 85,13p.

HOFFMAN, P., DEWEY, J. F., and BURKE, K., 1974, Aulacogens and their genetic relation to geosynclines with a Proterozoic example from Great Slave Lake Canada: American Association of Petroleum Geologists Bulletin 58, 856-867

JANITSKY, P., 1986, Laboratory methods: citrate–bicarbonate–dithionite (CBD) extractable iron and aluminum, in Singer, M.J., and Janitzky, P., eds., Field and laboratory procedures used in a Soil Chronosequence study: U.S. Geological Survey, Bulletin, 1648, 38–41.

JIONGXIN, X., 2004, Hyperconcentrated flows in the slope-channel systems in gullied hilly areas on the Loess Plateau, China: Geografiska Annaler. Series A, Physical Geography, 86(4), 349-366.

KELLER, G.R., LIDIAK, E.G., HINZE, W.J., and BRAILE, L.W.,1983, The role of rifting in the tectonic development of the midcontinent, U.S.A.: Tectonophysics, 94, 391-412.

KESSLER, J., SOREGHAN, G.S., and WACKER, H., 2001, Equatorial aridity in Western Pangea: Lower Permian loessite and dolomitic paleosols in northeastern New Mexico, USA: Journal of Sedimentary Research, 71(5), 817–832.

KOTTEK, M., GRIESER, J., BECK, C., RUDOLF, B., and RUBEL, F., 2006, World map of the Koppen-Geiger climate classification updated. Meteorologische Zeitschrift, 15(3), 259-264.

KRAUS, M. J.,1996, Avulsion deposits in lower Eocene alluvial rocks, Bighorn Basin, Wyoming. Journal of Sedimentary Research, 66(2), 354-363.

LYDOLPH, P.E., 1985, The Climate of the Earth: Totowa, N.J., Rowman &

Allanheld, 388p.

MACK, G.H., JAMES, W.C., and MONGER, H.C., 1993, Classification of paleosols. Geological Society of America Bulletin, 105(2), 129-136.

MAST, M.A., and TURK, J.T., 1999, Environmental characteristics and water quality of hydrologic benchmark network stations in the midwestern United States: US Geological Survey 1173, 1963-95.

MEHRA, O.P., and JACKSON, M.L., 1960, Iron oxide removal from soils and clays by a citrate–dithionite system buffered by sodium carbonate: Clays and Clay Mineralogy, 7, 317–327.

MILLER, K.B., MCCAHON, T.J., and WEST, R.R., 1996, Lower Permian (Wolfcampian) paleosol-bearing cycles of the U.S. midcontinent: Evidence of climatic cyclicity: Journal of Sedimentary Research, 66, 71-84.

NESBITT, H.W., YOUNG, G.M., MCLENNAN, S.M., and KEAYS, R.R., 1996, Effects of chemical weathering and sorting on petrogenesis of siliciclastic sediments with implications for provenance studies: The Journal of Geology, 104(5) 525-542.

NICHOLS, C.R., 1968, Alteration of Igneous Rocks in the Lugert Area, Kiowa County, Oklahoma: M.S. Thesis, University of Oklahoma, Norman, Oklahoma, 140p .

OBERLANDER, T.M., 1972, Morphogenesis of granitic boulder slopes in the Mojave Desert, California: The Journal of Geology, 80(1), 1-20.

PACK, J.M., 2010, Paleoclimatic implications of the depositional setting and origin of sediments in the Wellington Formation, Kay County, Oklahoma: M.S. University of Oklahoma, Norman, Oklahoma, 192p.

POPE, G. A., DORN, R. I., and DIXON, J. C., 1995, A new conceptual model for understanding geographical variations in weathering. Annals of the Association of American Geographers, 85(1), 38-64.

POWELL, B.N., and PHELPS, D.W., 1977, Igneous cumulates of the Wichita province and their tectonic implications: Geology, 5(1), 52-56.

PRICE, J.D., 1998, Petrology of the Mount Scott Granite: PhD dissertation, University of Oklahoma, Norman, Oklahoma, 240p .

RETALLACK, G.J., 2001, Soils of the past: An introduction to paleopedology. Wiley-Blackwell, 404p.

RETALLACK, G.J., 2013, Permian and Triassic greenhouse crises: Gondwana Research, 24, 90-103.

RIEBE, C.S., KIRCHNER, J.W., and FINKEL, R.C., 2004, Erosional and climatic effects on long-term chemical weathering rates in granitic landscapes spanning diverse climate regimes: Earth and Planetary Science Letters, 224, 547-562.

SINGH, P., 2010, Geochemistry and provenance of stream sediments of the Ganga River and its major tributaries in the Himalayan region, India: Chemical Geology, 269(3), 220-236.

SOIL SURVEY STAFF, Natural Resources Conservation Service, United States Department of Agriculture. Soil Series Classification Database. Available online at http://soils.usda.gov/technical/classification/scfile/index.html. Accessed [05/17/213].

SOREGHAN, G.S., KELLER, G.R., GILBERT, M.C., CHASE, C.G., and SWEET, D.E., 2012, Load-induced subsidence of the Ancestral Rocky Mountains recorded by preservation of Permian landscapes: Geosphere, 8(3), 654-668.

SMITH, G.A., and LOWE, D. R., 1991, Lahars: Volcano Hydrologic-Events and Deposition in the Debris Flow—Hyperconcentrated Flow Continuum in Fisher, R.V., and Smith, G.A., eds., Sedimentation in volcanic settings: SEPM (Society for Sedimentary Geology), Special Publication No. 45, p. 59-70.

SMITH, G.A.,1986, Coarse-grained nonmarine volcaniclastic sediment: Terminology and depositional process. Geological Society of America Bulletin, 97(1), 1-10.

STITH, D.A., 1968, Petrology of the Hennessey Shale (Permian) Wichita Mountains area, Oklahoma: M.S. Thesis, University of Oklahoma, Norman, Oklahoma, 113p.

STONE, W.B., 1977, Mineralogic and Textural Dispersal Patterns within the Permian Post Oak Formation of Southwestern Oklahoma: M.S. Thesis, University of Oklahoma, Norman, Oklahoma, 117p .

STRUDLEY, M. W., MURRAY, A. B., and HAFF, P. K., 2006, Emergence of pediments, tors, and piedmont junctions from a bedrock weathering– regolith thickness feedback. Geology, 34(10), 805-808.

SWEET, A. C., SOREGHAN, G. S., SWEET, D. E., SOREGHAN, M. J., and MADDEN, A. S., 2012, PermianDust in Oklahoma: Source and Origin for Middle Permian (Flowerpot-Blaine) Redbeds in Western Tropical Pangaea. Sedimentary Geology.

TABOR, N.J., and MONTAÑEZ, I.P., 2002, Shifts in late Paleozoic atmospheric circulation over western equatorial Pangea: Insights from pedogenic mineral δ18O compositions. Geology, 30(12), 1127-1130.

TABOR, N.J. and MONTANEZ, I.P., 2004, Morphology and distribution of fossil soils in the Permo-Pennsylvanian Wichita and Bowie Groups, north-central Texas, USA: implications for western equatorial Pangean palaeoclimate during icehouse–greenhouse transition. Sedimentology, 51(4), 851-884.

TABOR, N.J. and POULSEN, C.J., 2008, Palaeoclimate across the Late Pennsylvanian-Early Permian tropical palaeolatitudes: A review of climate indicators, their distribution, and relation to palaeophysiographic climate factors: Palaeogeography, Palaeoclimatology, Palaeoecology, 268(3), 293-310.

TAYLOR, G. and EGGLETON, R.A., 2010, Regolith Geology and Geomorphology: John Wiley and Sons, New York, 375p.

TAYLOR, S.R. and MCLENNAN, S.M., 1985, The continental crust: its composition and evolution: Blackwell Scientific, Palo Alto, CA, 120p.

TERRY JR, D.O., 2001, Paleopedology of the Chadron Formation of Northwestern Nebraska: implications for paleoclimatic change in the North American midcontinent across the Eocene–Oligocene boundary: Palaeogeography, Palaeoclimatology, Palaeoecology, 168(1), 1-38.

TWIDALE, C.R., and ROMANÍ, J.R.V., 2005, Landforms and geology of granite terrains: CRC Press, New York, 351p.

VAN DE KAMP, P.C., 2010, Arkose, subarkose, quartz sand, and associated muds derived from felsic plutonic rocks in glacial to tropical humid climates: Journal of Sedimentary Research, 80(10), 895-918.

WHITE, A.F., and BLUM, A.E., 1995, Effects of climate on chemical weathering in watersheds: Geochimica et Cosmochimica Acta, 59(9), 1729-1747.

WINKLER, J.E., KELLEY, S.A., and BERGMAN, S.C., 1999, Cenozoic denudation of the Wichita Mountains, Oklahoma, and southern mid-continent: apatite fission-track thermochronology constraints: Tectonophysics, 305(1), 339-353.

WOODHEAD, J., REISZ, R., FOX, D., DRYSDALE, R., HELLSTROM, J., MAAS, R., CHENG, H., and EDWARDS, L., 2010, Speleothem climate records from deep time? Exploring the potential with an example from the Permian: Geology, 38(5), 455-458.

YANG, S., JUNG, H-S, and LI, C., 2004, Two unique weathering regimes in the Changjiang and Juanghe drainage basins: geochemical evidence from river sediments: Sedimentary Geology, 164, 19-34.